THESIS

UNDERSTANDING THE IMPACTS OF POST-WILDFIRE PROCESS-BASED RESTORATION ON SEDIMENT ACCUMULATION AND TRANSIENT GROUNDWATER STORAGE IN A COLORADO HEADWATER STREAM

Submitted by

Brady Jones

Department of Civil and Environmental Engineering

In partial fulfillment of the requirements

For the Degree of Master of Science

Colorado State University

Fort Collins, Colorado

Fall 2025

Master's Committee:

Advisor: Ryan Morrison

Ryan Bailey

Sara Rathburn

ABSTRACT

UNDERSTANDING THE IMPACTS OF POST-WILDFIRE PROCESS-BASED RESTORATION ON SEDIMENT ACCUMULATION AND TRANSIENT GROUNDWATER STORAGE IN A COLORADO HEADWATER STREAM

Low-tech, process-based restoration (LTPBR) techniques are increasingly being implemented in headwater streams, especially in catchments affected or threatened by wildfire. Although many benefits of LTPBR have been thoroughly demonstrated, the influence of these restoration approaches on transient groundwater response and sediment size and storage following a wildfire are not well understood. This study focused on Elkhorn Creek, a small headwater stream (~4.5 km^2), consisting of a low-gradient beaver meadow in the Cache la Poudre River watershed that burned during the 2020 Cameron Peak Fire. The efficacy of LTPBR techniques was assessed, including Post-Assisted Log Structures (PALS), which were implemented at the study site. Groundwater monitoring wells were installed throughout the study reach and in a reference reach located downstream. Sediment surveys including pebble counts and sediment probing were also conducted. Groundwater monitoring wells showed an average increase in groundwater elevation of 0.21 m in the study reach during baseflow one-year post-restoration when compared to limited data pre-restoration. Pebble counts showed a decrease in D_{50} of 11.7 mm one-year post-restoration. Sediment probing surveys showed approximately 63 m^3 of sediment retention within the channel one-year post-restoration. Field data were then used to develop a linked hydrodynamic (SRH-2D) – groundwater (MODFLOW-NWT) model to observe the impacts of varying restoration scenarios involving location and number of PALS at varying flowrates on surface water volume and

groundwater volume. Surface water volume results from the hydrodynamic model showed an increase of up to 37.4% when compared to no restoration implemented. Groundwater volume differences showed up to an 8% increase during low flows when comparing the groundwater volume difference to the least intensive restoration scenario to the most intensive restoration scenario. The linked hydrodynamic-groundwater model indicates that the greatest increase in both the surface water stage and inundation extent as well as the groundwater table elevations occurs at low and intermediate flows.

ACKNOWLEDGMENTS

This work would not have been possible without the amazing support, guidance, and help from all the incredible people involved in this project. From the interdisciplinary team at CSU across the Engineering, Geosciences, and Fish, Wildlife, and Conservation Biology departments to our great community partners in the Coalition for the Poudre River Watershed and Ayres Associates, it's been an honor to learn and work with you during my time at CSU.

I would like to thank my advisor, Dr. Ryan Morrison, for his continued support, motivation, and mentorship throughout this process. Your professional knowledge, excitement for collaboration, and general advice for my professional career has been invaluable. My committee members, Dr. Sara Rathburn and Dr. Ryan Bailey, thank you for your expertise in geomorphology and groundwater modeling. This project would not have been completed without both of you being willing to frequently meet with me to answer my many questions. To all the professors at CSU that I would contact to borrow field equipment, get a second opinion on my work, and to ask questions. I am lucky to have experienced a community of people at CSU that are passionate about their work and willing to help.

I would like to thank Nicholas Christensen for your vital role in the methodology and execution of the hydrodynamic modeling portion of this research. To my fellow grad students at CSU, thank you for your collaboration, help, and all the shenanigans that made my time at CSU amazing. You all truly made my grad school experience special and I will cherish the memories.

Thank you to Stillwater Sciences for their flexibility and encouragement as I finished this research and began working full-time. I am grateful to have so many people on my team encouraging me to complete my master's research.

This publication and associated research was made possible in part through funding from the Intermountain West Transformation Network, generously supported by the National Science Foundation under grant #2115169.

TABLE OF CONTENTS

LIST OF TABLES

LIST OF FIGURES

1. INTRODUCTION

1.1 Importance of River Corridor Resiliency

The river corridor consists of the stream channel, floodplain, and subsurface components, such as groundwater and hyporheic flow (Boano et al., 2014). The river corridor can vary spatially and temporally based on stream size, the geology and hydrology of the area, seasonal and yearly climate patterns, elevation, gradient, size of the watershed, upland vegetation, land cover/management, and water use patterns (Svejcar, 1997). These variations result in segments of the river being bounded by bedrock which are straighter and steeper creating a sediment transport reach, referred to as strings, while other segments of the river are wider and lower gradient creating an open depositional reach, resembling beads on the string (Stanford et al., 1996; Wohl et al., 2018). Beads can promote a diversity of grain size distribution, stratigraphy, moisture level through a connected groundwater table, riparian and/or wetland vegetation, carbon storage, and denitrification rates in floodplain sediment (Appling et al., 2014; Collins et al., 2012; Wohl et al., 2018). This interface between terrestrial and aquatic ecosystems makes the river corridor one of the most dynamic and resilient portions of the landscape (Gregory et al., 1991; Swanson et al., 1988).

Sensitivity, resistance, and resilience are important properties of the river corridor (McCluney et al., 2014). With the increasing threat of extreme wildfires and the impact these wildfires have on the river corridor, the resiliency of the watershed is crucial to maintain biodiversity and ecosystem functionality (Di Virgilio et al., 2019; Oliver et al., 2015). Wildfires create a disturbance cascade, primarily in mountainous watersheds when an abrupt alteration of land cover and the removal of litter and duff layers commonly increases sediment and water yields to a river corridor for at least a year following the fire (Wohl et al., 2022). This disturbance

can cause the river corridor to go through considerable hydrological and geomorphological changes (Shakesby & Doerr, 2006), extreme flooding and debris flows (Parise & Cannon, 2012), degradation in water quality (Rhoades et al., 2019), and lasting impacts on riparian vegetation (Bendix & Cowell, 2010; Pettit & Naiman, 2007).

In areas where extreme wildfires are more prone to occur, an emphasis has been placed on preparing the watersheds, specifically the river corridor prior to wildfire to create a more resilient ecosystem (Huayhuaca et al., 2023). An example of river corridor resiliency includes areas where beavers (*Castor* canadensis) are active and present (Fairfax & Whittle, 2020). Beavers are commonly classified as ecosystem engineers by building and creating diverse ecosystems, as well as significantly changing the geomorphology of the area and the hydrological processes (Rosell et al., 2005). Beaver canals and dams improve floodplain connectivity by spreading water out into the landscape and storing it broadly in adjacent soils that can influence elevation of the groundwater table, thus creating a more wet landscape which becomes more resistance to wildfires and drought (Fairfax & Whittle, 2020).

The key to creating a resilient river corridor is through floodplain connectivity which can promote increases in surface water and groundwater stage across the landscape. Strategic small-scale wildfires are also beneficial to the river corridor. River restoration practitioners are beginning to use wildfires as a tool to promote river ecosystem biodiversity through patch mosaic burning in rivers with extensive floodplain connectivity (Pugh et al., 2022). By doing so, this allows natural processes, such as wildfires, to create biodiversity and restore natural ecosystem functions without decimating the landscape.

1.2 Low-tech Process-based Restoration

Process-based restoration aims to reestablish normative rates and magnitudes of physical, chemical, and biological processes that create and sustain river and surrounding floodplain ecosystems (Beechie et al., 2010). Low-tech process based restoration (LTPBR) utilizes minimally invasive techniques which don't require heavy machinery to restore the underlying processes (Wheaton et al., 2019). These processes include erosion and sediment transport, storage and routing of water, plant growth and successional processes, input of nutrients and thermal energy, and nutrient cycling in the aquatic food web (Beechie et al., 2010). By restoring these natural processes, this allows the riverscape to become more resilient to future disturbances (such as climate change, wildfires, etc.) through natural, physical, and biological adjustments, enabling the riverscape to evolve and continue to function (Beechie et al., 2010; Wohl et al., 2024). LTPBR does not look to create artificial and unnaturally static habitats but instead create a dynamic equilibrium that is driven by these natural processes (Beechie et al., 2010; Formann et al., 2014).

The application of process-based restoration varies site to site. It is important to note that not all LTPBR techniques are sensible for every site. A complete and thorough understanding of the geomorphology, hydrology, and biology and land use over time is crucial to applying the correct technique to a specific site (Castro & Thorne, 2019). In addition to a complete understanding of the river corridor, a clear understanding of the tradeoffs between ecological benefits of restoration practices and competing human demands for goods and services derived from rivers is also required (Beechie et al., 2010). LTPBR applications are intended to be primarily used in wadable streams, which include perennial, intermittent, and ephemerally flowing channels which are often found in the headwaters of stream network (Wheaton et al.,

2019). However, these same concepts can be applied to large river systems under the right circumstances.

LTPBR application often looks to reincorporate large woody material back into a riverscape as large wood is a crucial component to its physical processes (Wohl et al., 2019). Examples of LTPBR applications are Beaver Dam Analogs (BDAs) and Post-Assisted Log Structures (PALS). BDAs are channel-spanning structures with low permeability, a constant crest elevation, and constructed with a mixture of woody material and fill material to promote backwater and mimic a natural beaver dam (Wheaton et al., 2019). PALS are woody material of various sizes pinned together with untreated posts driven into the substrate to mimic natural wood accumulations (Wheaton et al., 2019). BDAs and PALS can take any shape and form depending on the structure location. The purpose of these structures is to add flow complexity, retain sediment, and enhance habitat along a river corridor while trying to mimic natural processes such as beaver dams and wood jams. When strategically placed, these structures can accelerate erosion/aggradation, create aquatic habitat for macroinvertebrates/fish, add roughness to create flow diversity and help reconnect floodplains, as well as facilitate in future wood recruitment and increase hyporheic exchange (Marshall et al., 2023).

LTPBR has become an increasingly popular tool used for river corridors affected by wildfire, specifically the sediment retention capacity both in the channel and on the floodplain (Scamardo et al., 2025). In order for LTPBR to be successful in a post-wildfire landscape, restoration projects requires restoring the physical structures of the river such as the input of large woody material which reduces stream velocities, initiates sediment deposition and enhances floodplain reconnection (Pugh et al., 2022). Several studies have quantified suspended sediment load in a river following a wildfire (Blake et al., 2009; Petticrew et al., 2006; Warrick et

al., 2012), but little is known about quantifying the total sediment retained within the channel influenced by LTPBR structures following a wildfire.

1.3 Modeling Groundwater and Surface Water Interactions

Surface water-groundwater interactions have been examined through various restoration projects and studies, but little is known about how to predict or model this process at a reach scale which can be used as a design tool in restoring riparian and wetland habitat within the river corridor (Kurth et al., 2015). Various methodologies have been developed to examine groundwater and surface water interactions through numerical modeling (Ntona et al., 2022). The majority of, if not all of these models couples a groundwater model with a hydrological model (Ntona et al., 2022). Examples of these hydrological models include the Soil and Water Assessment Tool (SWAT), MIKE SHE, GSFLOW, HydroGeoSphere, as well as others (Arnold et al., 1998; Brunner & Simmons, 2012; Graham & Butts, 2006; Markstrom et al., 2008). These models capture the surface water-groundwater interactions at large, watershed-size scales (Bailey et al., 2016; Hunt et al., 2013; Sahoo et al., 2006; Talebmorad & Ostad-Ali-Askari, 2022).

Waseem et al. (2020) attempted to capture these interactions using a coupled MIKE 11, a 1D hydrodynamic model, and MIKE SHE, a hydrological model that can simulate surface water and groundwater interactions within a catchment. However, this method was used to model a relatively large watershed area (400 km^2) while capturing hydrodynamic process caused by hydraulic structures within the river system (Waseem et al., 2020). Furman (2008) provides a review for coupling surface-subsurface flow processes providing an in-depth analysis of the governing equations. Specifically, that the governing equations used for large-scale modeling applications (i.e. watershed scale) are a reasonable approximation but may be less accurate in small-scale modeling applications such as reach scale (Furman, 2008).

The linked surface water-groundwater models that provide analysis over large watershed areas where hydraulic characteristics, such as inundation area and water depth are often not captured. These hydraulic characteristics can be used as a very useful design tool for restoration projects when creating wetland/riparian habitat based on location and depth to groundwater levels. The relationship between reach-scale hydraulics and groundwater levels is not well understood and is an active field of research (Lewandowski et al., 2020). This study aims to build on these modeling efforts by creating a reach scale model linking a fully hydrodynamic surface water model with a groundwater model to observe fluxes in both surface water and groundwater transient storage.

1.4 Research Objectives

Given the lack of understanding regarding the impact of LTPBR on sediment and groundwater storage following a wildfire, the research objectives of this study are to:

1) Analyze the impacts of low-tech, process-based restoration in an inactive beaver meadow on sediment storage within the channel and groundwater elevations throughout the floodplain.
2) Evaluate the relationships between groundwater transient storage and restoration implementation scenarios through numerical experiments.

2. METHODS

2.1 Background Information

This study focuses on a headwater stream impacted by the 2020 Cameron Peak Fire in northern Colorado. Elkhorn Creek is a perennial, second-order, headwater stream of the Cache la Poudre River, located near Red Feather Lakes, CO. Elkhorn Creek has a drainage area of approximately 4.5 km^2 upstream of the study site, a mean annual precipitation of approximately 61 cm, and an average stream gradient of approximately 3% through the project site. Elkhorn Creek once had a healthy and active beaver population occupying the majority of the watershed resulting in relic beaver dams and the deposition of fine sediment creating a low gradient beaver meadow (Figure 1). Beaver ponds at the study site can be seen as recently as 2013 via Google Earth imagery. The width of the active channel varies between 2 and 4 meters throughout the study site. Prior to restoration, channel incision occurred caused by the breaching of relic beaver dams, resulting in a disconnected floodplain and an increased rate in sediment transport during high flow events such as annual snowmelt runoff.

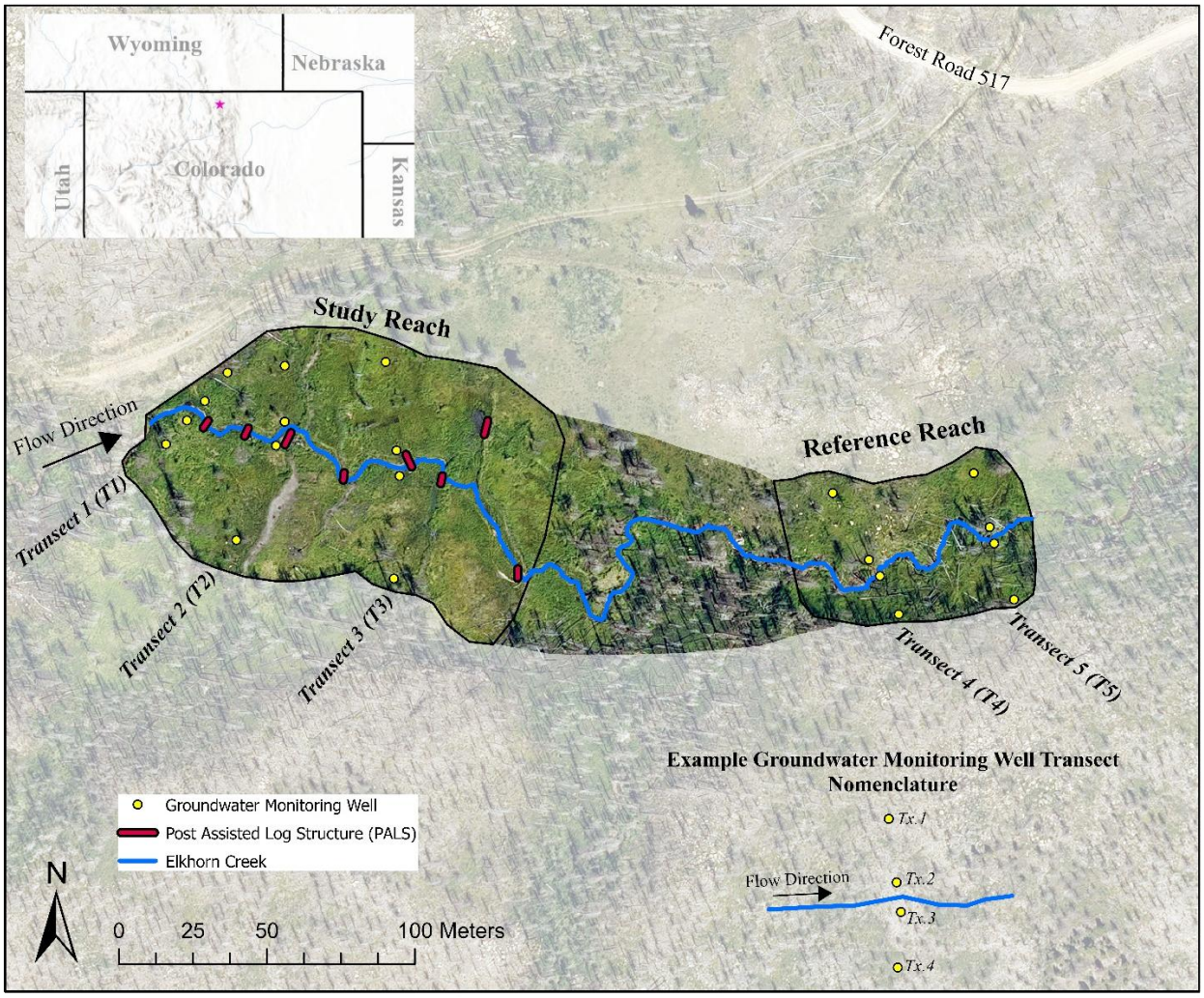

Figure 1. Map of Elkhorn Creek Study Site and Groundwater Monitoring Transects Nomenclature

Cameron Peak Fire restoration efforts, led by the Coalition for the Poudre River Watershed (CPRW) and Ayres Associates, were conducted at Elkhorn Creek to increase sediment deposition and reconnect the channel to the floodplain. LTPBR methods were applied through the installation of Post-Assisted Log Structures (PALS). PALS are hand-built structures meant to mimic and promote the processes of wood accumulation yet are still permeable temporary structures (Wheaton et al., 2019). A total of 8 PALS were installed throughout the study reach (Figure 1). PALS were constructed by a volunteer group using untreated wooden fence posts, introduced to the site, as well as woody material found on site (Figure 2). The fence posts were

driven into the stream bed using a sledgehammer and/or a gas-powered fence post driver. The fence posts were used to secure the woody material within the channel. A total of approximately 131 m of stream length resided in the restoration reach while an additional PALS was constructed in a secondary channel (Figure 1) to restore valley-wide dam structures and add more roughness in the floodplain.

Figure 2. Example of a Constructed PALS at Elkhorn Creek Study Site

2.2 Field Data Collection

Various field data collection methods were conducted over a 1-year time period to observe the study site following the installation of the PALS in the fall of 2022. These methods included Wolman pebble counts (Wolman, 1954), sediment probing within the channel, installation of groundwater monitoring wells, and survey of the site.

2.2.1 Topography

Airborne lidar data at approximately 0.3 m resolution collected by Ayres Associates Inc. in October 2023 was used in this project for numerical model creation. Lidar data were used to create a digital elevation model (DEM). The surface data were supplemented by survey data collected using an Emlid Reach RS2+ real time kinetic (RTK) positioning and global navigation satellite (GNSS) demonstrating centimeter accuracy (Emlid, 2025; Fencl, 2020; Nathan, 2024). Surveys included a bathymetric survey of the stream channel, groundwater well cap elevation measurements, a cross-sectional survey where stream discharge was collected, and water surface elevations during high flows. For numerical modeling, stream bathymetry was included within the DEM to account for channel morphology and water surface elevations during high slows were used for model calibration.

A total of four survey control points were installed throughout the study site using onsite features and rebar. During each survey of the site, three of these points were resurveyed to account for fluctuations in the Emlid Reach RS2+ while one control point was used for the Emlid Reach RS2+ Base Station. The location of the base station remained constant for all surveys. These survey points were used to correct each survey of the site to ensure each survey was relatively accurate to one another.

2.2.2 Sediment Size and Storage

To monitor the changes in sediment storage and size distribution at the project site, a combination of data collection methods was used. First, Wolman pebble counts were collected upstream and downstream of each in-channel PALS in the project reach to determine a relative baseline sediment size and distribution throughout the project reach. Pebble counts were repeated

at the same locations on September 25, 2022 (pre-construction) and August 3, 2023 (post-construction). During the initial pebble count, not all PALS were constructed. If the PALS were not constructed, pebble counts were taken in the channel at the proposed PALS location. However, for the purpose of this study, the pebble count surveys conducted on September 25, 2022, will be referred to as “pre-construction”.

Sediment probing was conducted on September 17, 2023, approximately one-year post-restoration to determine the amount of sediment captured within the channel. Sediment probing began 15 m upstream of the most upstream PALS and ended at the most downstream PALS within the study reach. The study reach was divided into seven sub-reaches for the sediment probing. Each sub-reach was directly upstream of a PALS. For example, the sub-reach titled PALS 2 was taken directly upstream of PALS 2 and extended upstream to directly downstream of PALS 1. Refer to Figure 3 for locations of sediment probing reaches. Sediment was probed at 1 m increments along each sub-reach. At each increment, three sediment probing measurements were taken at the cross-section. One at 25% of the channel width, one at 50% of the channel width, and one at 75% of the channel width. The stream width at each cross section was also recorded. Due to the coarse stream bed material prior to PALS implementation, sediment was probed depth-to-refusal assuming all the finer sediment is newly captured sediment post-construction.

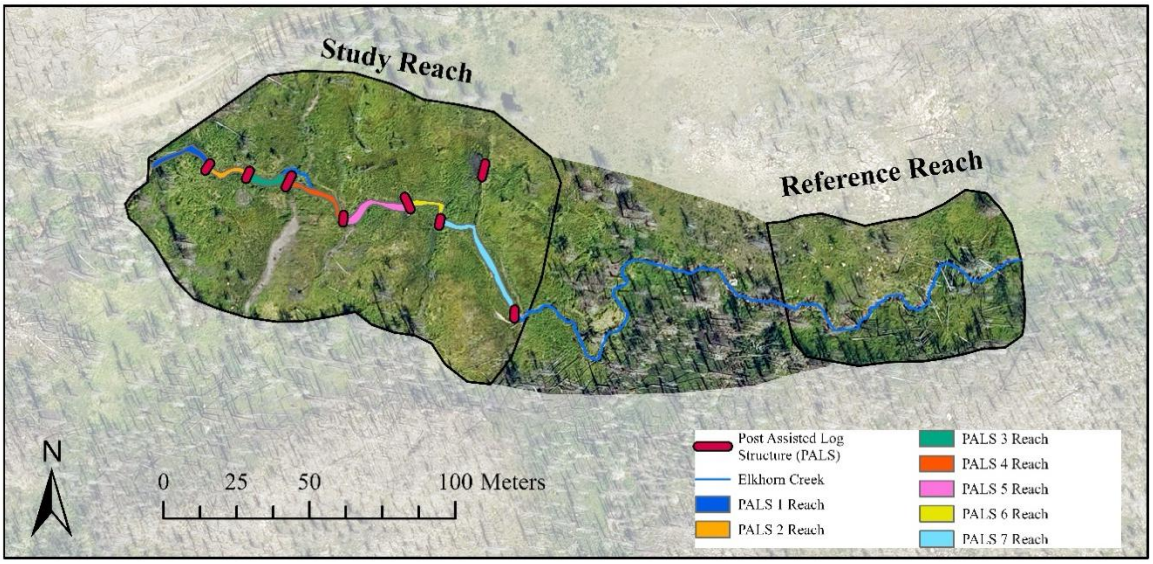

Figure 3. Sediment Probing Reaches

2.2.3 Groundwater Data

Groundwater monitoring well transects were installed to collect a time series of groundwater elevations, specifically during the receding limb of the hydrograph, as well as calibration data to create a numerical groundwater model. Groundwater data collection began on October 10, 2022, and ended on October 25, 2023, totaling 380 days.

Groundwater monitoring wells were perforated polyvinyl chloride (PVC) cylinders with a drive point that totaled approximately 122 cm in length. These wells were driven by hand into the ground, and all intersected the water table when installed. Fine sediment from the groundwater monitoring wells were removed using bailers throughout the study period. Groundwater monitoring wells were installed at five transects (Figure 1). Each transect consisted of four groundwater wells, two near the stream channel and two further into the floodplain. The transects were named T1 though T5. T1 is the most upstream transect while T5 is the most downstream. The wells were named Tx.x. For example, the furthest well on the stream left side

of the most upstream transect was named T1.1 and the furthest well on the stream right side of the most upstream transect was named T1.4. Three transects (T1-T3) were located in the study reach, while two transects (T4-T5) were located downstream in a reference reach. Refer to Figure 1 for a visual depiction of the groundwater well transects nomenclature. Initially, only ten groundwater monitoring wells were installed in the floodplain approximately two to four meters from the channel on October 10, 2022 (e.g., Tx.2 and Tx.3). On June 14, 2023, an additional ten groundwater monitoring wells (Tx.1 and Tx.4) were installed extending further into the floodplain. These groundwater monitoring wells were placed at the furthest location on the floodplain that would still intersect the water table. This was determined in the field identifying depressional areas in the floodplain while still horizontally aligned perpendicular to the channel with each respective transect. Figure 1 shows the location of each groundwater monitoring well in both the study reach and the reference reach.

Each groundwater monitoring well contained an Onset HOBO water level logger (U20L) to track groundwater levels in the well. The water level loggers collected hydrostatic pressure and temperature measurements every fifteen minutes. These data, along with survey data of the groundwater monitoring well caps, were used to estimate groundwater elevations at each well throughout the time period.

2.2.4 Stream Discharge

Stream discharge was measured at the upstream boundary of the study site using a SonTek FlowTracker accompanied by a staff gage. Stream discharge data were used to inform the hydrodynamic model runs. The observed baseflow discharge onsite was 0.11 m^3/s while the largest discharge recorded at the site was 0.57 m^3/s. In-stream pressure transducers (HOBO U20L; same as the loggers in groundwater wells) were installed at the upstream boundary of the

study reach and in the reference reach. The pressure transducers collected hydrostatic pressure and temperature at fifteen-minute intervals and were used to estimate stream stage. Stream stage data were used to inform the groundwater model runs. The goal was to develop a rating curve for Elkhorn Creek but due to unexpected sediment deposition at the staff gage and upstream pressure transducer during snowmelt runoff, the data were insufficient to develop a rating curve.

2.3 Numerical Modeling

This study focuses on using a hydrodynamic model and a groundwater model to predict the surface water-groundwater interactions through varying restoration scenarios at a reach scale (Figure 4). A total of five theoretical restoration scenarios were determined which varied the location and number of PALS installed throughout the study reach for this assessment. For each restoration scenario, a total of three discharges were modeled based on measured discharges at the site. First, a hydrodynamic model using Sedimentation and River Hydraulics – Two-Dimension (SRH-2D) in Aquaveo Surface-water Modeling System (SMS) was developed for the study site to observe water surface behavior, such as depth of water and inundation extent, between restoration scenarios and discharges (Lai, 2020; Aquaveo, 2024). PALS were included within the SRH-2D model at select locations dependent upon restoration scenario. The surface water inundation extent and water depth were exported from SMS for each model run. Next, a groundwater model using MODFLOW-NWT in ModelMuse was developed to observe how the surface water modeled in SRH-2D impacted the groundwater table. The SRH-2D results were imported into the River Package within MODFLOW to simulate surface water for each of the SRH-2D model runs. This process is depicted in Figure 4.

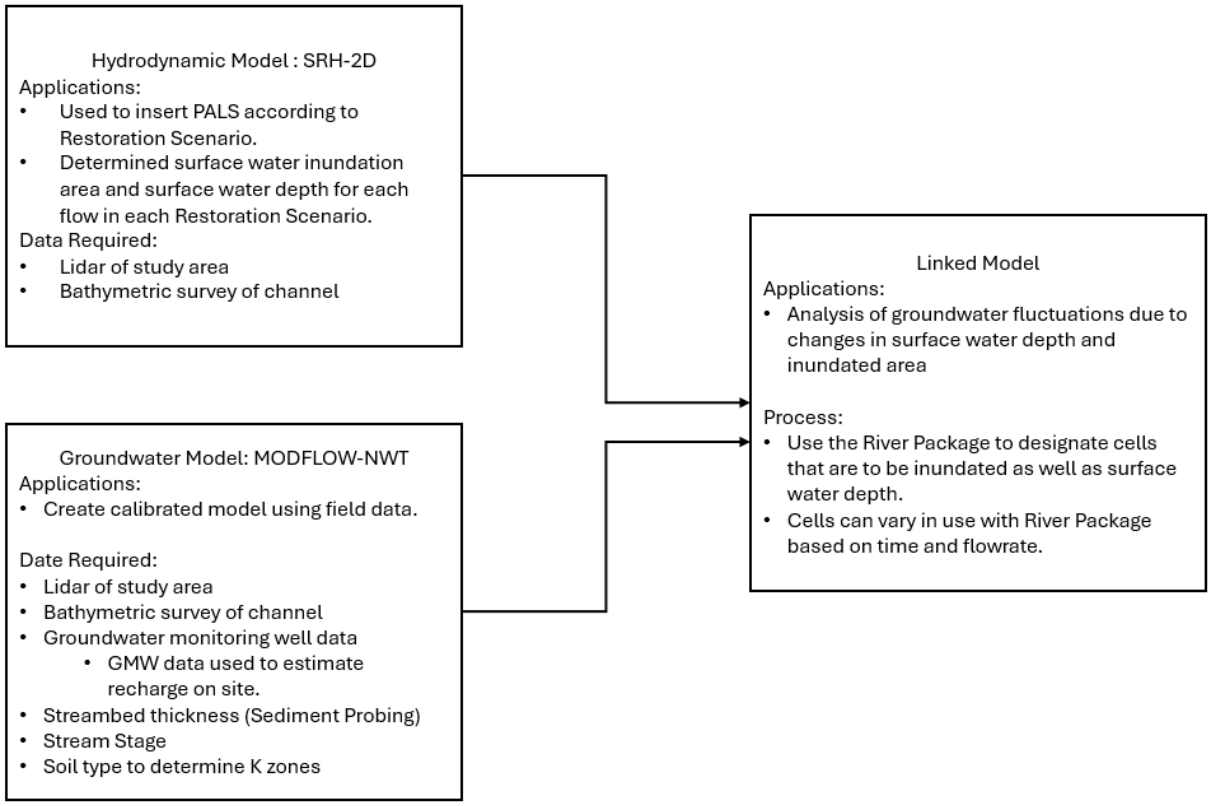

Figure 4. Hydrodynamic-Groundwater Linked Model Flow Chart

2.3.1 Hydrodynamic Modeling

Water depths and inundation boundaries were simulated for the entire study site using two-dimensional hydrodynamic modeling for 3 different discharges: 0.11 m^3/s, 0.34 m^3/s, and 0.57 m^3/s. The baseflow (0.11 m^3/s) and high flow (0.57 m^3/s) were observed at the study through discharge measurements while 0.34 m^3/s was included as an intermediate flowrate. During the high flow scenario, the floodplain is connected, and Elkhorn Creek is generally out of its banks. SRH-2D was chosen to model the water surface elevations for its ability to easily represent the PALS as porous obstructions. The hydrodynamic model geometry was developed using a stream bathymetry RTK survey and a lidar derived DEM for the floodplain topography. These datasets were merged by masking the lidar DEM in the baseflow channel where the data

are not valid and instead using the RTK survey to represent the channel morphology (Christensen et al., 2024). The roughness for the channel was estimated to be 0.118 based on Jarrett's equation (Jarrett, 1984) and the floodplain roughness was determined to be 0.2 due to the high variation in topography, steep slope, and grass-shrub vegetation. Each PALS was represented as a 0.9 m tall, 2.1 m long "obstruction" object with a drag coefficient C_d= 1, as determined for leafless shrubby emergent vegetation (Wunder et al., 2011). Porosity of the PALS were determined via calibration. Each model run utilized a steady inflow and was computed until steady state was reached with <1% change in inundation extent throughout the model in successive model outputs. The key output from the hydrodynamic model (inundation extent and water depth) was then exported as a shapefile and a raster at the final timestep for use in the groundwater model.

2.3.2 Groundwater Modeling

MODFLOW-NWT is a Newton-Raphson formulation variation of MODFLOW-2005 that is used for an improved solution involving unconfined aquifers and surface-water/groundwater interactions (Niswonger et al., 2011). MODFLOW-NWT uses the upstream-weighting (UPW) function as opposed to Picard method, which is the only method available in MODFLOW-2005, to solve nonlinear equations which occur when representing unconfined aquifers and nonlinear boundary conditions (Niswonger et al., 2011).

The model was set up using daily time steps resulting in 380 days, the timespan in which data were collected. The model area was approximately 33,700 m^2. The model consisted of 29,110 cells. The dimensions of each cell was 1.524 m. x 1.524 m. in size. The model contains two layers to account for vertical flow of water to an undefined aquifer location subsurface. The top layer was 1.524 m thick and the bottom layer was 3.048 m thick in the model. The bottom

layer represented a depth to a deeper aquifer into which groundwater could flow. MODFLOW packages used to represent certain processes can be found in Table 1.

The topographical model surface was developed using the same method used for the hydrodynamic model. Initial conditions of groundwater elevation were defined as 1.22 m below the model surface, due to the shallow groundwater table observed on site. The majority of groundwater monitoring wells onsite consistently observed groundwater elevation within 1.22 m below the ground surface inferring a reasonable assumption for initial conditions.

The River (RIV) Package was used to represent stream flow and conductance between the river and surrounding groundwater table. The RIV package is applied to certain cells within the model, and these cells can be selected by using a polygon object. The stage values used within the RIV Package were determined via an in-stream pressure transducer upstream of the study site as well as another in-stream pressure transducer located at the PALS 3 transect. Stream stage data were initially collected from a pressure transducer upstream of the study reach. However, sediment retention within the channel resulted in periods of inaccurate stream stage data collected from the pressure transducer. Due to sediment deposition, a portion of the channel avulsed causing the channel to intersect a groundwater monitoring well (T2.3) placed near the stream. Fortunately, there is an overlap of time-series data between the upstream pressure transducer and the in-stream groundwater well in which a continuous time-series estimate of stream stage was determined.

Conductance within the RIV package was calculated by dividing the vertical hydraulic conductivity (K_z) by the “DrainSedimentThickness” parameter. The “DrainSedimentThickness” represents the thickness of the stream bed and was estimated to be approximately 0.30 m via sediment probing at Elkhorn Creek. This value was used for the entire reach.

The Recharge (RCH) Package was used to represent recharge for the entire study area. Because the study area is relatively small, recharge values were the same for all cells in the model. Due to the remote location and size of the study site, hydrological data were unavailable at the site. Therefore, the water-table fluctuation method using the time-series of groundwater well data was used to estimate the recharge at the site. The water-table fluctuation method assumes that the change in groundwater elevation is an indicator of recharge across the water table, shown as:

$$R = SY * \Delta Z$$

Where R is recharge, SY is the specific yield of the aquifer, and ΔZ is the change in groundwater elevation.

The water-table fluctuation method is only valid for a singular "storm event", thus each storm event was identified via spikes in the groundwater monitoring well data for each well throughout the time period. Recharge was then determined for each storm event for each groundwater well using a standard specific yield value of 0.25, which is common for unconfined aquifer (*UNSW Connected Waters Initiative*, 2017). Snowmelt runoff was not included in recharge and was represented through stream stage via the RIV package. To accurately estimate recharge over the entire site, the recharge rate was calculated via the water-table fluctuation for each groundwater monitoring well throughout the observation time period. These recharge values were then averaged across the study site and converted to a daily recharge to be inserted into the groundwater model.

Table 1. Description of Each MODFLOW Package Used

MODFLOW Package	Purpose	Use in Model
Upstream Weighting Package (UPW)	To solve nonlinear equations which occur when representing unconfined aquifers and nonlinear boundary conditions (Niswonger et al., 2011)	Used to apply horizontal and vertical hydraulic conductivity values to the model as well as specific yield.
Time-Variant Specified-Head Package (CHD)	To simulate specified head boundaries that vary within or between stress periods (Harbaugh, 2005)	Used to set inflow and outflow boundary conditions at constant groundwater elevations.
River (RIV)	To simulate surface water as head-dependent flux boundaries (Harbaugh, 2005)	Used to simulate surface water and conductance between the surface water and the groundwater table.
Recharge (RCH)	To simulate a specified flux distribution over the top of the model (Harbaugh, 2005)	Used to represent recharge to the groundwater system ONLY in the base model.
Newton Solver (NWT)	To solve the finite difference equations in each step of the MODFLOW-NWT stress period (Niswonger et al., 2011)	Used to determine groundwater flow processes.
Head Observation Package (HOB)	To specify observations of head for use in the Observation Process (Hill et al., 2000)	Used in PEST to compare modeled groundwater elevations to observed groundwater elevations.

The Time-Variant Specified Head (CHD) Package was used to set the upstream and downstream boundary conditions for the model. The upstream constant groundwater elevation was set to 2712.7 m. The downstream constant groundwater elevation was set to 2693.5 m. These values were derived from the stream surface of the lidar flown and were used to moderate flow into and out of the system. These values were kept constant throughout the entire duration of the model, assuming the boundary conditions were far away from the study area.

The Head Observation (HOB) package was used to input the observed time series of groundwater elevation data, collected at each well, used for model calibration. The groundwater elevation observations used to calibrate the model were collected at 15-minute intervals. Because

the model uses a daily time interval, the average groundwater elevation for each day was used in the model calibration. This accounted for the quick storm events producing fast rising and receding water table observations as well as stream stage observations.

Within the Upstream Weighting (UPW) package, hydraulic conductivity, specific yield, and horizontal anisotropy can be defined. Hydraulic conductivity regions were determined using soil type, derived from using the Web Soil Survey tool (Soil Survey Staff, 2024). This resulted in five regions that varied in hydraulic conductivity values. These regions were used for both horizontal hydraulic conductivity as well as vertical hydraulic conductivity. Additionally, a separate hydraulic conductivity zone was applied to the Elkhorn Creek riverbed in both horizontal and vertical directions. Specific yield and horizontal anisotropy were applied as a singular value to the entire model area.

2.3.3 Model Calibration

2.3.3.1 Hydrodynamic Model Calibration

The surface water model was calibrated by adjusting the porosity of the simulated obstructions to match the observed water surface elevations. WSE was surveyed throughout the site using an RTK while a flow measurement was taken. This flow was simulated in the hydrodynamic model and then compared with the observed WSE (Christensen et al., 2024). The porosity of the obstructions then adjusted from 0.20 to 0.90 to minimize the Root Mean Square Error (RMSE) between the observed and modeled WSE. This porosity was then applied to create the additional scenarios with varying PALS quantities and positioning for each of the simplified hydrograph flows.

2.3.3.2 Groundwater Model Calibration

Parameter Estimation (PEST) is a model-independent parameter estimation and uncertainty analysis software used for automatic calibration of various models (Doherty, 2015). PEST can be applied within ModelMuse to the MODFLOW-NWT model. Parameters included in PEST cover a range of soil characteristic parameters such as horizontal and vertical hydraulic conductivity, riverbed conductivity, specific yield, and horizontal anisotropy. A total of 14 calibration parameters were varied based on soil characteristic zone. Observed groundwater elevations were inserted into the model using the HOB package as comparison to modeled groundwater elevation. These calibration parameters were used by PEST to minimize the RMSE at the groundwater elevation locations used in the HOB package.

2.3.4 Linking of SRH-2D and MODFLOW-NWT

To examine the varying surface water impacts on the groundwater system, five restoration scenario models were created in MODFLOW-NWT. The restoration scenario models include the calibrated parameters from the calibrated hydrodynamic model and groundwater model. Recharge was excluded from the model runs as only surface water interactions were being examined. A simplified hydrograph over a given calendar year, with flowrates of 0.11 m^3/s (base flow), 0.34 m^3/s (intermediate flow), and 0.57 m^3/s (high flow), were used to estimate how the different restoration scenarios would affect the groundwater elevation throughout a year. The details of the simplified hydrograph and model time controls are shown in Table 2.

Table 2. Restoration Scenario Model Time and Flowrate Control

Start Day	End Day	Flowrate (m^3/s)
0	80	0.11
80	130	0.34
130	180	0.57
180	200	0.34
200	365	0.11

Shapefiles were created from the inundation area for each flowrate, determined by the hydrodynamic model. These shapefiles represent the area containing surface water. Each flow rate for each scenario created a different inundated area. The shapefiles were imported into ModelMuse as objects, for its respective scenario. The River Package was then applied to each object for each flowrate for all scenarios. Water depth rasters were exported from the hydrodynamic model, indicating the water stage in each cell for the various restoration scenarios and flowrates. The water depth rasters were applied to the inundation area shapefiles within the River Package as the stage to represent active surface water in the respected cell. The other components of the River Package remain the same as the calibrated groundwater model.

2.3.5 Restoration Scenarios

Five restoration scenarios were used to assess the effectiveness of PALS as a restoration tool in relation to groundwater transient storage (Table 3). Restoration Scenario (RS) 1 is the site without any restoration implementation; therefore, no PALS were installed. RS 2 has PALS only at locations along Elkhorn Creek where a relic beaver dam historically intersected the channel. Relic beaver dams were identified using a combination of aerial imagery, field reconnaissance, and DEM (Refer to Figure C-1 in Appendix C for map of existing beaver dams). RS 3 is the existing conditions implemented by CPRW and Ayres Associates Inc. including PALS installed in RS 2 as well as additional PALS installed throughout the stream reach. RS 4 includes PALS

installed in RS 3 as well as 5 additional PALS installed within the project reach. RS 5 includes PALS installed every ~5m throughout the study reach. RS 4 and RS 5 were included to assess how increased restoration scenario intensity, than what was observed onsite (RS 3) affects both the surface water and groundwater table. Refer to Appendix C for maps of PALS locations for each restoration scenario. For each scenario, three different flowrates were tested. The first flowrate represents observed baseflow at Elkhorn Creek of 0.11 m^3/s. The next flowrate is an intermediate flow of 0.34 m^3/s. The final flowrate represents the highest flow observed at Elkhorn Creek of 0.57 m^3/s.

Table 3. Restoration Scenarios

Restoration Scenario	Number of PALS	Description
Restoration Scenario 1	0	Pre-Restoration Conditions
Restoration Scenario 2	5	PALS only where historical beaver dams intersected Elkhorn Creek
Restoration Scenario 3	9	Existing Restoration Scenario Implemented by CPRW and Ayres Associates
Restoration Scenario 4	14	Additional PALS to Restoration Scenario 3
Restoration Scenario 5	30	PALS installed every ~5 m.

3 RESULTS

3.1 Stream Stage

A rating curve was not developed due to sediment aggradation at the upstream cross section where streamflow data were being recorded. However, stream stage data were captured over the study period between two locations. The pressure transducer in the upstream cross section collected stage data from October 10, 2022, until May 7, 2023. On approximately May 7, 2023, sediment aggradation occurred, and the pressure transducer was buried. Fortunately, due to sediment aggradation in the channel, the channel avulsed thus intercepting a groundwater monitoring well (T2.2). This allowed the stage time series to be continuous throughout the study period. Groundwater monitoring well T2.2 was used from May 7, 2023, to October 25, 2023, to capture stream stage data. This continues time-series can be viewed in Figure 5 to observe temporal patterns of stream stage throughout the study period. Stream stage peaked between April 13, 2023, and June 26, 2023, due to snowmelt runoff and seasonal summer thunderstorms.

Due to project and time constraints, stream stage data were not collected prior to implementation. However, major morphological changes to the study site, such as sediment aggradation, did not occur until the snowmelt runoff season, allowing for a relative pre-runoff baseflow condition to be established prior to sediment aggradation. The relative baseflow period was determined to occur between November 1, 2022, through April 1, 2023. This was determined through analyzing the steam stage and groundwater elevation results and identifying a “baseflow” period before snowmelt runoff. Next, a post-runoff relative baseflow period was identified to compare the results to the pre-runoff relative baseflow period to quantify stream stage differences. The post-runoff baseflow period was determined to occur from August 1, 2023, to October 25, 2023, and was determined using the same method as the pre-runoff baseflow

period. Figure 5 shows a decrease in stream stage of 0.08 m between the two baseline periods. It is important to note that Figure 5 was created using two different sensors at different locations as explained previously.

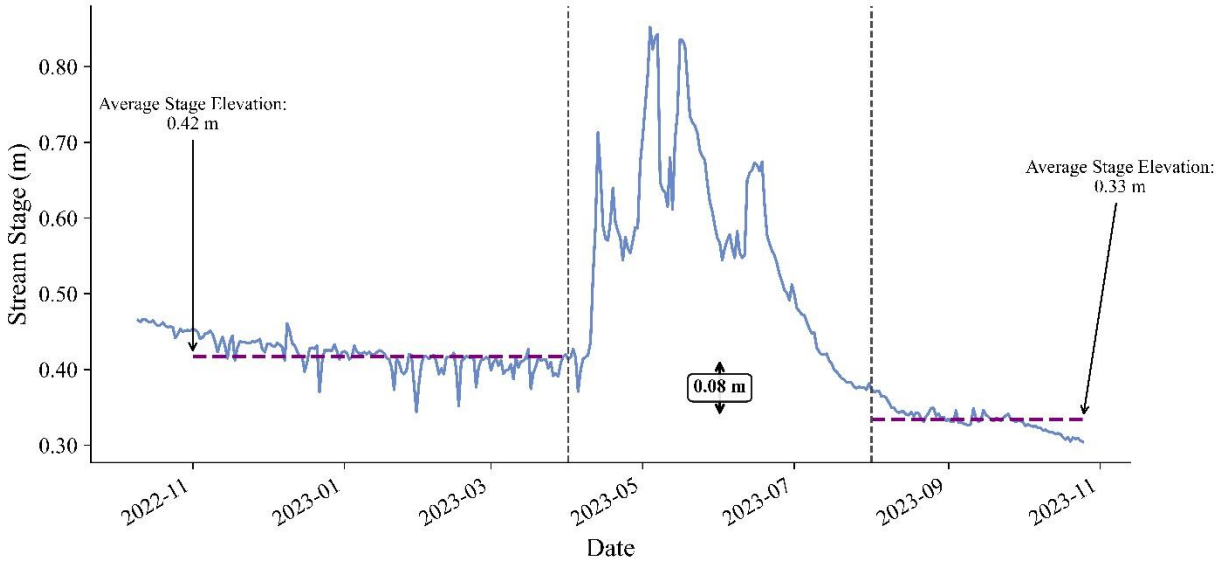

Figure 5. Stream Stage Observations. Average stage elevation showed a decrease of 0.08 m between the pre-runoff baseflow period and the post-runoff baseflow period as indicated by the vertical dotted lines.

3.2 Sediment Size and Storage

Pebble count analysis consistently showed a decrease in D_{50} both upstream and downstream of the PALS when comparing pre-construction sediment size data to post-construction sediment size data (Figure 6). Sediment transported to the study reach was finer in grain size than what was initially surveyed with an average D_{50} of 15.4 mm pre-installation to an average D_{50} of 3.70 mm post-installation (Figure 6). The "pre-construction" pebble count occurred during construction of some of the upstream PALS. This caused an increase of fine sediment upstream of the PALS, specifically PALS 3 and PALS 4 (Figure 6). For additional grain size distribution data from pebble counts, refer to Appendix E.

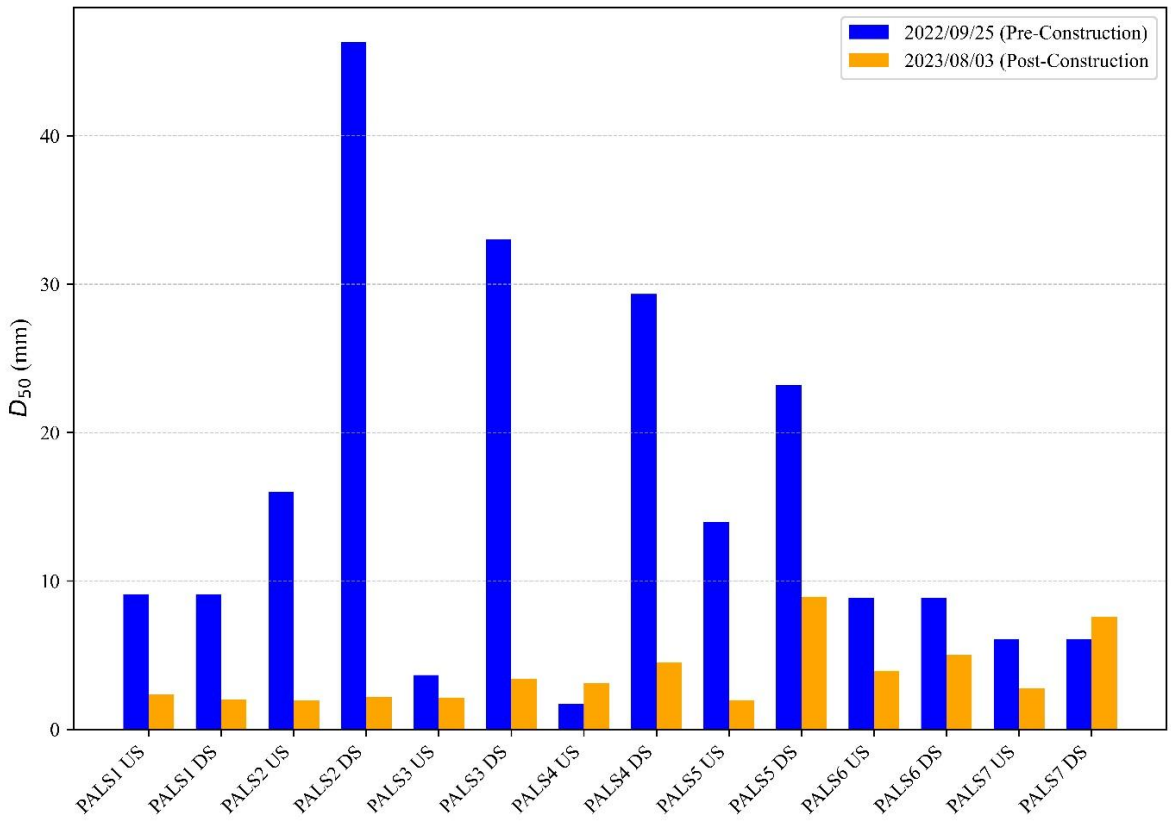

Figure 6. Comparison of D_{50} Grain Size Pre- and Post-Construction at Each PALS

Sediment probing estimated a volume of approximately 63 m^3 deposited in the stream channel. There was an average depth of 0.30 m of sediment deposited throughout the study reach. Sediment volumes for each sediment probing reach ranged from 1.37 m^3 for the PALS 6 reach to 21.6 m^3 for the PALS 7 reach (Figure 7A). However, the length of each sediment probing survey reach varies (Figure 3) so sediment volume values for each reach could be impacted by the length of the reach. Due to the extent of sediment deposited upstream of PALS 1 and the extent of the sediment probing survey, the sediment aggradation associated with PALS 1 could be an underestimate of the sediment aggradation that occurred.

To account for reach lengths, the values were normalized by dividing the total aggradation per sediment probing reach by the length of stream surveyed (Figure 7B). Normalized sediment aggradation for each sediment probing reach ranged from 0.09 m^3/m for the PALS 5 reach to 1.00 m^3/m for the PALS 2 reach. Sediment retained in PALS 7 was greatly reduced when normalizing, however it is still greater than PALS 4-6. Figure 7B depicts the general downstream decreasing trend in sediment aggradation.

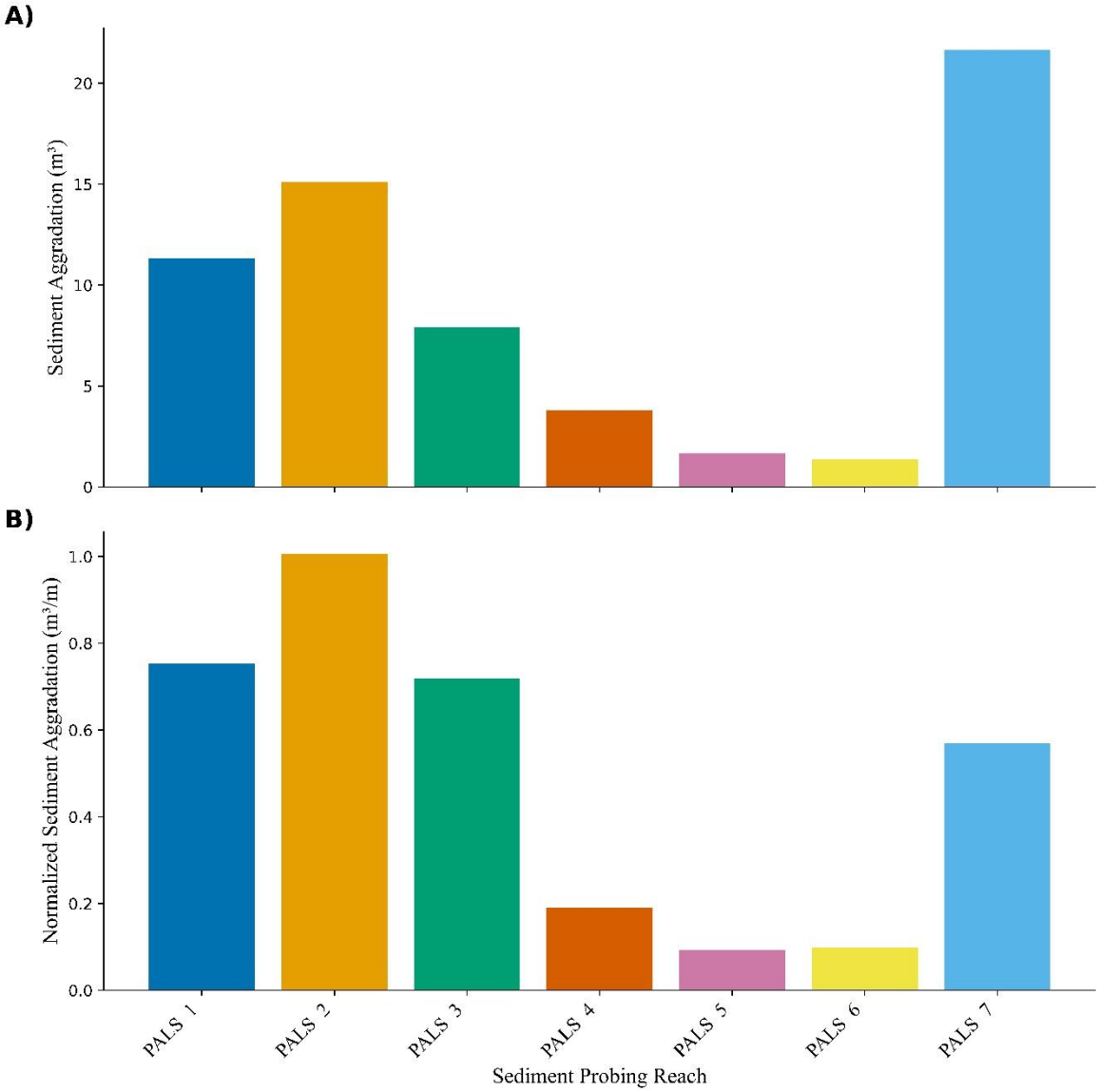

Figure 7. Normalized In-channel Sediment Distribution

3.3 Groundwater Observations

Due to project and time constraints, groundwater elevation data was not collected prior to implementation. However, major changes to the study site, such as sediment aggradation did not occur until during the snowmelt runoff season, allowing for a relative pre-runoff baseflow condition to be established prior to sediment aggradation. The relative baseflow periods was determined using the same method as stream stage described in Section 3.1. During the initial baseflow period (pre-snowmelt runoff), only groundwater monitoring wells near the stream (Tx.2 and Tx.3) were installed.

Groundwater elevation differences between the pre-snowmelt runoff and post-snowmelt runoff ranged from -0.02 m of difference in Transect 5 (indicating a decrease in groundwater elevation), which is located in the reference reach, to 0.32 m at Transect 2, in the study reach (Table 5). Elkhorn Creek avulsed at Transect 2 and intercepted groundwater monitoring well T2.2, which is the reason only T2.3 is shown in Figure 9. Transect 1 experienced an increase in relative baseflow groundwater elevation of 0.24 m and 0.23 m following the snowmelt runoff high flows indicating a higher water table (Figure 8). Transect 5 in the reference reach (Figure 10) depicts little to no change in groundwater elevation during baseflow.

Table 4. Groundwater Elevation Difference for Each Groundwater Monitoring Well

Groundwater Monitoring Well	Groundwater Elevation Difference (m)
T1.2	0.24
T1.3	0.23
T2.3	0.32
T3.2	0.15
T3.3	0.13
T4.2	0.17
T4.3	0.05
T5.2	-0.02
T5.3	0.02

The data collected represents approximately one year of data, therefore the increase in groundwater elevation in the reference reach could be a result of a wetter hydrological year. The 2023 hydrological year had approximately 27.7 additional centimeters of total liquid content than the 2022 hydrological year. See Appendix G for yearly precipitation data during the study duration provided by the National Oceanic and Atmospheric Administration (NOAA).

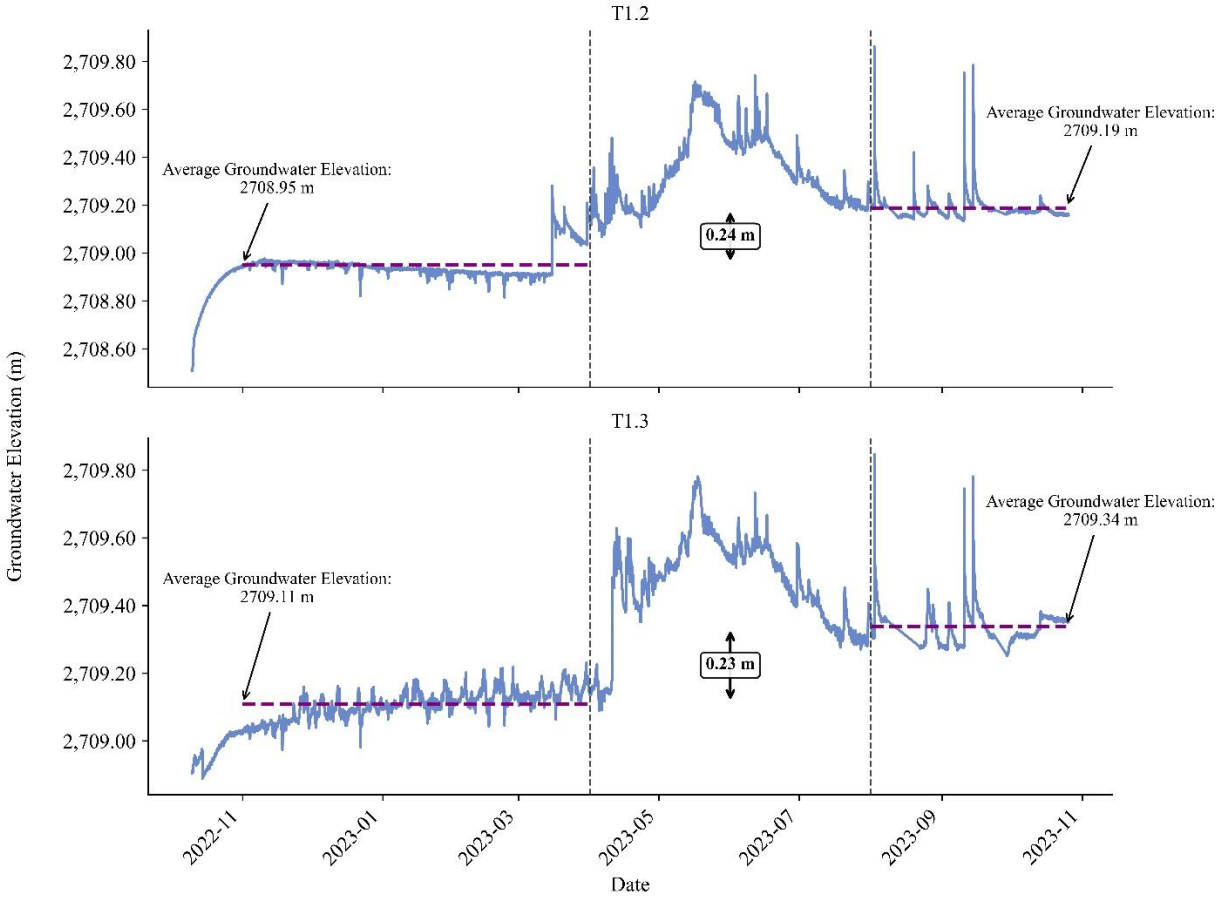

Figure 8. Transect 1 Groundwater Elevation Time Series. Average groundwater elevation showed an increase of 0.24 m (T1.2) and 0.23 m (T1.3) between the pre-runoff baseflow period and the post-runoff baseflow period as indicated by the vertical dotted lines.

The greater increase in groundwater elevation for transects located in the study reach when compared to the reference reach is true for all groundwater monitoring well transects. Refer to Table 5 for groundwater elevation difference values for each transect and Appendix D for additional figures.

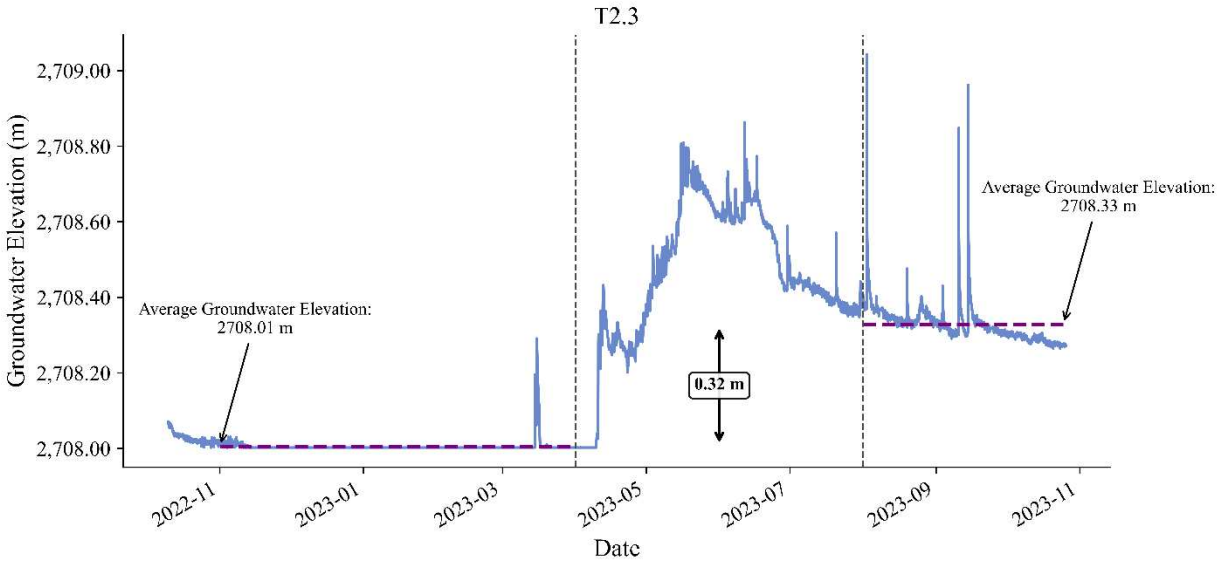

Figure 9. Transect 2 Groundwater Elevation Time Series. Average groundwater elevation showed an increase of 0.32 m at T2.3 between the pre-runoff baseflow period and the post-runoff baseflow period as indicated by the vertical dotted lines.

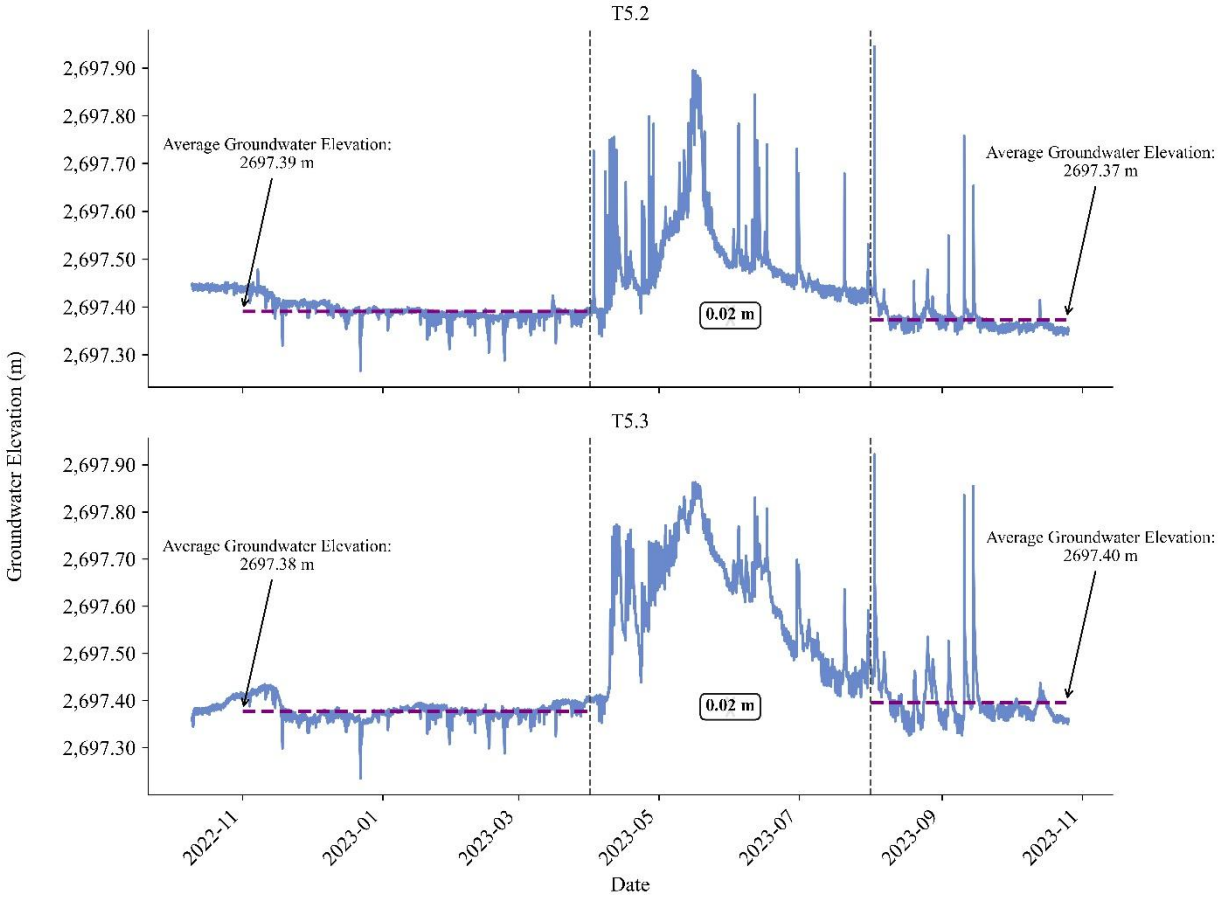

Figure 10. Transect 5 Groundwater Elevation Time Series. Average groundwater elevation showed a decrease of 0.02 m (T5.2) and an increase of 0.02 m (T5.3) between the pre-runoff baseflow period and the post-runoff baseflow period as indicated by the vertical dotted lines.

3.4 Numerical Modeling

3.4.1 Calibration Metrics

Model calibration for the hydrodynamic model consisted of determining porosity of the PALS through known discharges and WSE. Calibration of the obstruction porosity yielded a porosity value of 0.4 or 40%. Using a porosity of 0.4, a root mean square error of 0.14 m occurred between the modeled and observed WSE (Figure 11). This calibrated model effectively predicted the water surface elevation at the calibrated flow with an NSE of 0.997.

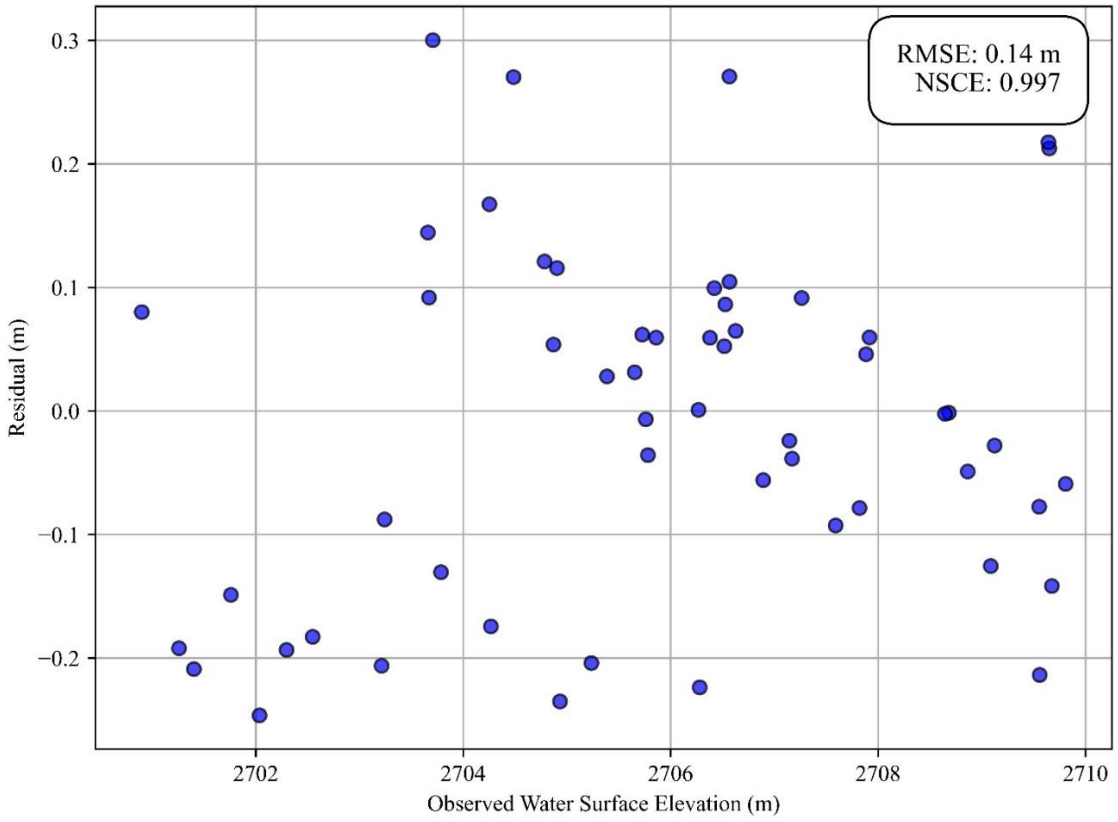

Figure 11. Model Residual Across the Site for the Hydrodynamic Model

Model calibration of the groundwater model consisted of utilizing PEST to minimize the RMSE for 14 calibration parameters including horizontal and vertical conductivity, riverbed

conductivity, specific yield, and horizontal anisotropy. These values were calibrated for varying zones within the model boundary that were determined based on soil characteristics. Table 5 contains the 14 calibration parameters for the varying zones and their calibrated values.

Table 5. Groundwater Model Calibrated Parameters

Parameter	Description	Calibrated Value	Units
LeftK	Horizontal Hydraulic Conductivity	61.3	m/day
LeftK_Vert	Vertical Hydraulic Conductivity	6.1	m/day
UpperK	Horizontal Hydraulic Conductivity	59.2	m/day
UpperK_Ver	Vertical Hydraulic Conductivity	6.1	m/day
MainK_Up	Horizontal Hydraulic Conductivity	135.2	m/day
MainK_Up_V	Vertical Hydraulic Conductivity	6.1	m/day
MainK_Low	Horizontal Hydraulic Conductivity	169.6	m/day
MainK_Lo_V	Vertical Hydraulic Conductivity	6.1	m/day
RightK	Horizontal Hydraulic Conductivity	61.0	m/day
RightK_V	Vertical Hydraulic Conductivity	6.1	m/day
SY	Specific Yield	0.32	-
HANI	Horizontal Anisotropy	0.71	-
RBK	Riverbed Horizontal Hydraulic Conductivity	73.6	m/day
RBK_Vert	Riverbed Vertical Hydraulic Conductivity	6.1	m/day

To evaluate the performance of the calibrated groundwater model, three different statistical analyses were completed. The first is using all model and observation values. The next was eliminating model values that produced a residual of more than 30.48 m, which was determined to be a completely unrealistic value. These spikes are unrealistic and can be attributed to an overestimate of recharge into the system. These spikes only accounted for 0.22% of the values but were excluded to determine the general behavior of the model. Finally, spikes over 1.83 m. (which was determined to be the realistic threshold based on field observations) were excluded and accounted for 3.5% of values. The performance metrics chosen for this analysis include R^2 and RMSE are shown in Table 3. To observe performance metrics for each individual groundwater monitoring well, refer to Appendix B.

Table 6. Performance metrics of the Groundwater Model

Type	R^2	RMSE (m)	# of Spikes
All Data	0.8400	2.325	-
Excluding 30.48 m Spikes	0.9169	1.614	9
Excluding 1.83 m Spikes	0.9967	0.3956	145

3.4.1 Surface Water

Water depth and inundation extent varied between restoration scenarios and flowrate in the hydrodynamic model. These differences are accredited to the frequency and locations of PALS based on the restoration scenario. Inundation extent area ranged from 1,220 m^2 in RS 1 at 0.11 m^3/s to 4,338 m^2 in RS 5 at 0.57 m^3/s (Figure 12).

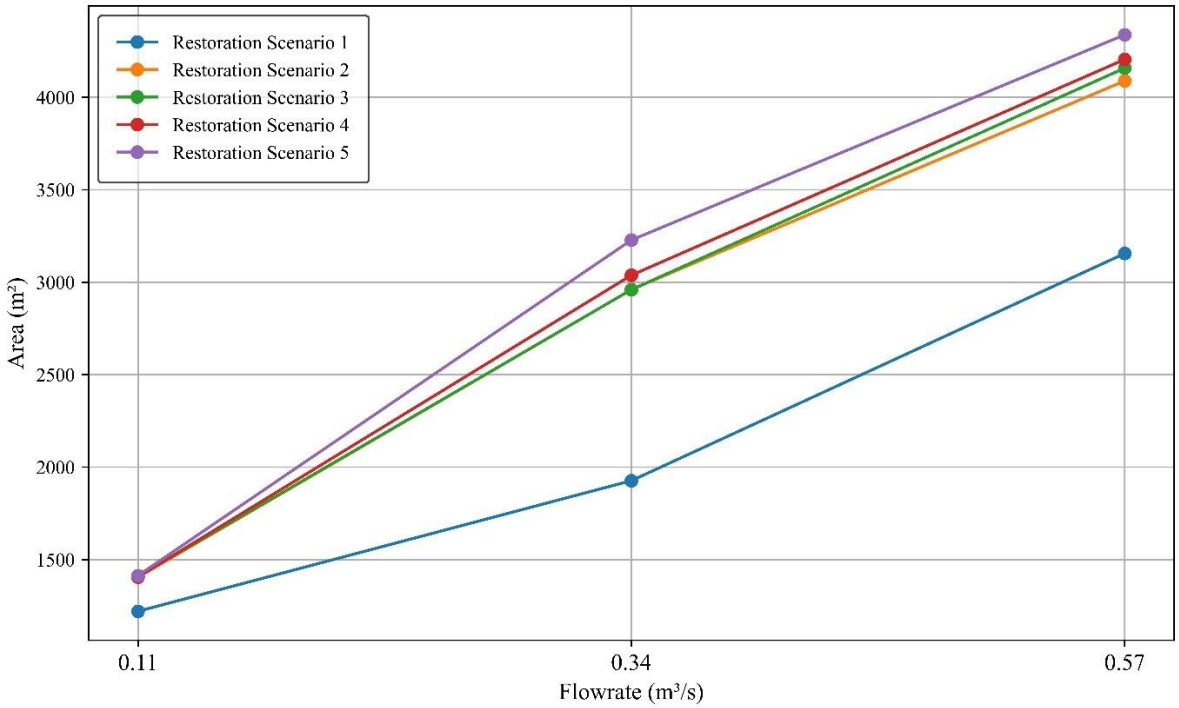

Figure 12. Inundation Extent Area Comparison Across All Restoration Scenarios

Water depth was greatest within the channel in each model run. The maximum water depth occurred during RS 5 at 0.57 m^3/s with a water depth of 1.24 m. The water depth and inundation extent can be visually represented in Figures 13-15.

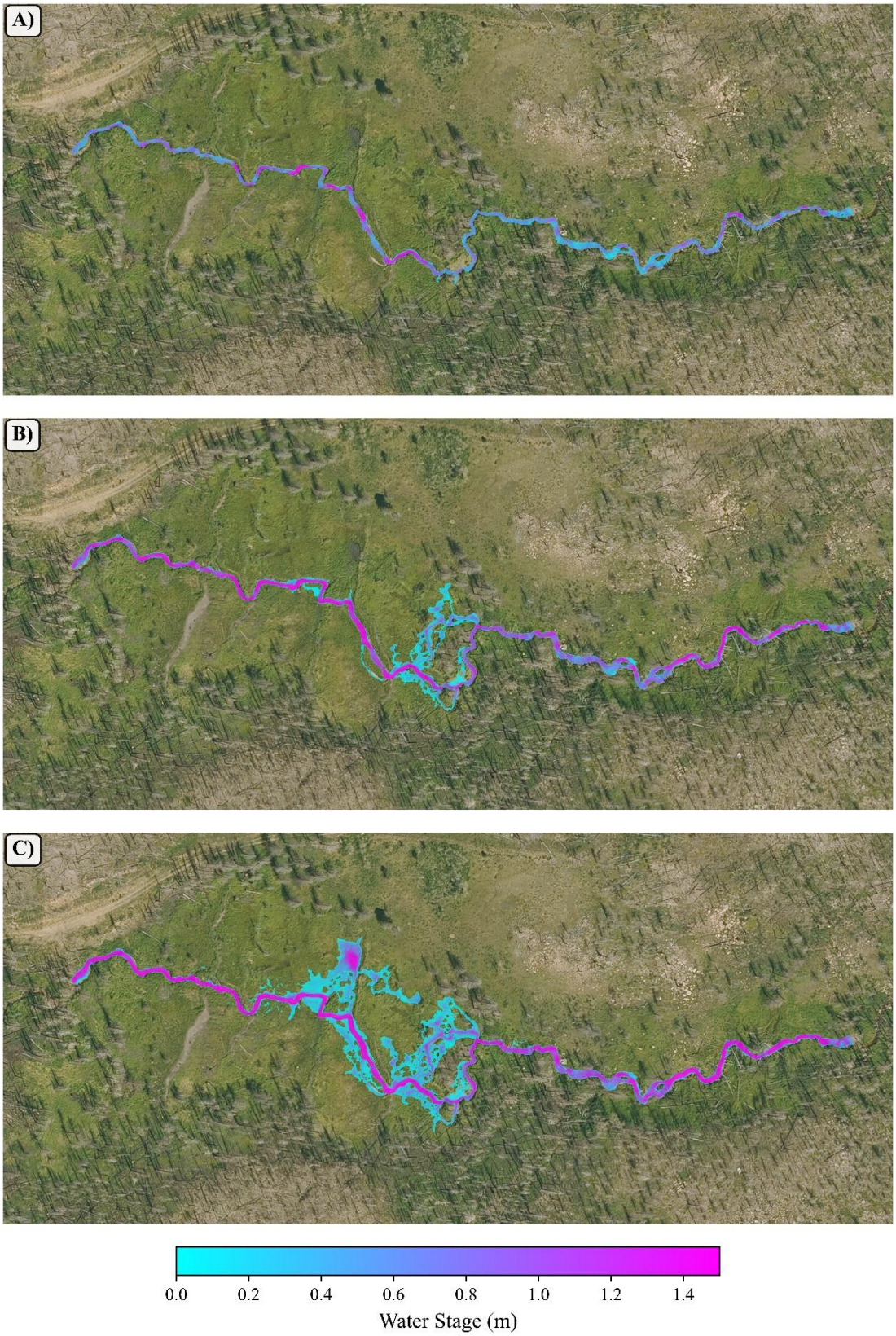

Figure 13. Restoration Scenario 1 SRH-2D Results. A) Flowrate: 0.11 m^3/s B) Flowrate: 0.34 m^3/s C) Flowrate: 0.57 m^3/s

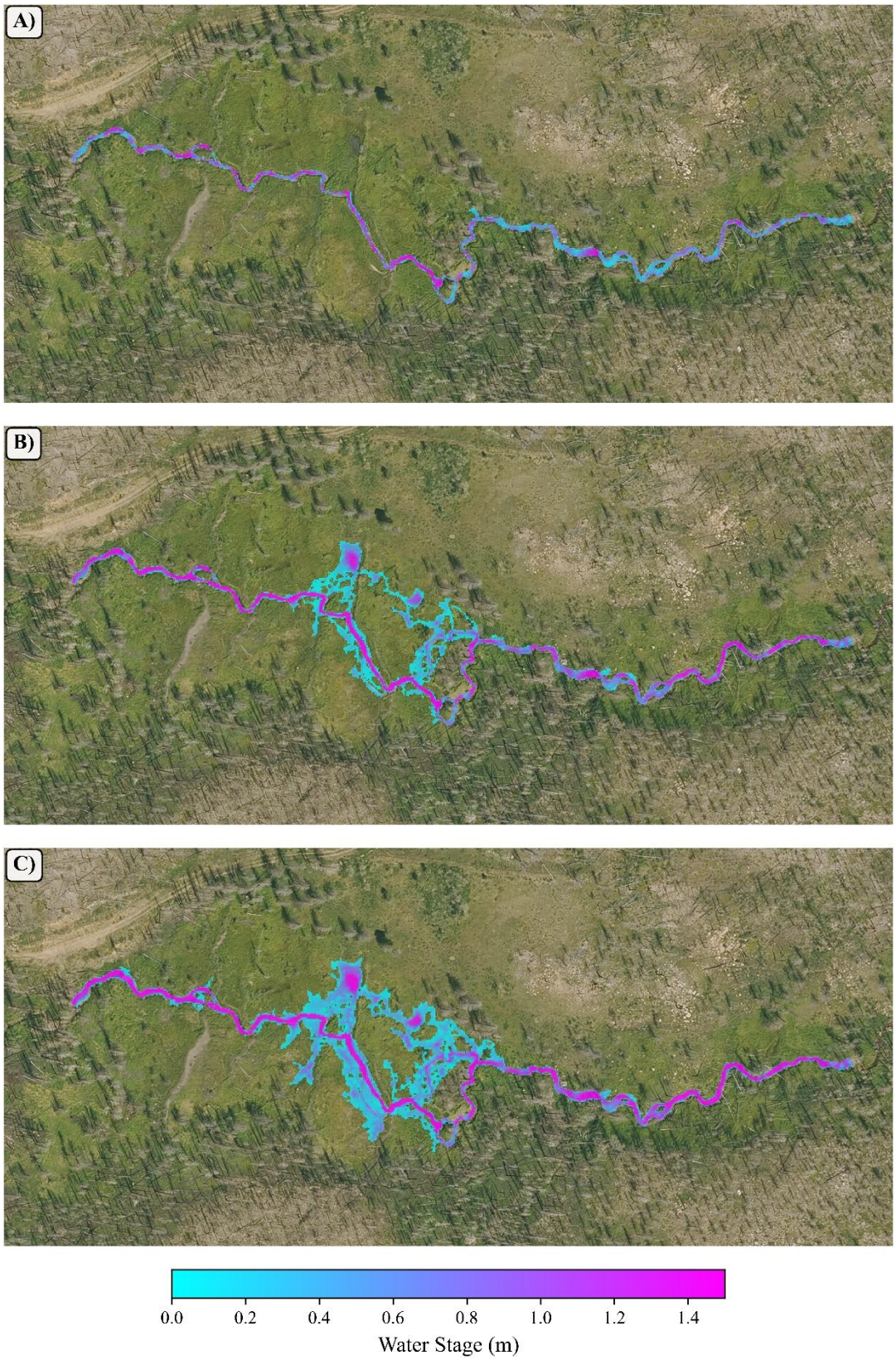

Figure 14. Restoration Scenario 3 SRH-2D Results. A) Flowrate: 0.11 m^3/s B) Flowrate: 0.34 m^3/s C) Flowrate: 0.57 m^3/s

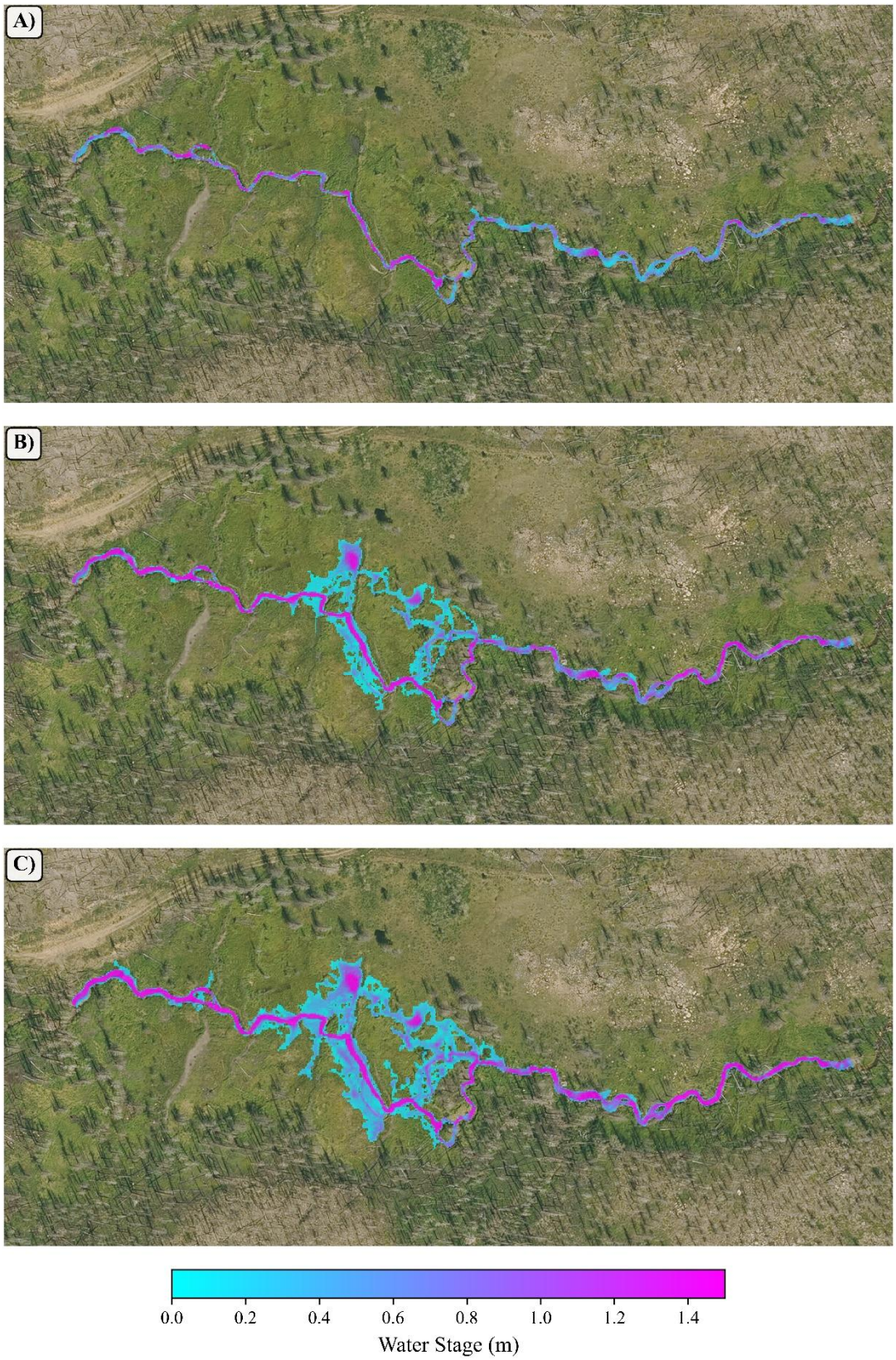

Figure 15. Restoration Scenario 5 SRH-2D Results. A) Flowrate: 0.11 m^3/s B) Flowrate: 0.34 m^3/s C) Flowrate: 0.57 m^3/s

Surface water volumes were calculated to analyze water depth and inundation extent simultaneously. Figure 16 compares surface water volumes between restoration scenario and flowrate. Surface water volumes ranged from 166 m^3 for RS 1 at 0.11 m^3/s to 725 m^3 at RS 5 at 0.57 m^3/s. Restoration Scenarios 2-5 produced very similar surface water volume results at low flow (0.11 m^3/s) but RS 5 diverged as flowrate increased. Restoration Scenarios 2-4 stayed very similar throughout all flowrates with only slight divergence as restoration scenario increased. RS 1 showed stark contrasts in surface water volume when compared to the other restoration scenarios.

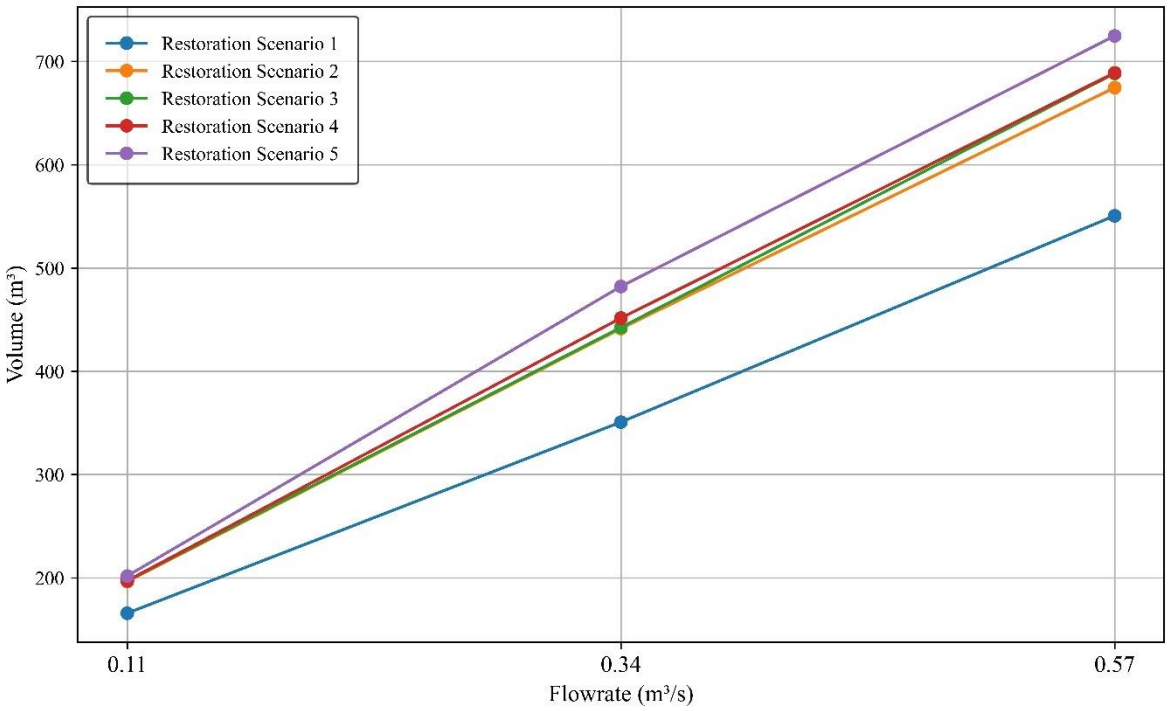

Figure 16. Surface Water Volume Comparison Across All Restoration Scenarios

The stark contrasts between RS 1 and the other restorations scenarios are shown in Table 6. There was a maximum increase of 37.4% in surface water volume between RS 5 and RS 1 at 0.34 m^3/s. The percentage increases as the restoration scenario intensity increases. The greatest increase between restoration comparison scenarios occurred between RS 4 and RS 5 at 0.34 m^3/s with a percentage difference of 8.7% while minimal differences were observed between RS 3 and RS4 at 0.11 m^3/s and 0.57 m^3/s. When comparing storage volume difference between flowrates, the greatest increase in surface water volume occurred at a flowrate of 0.34 m^3/s with an average percent increase of 29.5 % across restoration scenarios, while 0.11 m^3/s and 0.57 m^3/s showed an average increase of 19.5% and 26%, respectively. The flowrate of 0.34 m^3/s also showed the greatest increase in surface water volume between RS 2 and RS 5 with a 11.6% increase, while 0.11 m^3/s and 0.57 m^3/s increased by 3.2% and 9.1%, respectively.

Table 7. Percent Increase in Surface Water Volume Compared to RS 1

Flowrate (m^3/s)	**RS 2**	**RS 3**	**RS 4**	**RS 5**
0.11	18.5 %	18.9 %	18.9 %	21.7 %
0.34	25.8 %	26.1 %	28.7 %	37.4 %
0.57	22.5%	25.0%	25.1%	31.6%

3.4.2 Groundwater

Groundwater elevation and groundwater volume from the linked hydrodynamic model (SRH-2D) and groundwater model (MODFLOW-NWT) vary between restoration scenario and flowrate. To observe these changes in groundwater elevation and in groundwater volume, RS 1 was used as the relative baseline scenario where no implementation was applied to this restoration scenario. RS 1 was then subtracted from each of the remaining restoration scenarios to create a difference raster showing groundwater elevation difference between each respective restoration scenario, referred to as a comparison scenario.

To quantify the total estimated groundwater volume, each comparison restoration scenario was shown throughout the model time (Figure 17), by taking the groundwater volume difference (e.g., R5 minus R1 volumes) at each time step of the model. The greatest volume difference occurred during the low flow (0.11 m^3/s) scenario which occurred from Day 0 to 80 and again from Day 200 to 365. RS 5 showed as much as a 6,070 m^3 volume difference on Day 7 when compared to RS 1 while RS 2 showed a 5,620 m^3 volume difference on the same day, an 8% increase. As the flowrate increases, the volume differences decrease. During the high flow (0.57 m^3/s) scenario, RS 5 dropped to only a 1,910 m^3 volume difference on Day 169 when compared to RS 1 while RS 2 fell to 1,290 m^3 volume difference on the same day.

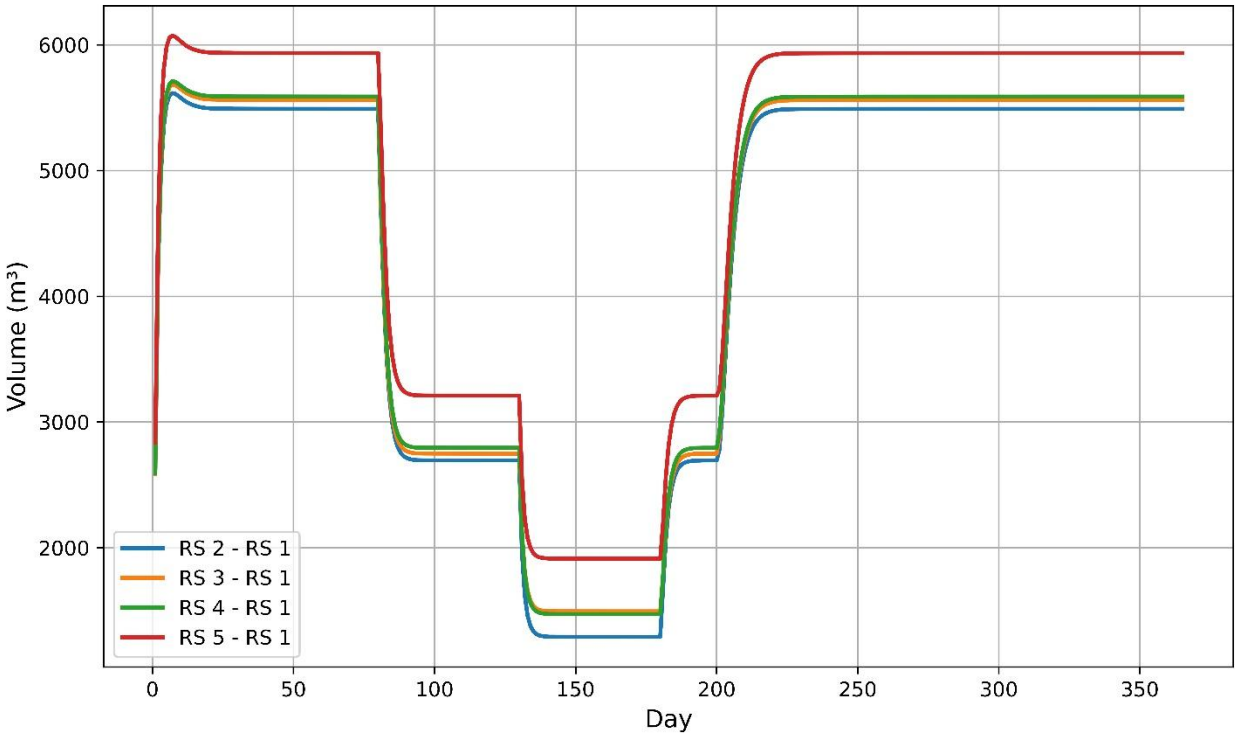

Figure 17. Groundwater Volume Comparison of All Restoration Scenarios through time.

The average groundwater volume difference for the entire model period was calculated for each comparison scenario (Figure 18). To compute these values, the groundwater volume difference (Figure 17) was averaged through the model time. The average groundwater volume difference for the model duration ranged from 4,340 m^3 for RS 2 – RS 1 up to 4,820 m^3 for RS5 – RS 1. A percent increase was then applied using RS 2 – RS 1 as the relative baseline value. A 2% increase in average groundwater volume difference was observed between RS 2 – RS 1 and RS 3 – RS 1. A 0.5% increase in average groundwater volume difference was observed between RS 3 – RS 1 and RS 4 – RS 1, with RS 4 – RS 1 increasing by 2.5% when compared to RS 2 – RS 1. Finally, the largest increase occurred between RS 5 – RS 1 and RS 4 – RS 1 with an 8.6% increase, with RS 5 – RS 1 showing a maximum increase of 11.1% when compared to RS 2 – RS 1.

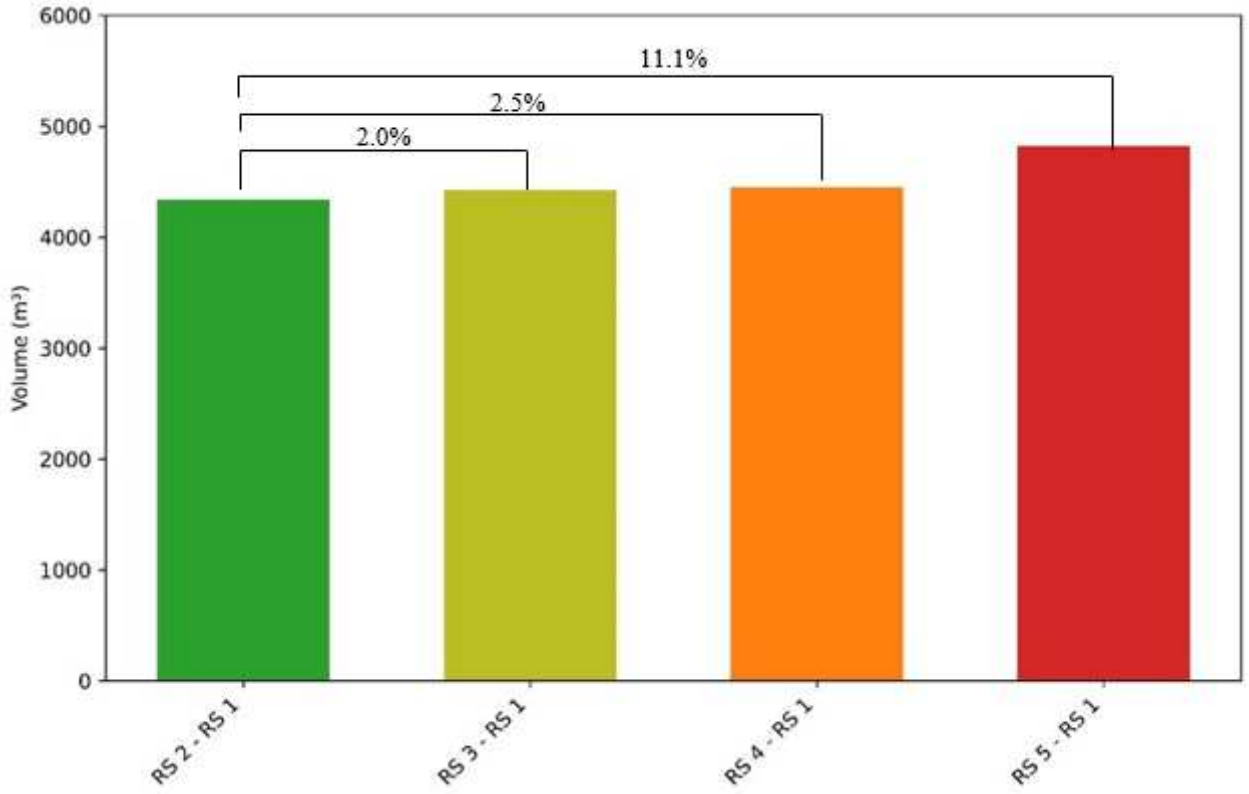

Figure 18. Average Groundwater Storage Volume Difference and Percent Increase Compared to RS 2- RS 1

Change in groundwater elevation rasters were created to assess the changes spatially between the varying restoration scenarios (Figures 19-21). RS 1 is used as the relative baseline scenario, similar to the groundwater volume analysis. Figure 19 shows the groundwater elevation difference rasters for each comparison scenario on Day 40 (0.11 m^3/s) of the model period. Groundwater elevation difference was averaged for each comparison scenario. RS 2 – RS 1 showed an average change in groundwater elevation of 0.318 m. RS 3 – RS 1 showed an average change in groundwater elevation of 0.322 m. RS 4 – RS 1 showed an average change in groundwater elevation of 0.324 m. RS 5 – RS 1 showed an average change in groundwater elevation of 0.344 m.

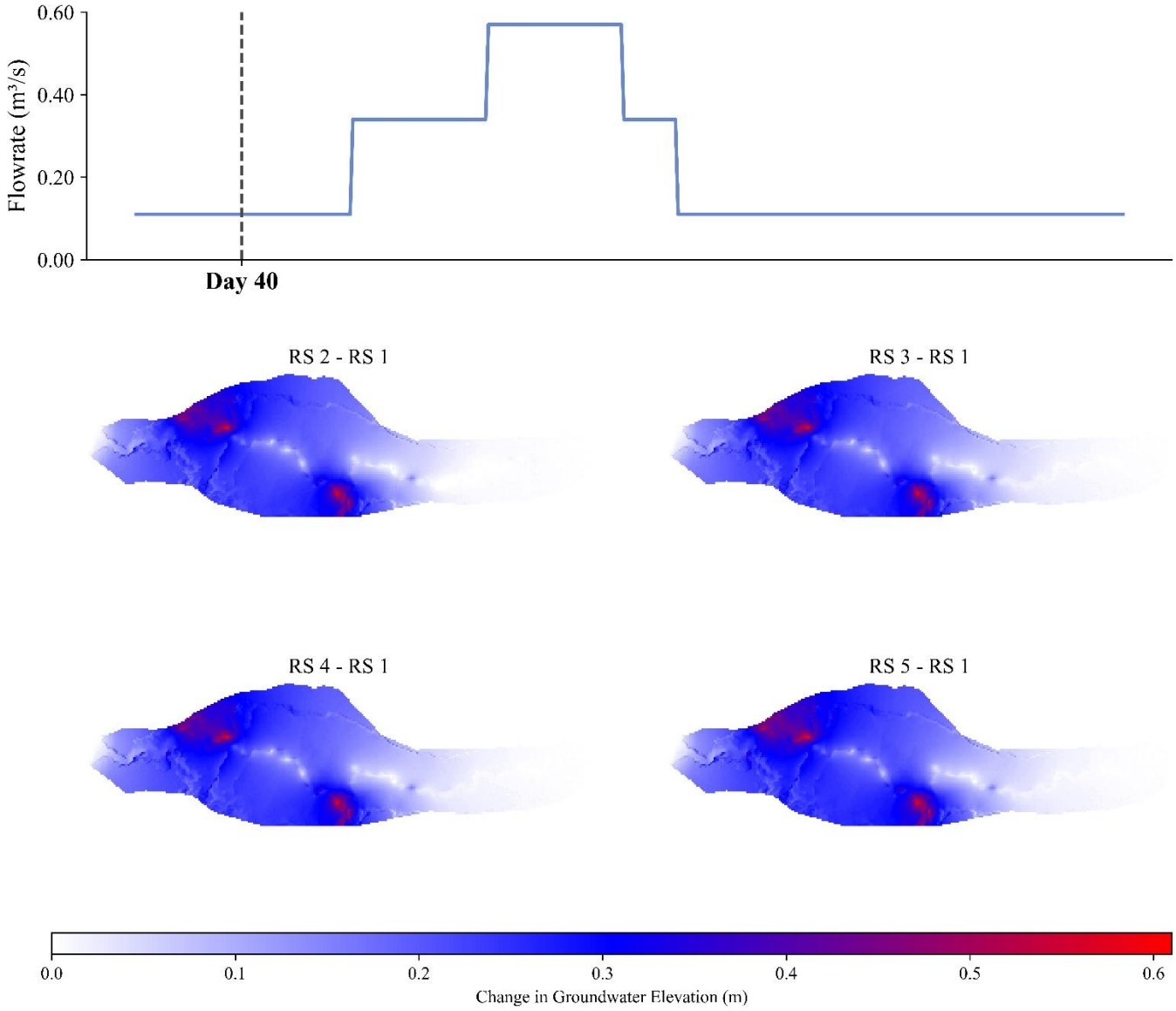

Figure 19. Groundwater Elevation Difference Maps at Day 40, 0.11 m^3/s

Figure 20 shows the groundwater elevation difference rasters for each comparison scenario on Day 105 (0.34 m^3/s) of the model period. Groundwater elevation difference values range from no change to 0.60 m of change in RS 5 – RS 1 in certain locations, similar to Day 40. Groundwater elevation difference was averaged for each comparison scenario. RS 2 – RS 1 showed an average change in groundwater elevation of 0.156 m. RS 3 – RS 1 showed an average change in groundwater elevation of 0.159 m. RS 4 – RS 1 showed an average change in groundwater elevation of 0.162 m. RS 5 – RS 1 showed an average change in groundwater elevation of 0.186 m.

Figure 21 shows the groundwater elevation difference rasters for each comparison scenario on Day 155 (0.57 m^3/s) of the model period. Groundwater elevation difference values range from no change occurred to 0.39 m of change in RS 5 – RS 1 in certain locations, lower than Days 40 and 105. Groundwater elevation difference was averaged for each comparison scenario. RS 2 – RS 1 showed an average change in groundwater elevation of 0.075 m. RS 3 – RS 1 showed an average change in groundwater elevation of 0.086 m. RS 4 – RS 1 showed an average change in groundwater elevation of 0.085 m. RS 5 – RS 1 showed an average change in groundwater elevation of 0.111 m.

The decreasing trend in groundwater elevation difference maximums is in agreement with the decrease in groundwater volume difference observed through model duration and changes in flowrates as seen in Figure 17. Because this analysis focuses on groundwater elevation difference, an increase in flowrate does not show an increase in groundwater difference when comparing to the RS 1, the relative baseline scenario. Additional groundwater elevation difference figures can be found in Appendix F for Days 190 (0.34 m^3/s) and 282 (0.11 m^3/s). However, these maps closely resemble Days 40 and 105, respectively, as shown in Figure 17.

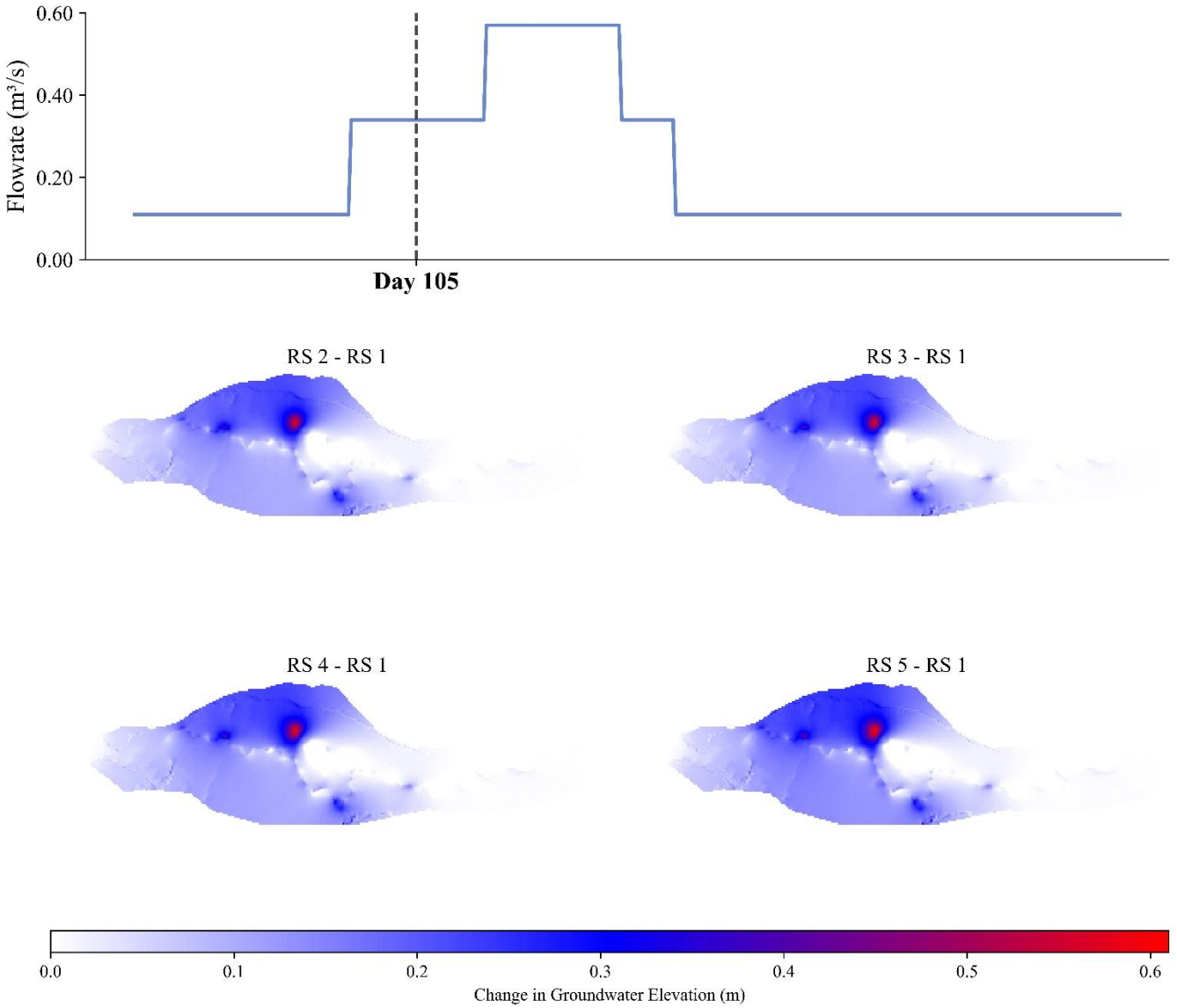

Figure 20. Groundwater Elevation Difference Maps at Day 105, 0.34 m^3/s.

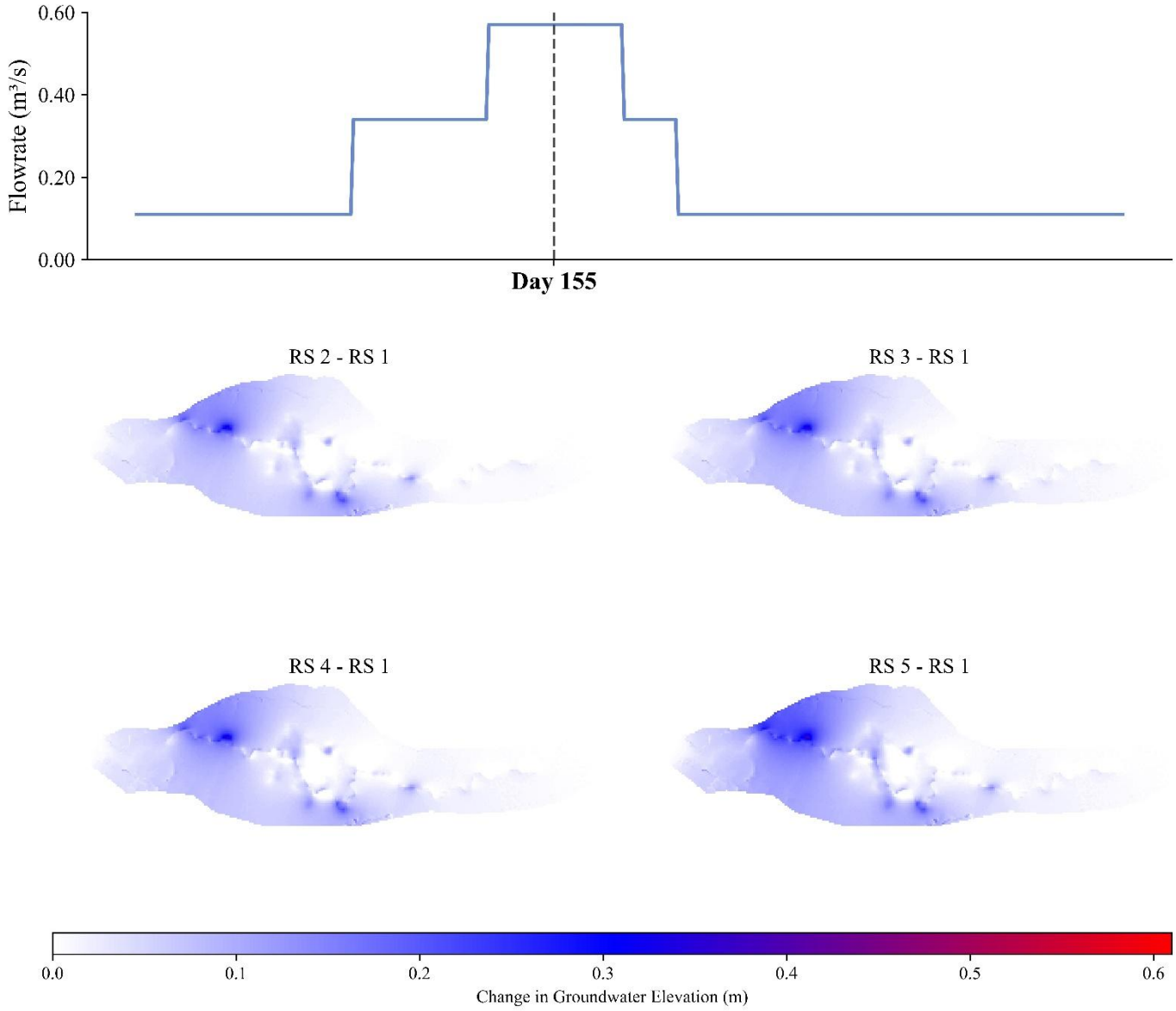

Figure 21. Groundwater Elevation Difference Maps at Day 155, 0.57 m^3/s.

Groundwater elevation difference rasters were compared through time to assess how gorundwater elevation differences vary spatially and temporally for a specific restoration scenario (Figures 22-23). These groundwater elevation difference rasters were developed using the same method as Figures 19-21. Days 40 and 282 each represent 0.11 m^3/s, Days 105 and 190 each represent 0.34 m^3/s, and Day 155 represents 0.57 m^3/s.

Figure 22 assess the RS 3 – RS 1 comparison scenario for each flowrate during the model duration. Groundwater elevation difference ranged from no change at all to 0.59 m on Days 40 and 282 (0.11 m^3/s). The average groundwater elevation difference for the entire model area ranged from 0.026 m on Day 155 (0.57 m^3/s) to 0.098 m on Days 40 and 282 (0.11 m^3/s).

Figure 23 assess the RS 5 – RS 1 comparison scenario for each flowrate during the model duration. Groundwater elevation difference ranged from no change at all to 0.60 m on Days 40 and 282 (0.11 m^3/s). The average groundwater elevation difference for the entire model area ranged from 0.034 m on Day 155 (0.57 m^3/s) to 0.105 m on Days 40 and 282 (0.11 m^3/s). Both the groundwater elevation difference maximum and the average groundwater elevation difference values are higher than RS 3-RS 1 scenario comparison.

Days 40 and 282, as well as Days 105 and 190 produce nearly identical groundwater elevation results due to those days both use the same flowrates. Similar to Figures 19-21, the decreasing trend in groundwater elevation difference maximums and average groundwater elevation difference is in agreement with the decrease in groundwater volume difference observed through model duration and changes in flowrates as seen in Figure 17. Additional groundwater elevation difference figures can be found in Appendix F for RS 2 – RS 1 comparison scenario and RS 4 – RS 1 comparison scenario, though the trends are the same as Figures 22-23.

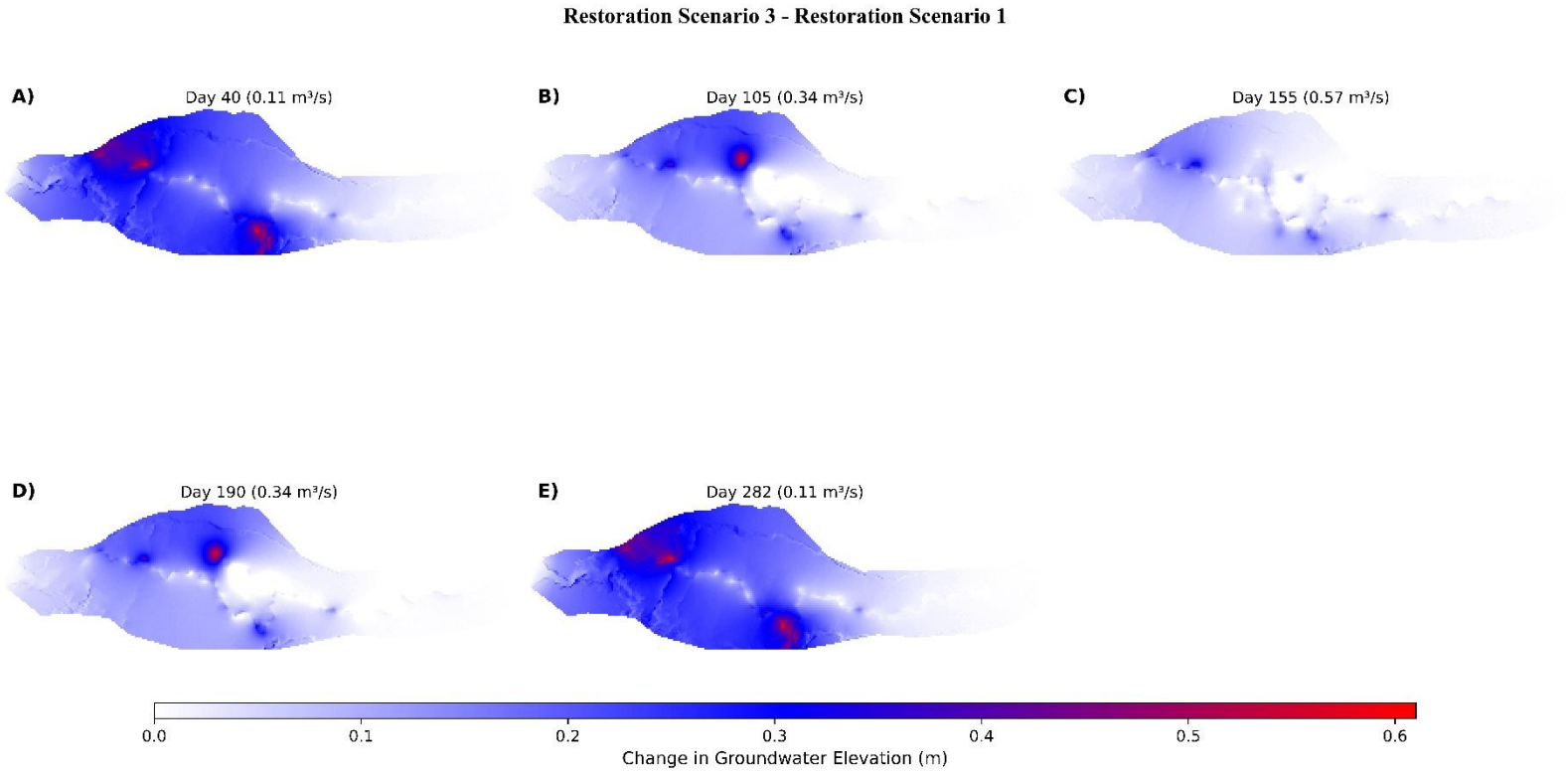

Figure 22. Scenario 3 – Scenario 1 Groundwater Difference Maps through Model Time.

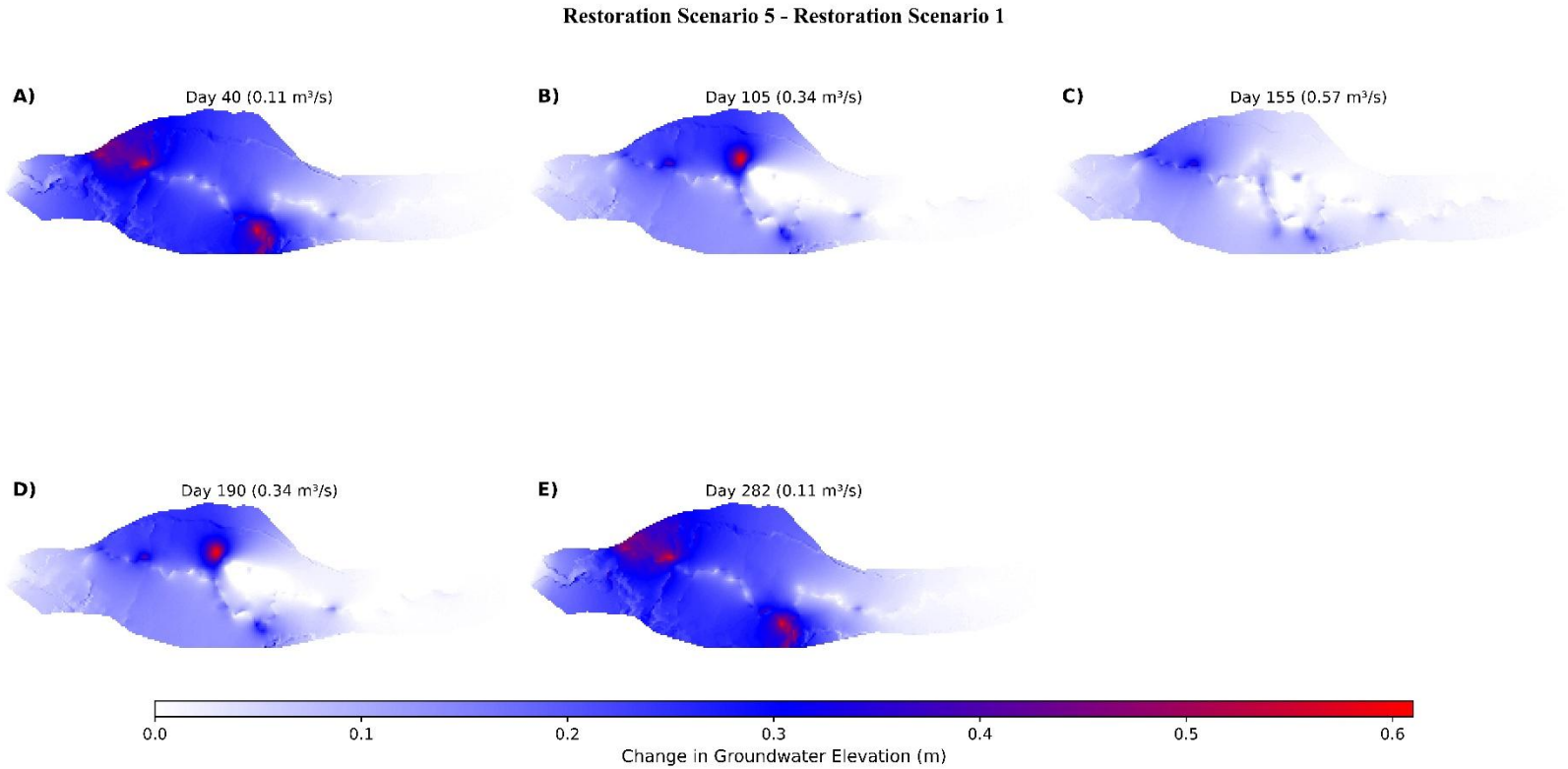

Figure 23. Scenario 5 – Scenario 1 Groundwater Difference Maps through Model Time

4 DISCUSSION

4.1 Sediment Transport, Grain Size Distribution, and Storage Following a Wildfire

In a post-fire setting, the potential for floods, debris flows, and high sediment transport in a fluvial system is significantly increased due to alterations in vegetation and soil properties (Swanson, 1981). No significant flooding or debris flows were observed during the study period. All the sediment transport occurred during typical seasonal patterns of snowmelt runoff and summer convective thunderstorms.

Sediment deposition along the study reach varied spatially. Sediment deposition generally decreased downstream from structures (Figure 7). However, there was less sediment deposition in the PALS 1 reach. Because the sediment probing reach was only conducted 15 m upstream of PALS 1, not all sediment deposition was potentially captured. Similarly, PALS 7 reach retained significantly more sediment than PALS 5 and PALS 6 reaches, even when normalized to account for reach length (Figure 7B). This could be accredited to the characteristics of the channel. Upstream of PALS 7, Elkhorn Creek runs along a relic beaver dam (Figure 3) providing roughness to high, sediment-transporting flows which causes a decrease in both stream velocity and stream power, allowing sediment deposition.

Fine sediment transport loads through a watershed have proven to be significantly higher five years following a wildfire when compared to pre-fire averages (Reneau et al., 2007). This study was conducted approximately 2.5 years following the 2020 Cameron Peak Fire. Most of the sediment transported to the study reach was finer in grain size than what was initially surveyed with an average D_{50} of 15.4 mm pre-installation of PALS to an average D_{50} of 3.70 mm one-year post-installation of PALS (Figure 6) indicating the majority of sediment being

transported through system consisted of finer grained sediment. Florsheim et al. (2017) monitored the effects of sediment size in the headwaters of Big Sycamore Creek in southern California following the 2013 Springs Fire and observed a similar pattern of finer bed grain sediment deposition. During the study period, two substantial rainfall events (2014 and 2015) occurred after a drought period (Florsheim et al., 2017). Sediment size before the 2014 storm was measured to be a D_{50} of 88 mm (Florsheim et al., 2017). Sediment size following the 2014 storm was measured to be a D_{50} of 5.8 mm (Florsheim et al., 2017). Sediment size following the 2015 storm event was measured to be a D_{50} 2.6 mm (Florsheim et al., 2017).

During the first snowmelt runoff season at the site, approximately 63 m^3 of sediment was deposited within the channel determined by sediment probing surveys (Figure 7), as well as sediment deposition on the floodplain which was observed visually at the study site. A similar study focusing on sediment deposition following a wildfire in a reservoir observed an increase of approximately 140 times the annual pre-wildfire rate in the first year following wildfire (Reneau et al., 2007). Approximately 70% of the total sediment deposition was fine-grained sediment (Reneau et al., 2007). The channel bed elevation of Elkhorn Creek increased by an average of approximately 0.30 m during the study period, heavily influenced by the addition of PALS. In the Florsheim et al., (2017) study, the channel bed elevation of Big Sycamore Creek increased by approximately 0.60 m after the 2014 storm and an additional 0.64 m following the 2015 storm.

4.2 Influence of LTPBR on Sediment Storage, Floodplain Connection, and the Groundwater Table

Sediment retention occurred through two contributing factors: post-wildfire landscape setting and the implementation of PALS through LTPBR within the study site. Through a similar study in which numerous LTPBR treatments were observed, (Scamardo et al., 2025) recorded an

average increase in sediment volume of 314 m^3 and an average increase in sediment depth of 0.7 m. Of the sites where sediment storage was monitored (33 sites), 91% showed net sediment deposition (Scamardo et al., 2025). The results of this study agree with the Scamardo et al., (2025) analysis of 30 LTPBR sites that found net sediment deposition indicating the effectiveness of LTPBR on sediment storage within the channel. These studies do not quantify the annual sediment that is transported through the river system, only the sediment that was deposited. These river systems vary in the amount of sediment that is available for transport as well as the rivers capacity to transport the sediment. The influence of LTPBR on sediment storage is dependent on the sediment available in transport and the quantities may vary site to site based on both the sediment available to be stored in transport and the sediment storage capacity of the LTPBR structure.

Scamardo et al., (2025) found an average increase of 0.6 m in stream stage through their analysis of 23 LTPBR sites. This increase in stage along with the average increase in channel bed elevation indicates a higher potential for floodplain connectivity of the restoration site. Our surface water modeling results agree with these findings indicating that there were increases in surface water volume with a greater density of PALS (Figure 16). Notably, this study did not have access to pre-implementation stage data to calibrate the no PALS scenario. Future work should begin before project implementation to determine more conclusive results.

Groundwater response could be correlated to floodplain connectivity. On average, an increase of approximately 0.21 m in groundwater elevations were observed in the study reach when comparing pre-snowmelt runoff to post-snowmelt runoff while monitoring wells in the reference reach increased an average increase in groundwater elevation by approximately 0.06 m

(Table 5). The increase in groundwater elevation in the reference reach can be accredited to wetter hydrological year for the site, refer to Appendix G.

Results have been fairly conclusive when observing groundwater levels post-implementation of LTPBR projects across the western US. Scamardo et al., (2025) observed an average decrease of 0.3 m in depth to groundwater over 16 project sites indicating an increase in the water table. In a similar study in a mountain meadow in the Sierra Nevada range, an increase of 3,700 m^3 of water storage across the meadow was estimated only 1 year post-restoration (Sevier et al., 2024). Our model results agree with this observation with an increase in groundwater storage, with a minimum increase of 4,340 m^3 in groundwater storage observed in the RS 2 – RS 1 comparison scenario. A study in which 2 years of pre- and post-installation of BDAs data in a first-order stream in Utah observed a significant increase in shallow groundwater table elevations of up to 0.14 m (Bosworth et al., 2025). However, a study geographically close to this study in the Front Range of Colorado in which BDAs were studied saw similar stored volumes of sediment but no significant influence on shallow groundwater (Scamardo & Wohl, 2020). The short-term results found in this study support the fast-acting capabilities of LTPBR in achieving post-wildfire, restoration goals on sediment retention, enhanced floodplain connectivity, and elevating the groundwater table.

4.3 Restoration Scenarios Through Numerical Modeling and Impacts for Practitioners

Numerical modeling was used to compare varying LTPBR restoration scenarios ranging from no implementation on site to PALS installed every 5 m along the stream channel to examine both surface water inundation extent and depth in addition to groundwater elevation changes between scenarios. Through hydrodynamic modeling with SRH-2D, water inundation area and surface water volume increased as restoration scenario intensity increased. However,

Restoration Scenarios (RS) 2 through 4 were relatively similar in both inundation area and surface water volume (Figures 12 and 16). This result combined with financial and time constraints of any typical restoration project indicate that when working in an historic beaver meadow where relic beaver dams are present, similar results could be achieved by plugging the relic beaver dams where they intersect the channel (RS 2) as opposed to adding additional structures throughout channel (RS 3, 4, and 5). This would greatly improve floodplain connectivity and river corridor resiliency while keeping the project budget reasonable and on a short timeline. While RS 5 was the most impactful when observing inundation extent and surface water volume, 30 PALS were simulated in this scenario while only 5 PALS were simulated in RS 2 (Table 3). Assuming each PALS costs the same to construct; RS 5 is 600% more expensive to construct than RS 2. RS 5 demonstrated an 11.1% increase in groundwater volume when compared to RS 2 (Figure 18). This hypothetical comparison shows that the additional cost of a more intensive restoration treatment does not linearly increase the potential impact on the system. Less intensive and cost-effective restoration treatments, such as RS 2 can have major impacts on both the surface water and groundwater system and are budget-friendly when compared to more intensive restoration treatments, such as RS 5. Reduced cost methods may allow practitioners to implement projects at larger scales to match the daunting task of restoring the processes of our many impaired streams (Bernhardt et al., 2005).

Through the linked hydrodynamic-groundwater model, there was a decrease in groundwater elevation difference as the flowrate increased (Figure 17). Flowrate was seen as a major driver of the model and indicates that restoration scenario intensity is less impactful at high flows when the surface water is spread out across the floodplain. This makes the case for LTPBR to be most impactful at low and intermediate flows when wetland and riparian

restoration is a major component of the project since the groundwater table will be more connected to surface vegetation at baseflows.

The numerical modeling results support the field observations from Elkhorn Creek and similar study results in that LTPBR has shown to increase the stream stage, increase surface water volume, and increase groundwater elevations (Bosworth et al., 2025; Scamardo et al., 2025). LTPBR has proven, through field observations and numerical modeling, to improve river corridor resiliency and can be used as a tool to make headwater streams in the fire-prone Western US more resilient to wildfire while also mitigating the impacts in a post-wildfire setting.

4.4 Limitations and Considerations

The linking of the SRH-2D and MODFLOW-NWT models took advantage of packages previously developed. The scheme used allowed the groundwater model to be influenced by the surface model but did not utilize the groundwater data in determining surface water. In reality, water may travel between the surface and groundwater flow paths readily. This pairing could also lead to inaccuracies in the unsaturated zone, also referred to as the vadose zone (Arora et al., 2019). In using the RIV Package, each cell was activated and deactivated based on restoration scenario and flowrate determined by the inundation extent of the hydrodynamic model. When a cell is inactive, the groundwater table is typically below the ground surface, exposing the vadose zone. When the cell is then activated with a specific stage of surface water, there is a discontinuity between the surface water and groundwater. To account for infiltration rates through the vadose zone, the conductance calculation within the RIV package was utilized to create spatially varying conductance based on the vertical hydraulic conductivity of the soil in its respective zone. Conductance was determined and remained consistent for all restoration scenario models and was not investigated further as to determine the model's sensitivity to

different conductance values. However, the model may have inaccurately captured the surface water infiltration process through the vadose zone and into the groundwater table. This is a crucial interface when assessing the impacts of surface water on the groundwater table. This uncertainty may have led to inaccurate assumptions on groundwater elevations and for that reason, must be acknowledged.

MODFLOW-NWT does have a package to simulate unsaturated zone flow, the Unsaturated Zone Flow (UZF) Package. The UZF package simulates vertical flow of water through the unsaturated zone to the saturated zone and can work in conjunction with the Recharge Package, Evapotranspiration Package, and Evapotranspiration Segments Package (Niswonger et al., 2006). This package does not work in conjunction with the RIV package. For this reason and to attempt to not overcomplicate the model, the UZF package was not applied. Future refining of the groundwater model should include the addition of the UZF package to better represent flow through the unsaturated zone.

Due to the remote location of the study site, recharge was difficult to estimate due to the lack of available hydrological data. As previously stated, the water table fluctuation method was used which assumes a specific yield value and is dependent on a time series of groundwater data. During model calibration, large groundwater spikes were observed which correlated with large recharge periods based on the water table fluctuation method. The occurrence of the large spikes can be attributed to inaccuracies in recharge estimation used for this specific site.

Performance metrics computed after the calibration of the groundwater model (MODFLOW-NWT) were less than ideal due to uncertainties in model creation such as recharge and other inputs into the model. Similar studies using MODFLOW-NWT achieved an R^2 values of 0.97 and a RMSE of 0.59 m whereas in this study, the R^2 was 0.84 and a RMSE of 2.32 m

(Eyster, 2018). The model area used in this study (approximately 33,700 m^2) is considerably smaller than the comparison study (27,000,000 m^2) (Eyster, 2018). Reach (or small) scale can be defined as a reach along a stream withing a watershed while watershed (or large) scale can be defined as full watersheds consisting of multiple stream networks. Other large differences were the Eyster (2018) study had greater hydrological data availability and accounted for evapotranspiration and drains within the modeled area, while the intent of the linked model in this study was to compare restoration scenarios that varied on frequency and location of PALS. Swain, (2021) used a MODFLOW-NWT model to observe groundwater levels of the Northern Cities Management Area in central California with a model area of approximately 33,588,908 m^2. PEST was used for calibration along with observed groundwater elevations throughout the site obtained a combined calibrated R^2 value of 0.50 for the calibrated model (Swain, 2021).

The elevated manning's n roughness estimation of 0.118, calculated from Jarrett's equation (Jarrett, 1984) may provide additional uncertainty in surface water inundation extents and surface water depths. Comparisons with observed low discharge and water surface pairs provided adequate accuracy (RMSE: 0.14 m) and are likely insignificant contributions in the linked surface water-groundwater modeling error (RMSE: 2.32 m including all data). Additional calibration of manning's roughness may reduce surface water error though this would not significantly impact overall error in groundwater elevations.

Capturing surface water-groundwater interactions at a reach scale using hydrodynamic models is an active field of study. Modeling at a reach scale presents its own inaccuracies and assumptions. When looking at the reach scale, it is still not possible to calculate closed balances for the groundwater and surface water bodies involved (Barthel & Banzhaf, 2016). This is due to water catchments (i.e. watersheds) and the groundwater aquifer are larger than the area of

interests forcing the modeler to determine boundary conditions and make assumptions (Barthel & Banzhaf, 2016). Studying the surface water-groundwater interaction at small scales consists of detailed observations in a small area while making assumptions and simplifying the process that occur outside of this small area (Barthel & Banzhaf, 2016). On the contrary, studying surface water-groundwater interaction at large scales simplifies the process at the immediate surface water-groundwater interface while using observations at the larger scale (Barthel & Banzhaf, 2016). When focusing on the reach scale, the disadvantages of these two scenarios are combined thus creating a complex modeling approach or a simplified modeling approach incorporating many assumptions.

The study site included a bedrock outcrop separating the study reach and the reference reach. This geological feature was not accounted for in both field data analysis nor the numerical modeling which could have impacted results and potentially skewing groundwater well data within the study reach. This does not discredit the findings of this study but it is important to note.

4.5 Considerations for Future Work

LTPBR is becoming a more popular restoration method to restore riparian areas, improve river corridor resiliency, and as a mitigation tool in post-wildfire systems. Continued monitoring and research of these LTPBR sites is needed to better understand their impacts on the river corridor such as carbon sequestration in the floodplain in addition to sediment retention and groundwater fluxes.

Continued improvement of the linked hydrodynamic-groundwater model is needed to better represent the natural groundwater processes occurring at the Elkhorn Creek study site.

First, a reanalysis of recharge is needed to accurately represent the water inputs into the system and to reduce the large spikes that occurred. Second, further investigation into other water inputs such as natural springs and/or seeps into the system. Finally, to develop a better understanding of the subsurface materials such as aquifer depths and sediment composition used in estimating conductance, hydraulic conductivity and specific yield values. Even though these are calibrated values, a better estimate of the system would improve the MODFLOW-NWT model.

The surface water-groundwater interface during the activation and deactivation of surface water cells is crucial to determine how the entire system reacts to a transient model. Further investigation into flow through the vadose zone while incorporating the UZF package and/or modifying the RIV package to more accurately represent unsaturated flow processes. This would be a great opportunity to create a more accurate model used for restoration practitioners in river projects globally.

This method is applied to a small, headwater stream with a relatively small channel width, flowrates, and floodplain. The application of this method to larger river systems would be useful to analyze differences (if any) in how larger flowrates with higher stage depths could impact the groundwater table. Next, using this method to not only compare varying sized rivers but also varying impacted rivers due to wildfire, land use practices, and restoration techniques. Continued refinement of a linked hydrodynamic-groundwater model at a reach scale and how it treats different sized systems would be interesting to develop into a widely used and trusted method of examining natural systems.

5 CONCLUSIONS

This research provides a monitoring analysis of the sediment grain size distribution, sediment storage, and groundwater observations of a LTPBR project in a post-wildfire setting. This research attempts to link a hydrodynamic model (SRH-2D) and groundwater model (MODFLOW-NWT) to observe groundwater elevation and groundwater volume differences across five restoration scenarios, ranging in intensity.

After one-year of monitoring post-implementation, the average D_{50} of the sediment grain size in the channel reduced from 15.4 mm prior to construction to 3.70 mm post-construction, approximately 63 m^3 of sediment was deposited within the channel, and observed groundwater elevations within the study reach showed an average increase of 0.21 m a year following LTPBR construction while observed groundwater elevations in the reference reach showed an average increase of 0.06 m.

Numerical modeling was used to analyze the effects of five restoration scenarios that vary on location and number of PALS installed throughout the study site. Hydrodynamic modeling using SRH-2D of the restoration scenario showed an increase of up to 37.4 % in surface water volume when compared to RS 1 which contained no PALS installed within the study site. This occurred at the most intensive restoration scenario (RS 5) at the intermediate flow (0.34 m^3/s). Restoration Scenarios 2, 3, and 4 produced similar surface water volume results indicating that the installation of more PALS is not necessarily worth the increase in cost and time fame for river restoration practitioners.

Hydrodynamic model results such as inundation extent and surface water depth were used as inputs into the groundwater model using MODFLOW-NWT. An increase of 11.1% in

groundwater volume was observed in comparison scenario RS 5 – RS 1 when compared to RS 2 – RS 1. The groundwater model produced similar results to the hydrodynamic model in terms of water volume. However, the groundwater model demonstrated the greatest groundwater volume difference during low flow indicating LTPBR influences the groundwater table the most at lower flows. This result can contribute to a more suitable habitat for riparian vegetation, along with other benefits which can create diversity within the ecosystem.

This research provided further data supporting the effectiveness of LTPBR on river corridor resiliency, mitigating wildfire impacts, and attempts at creating a linked hydrodynamic-groundwater model to observe various LTPBR techniques and their impacts on the groundwater system. This research helps to provide a better understanding of LTPBR on the river corridor of headwater streams affected by wildfire and to identify the need for a more complete linked hydrodynamic-groundwater model. This model can be used by practitioners to identify key areas as a design tool to better understand the river corridor, the inundation extent at varying flows, and to aid in riparian vegetation placement based on the groundwater table. Because modeling groundwater at a reach scale presents unique difficulties leading to higher RMSE values when compared to studies modeling at a larger, watershed scale, further research is needed to better understand the impacts of LTPBR on the river corridor and the development and/or creation of additional MODFLOW packages are needed to improve the understanding and accuracy of modeling the interactions between surface water and groundwater at a reach scale.

REFERENCES

Appling, A. P., Bernhardt, E. S., & Stanford, J. A. (2014). Floodplain biogeochemical mosaics: A multidimensional view of alluvial soils. *Journal of Geophysical Research: Biogeosciences*, *119*(8), 1538–1553. https://doi.org/10.1002/2013JG002543

Aquaveo. (2024). *SMS 13.3—The Complete Surface-water Solution | Aquaveo.com*. Aquaveo. https://aquaveo.com/software/sms/introduction

Arnold, J. G., Srinivasan, R., Muttiah, R. S., & Williams, J. R. (1998). Large Area Hydrologic Modeling and Assessment Part I: Model Development. *JAWRA Journal of the American Water Resources Association*, *34*(1), 73–89. https://doi.org/10.1111/j.1752-1688.1998.tb05961.x

Arora, B., Dwivedi, D., Faybishenko, B., Jana, R. B., & Wainwright, H. M. (2019). Understanding and Predicting Vadose Zone Processes. *Reviews in Mineralogy and Geochemistry*, *85*(1), 303–328. https://doi.org/10.2138/rmg.2019.85.10

Bailey, R. T., Wible, T. C., Arabi, M., Records, R. M., & Ditty, J. (2016). Assessing regional-scale spatio-temporal patterns of groundwater–surface water interactions using a coupled SWAT-MODFLOW model. *Hydrological Processes*, *30*(23), 4420–4433. https://doi.org/10.1002/hyp.10933

Barthel, R., & Banzhaf, S. (2016). Groundwater and Surface Water Interaction at the Regional-scale – A Review with Focus on Regional Integrated Models. *Water Resources Management*, *30*(1), 1–32. https://doi.org/10.1007/s11269-015-1163-z

Beechie, T. J., Sear, D. A., Olden, J. D., Pess, G. R., Buffington, J. M., Moir, H., Roni, P., & Pollock, M. M. (2010). Process-based Principles for Restoring River Ecosystems. *BioScience*, *60*(3), 209–222. https://doi.org/10.1525/bio.2010.60.3.7

Bendix, J., & Cowell, C. M. (2010). Impacts of Wildfire on the Composition and Structure of Riparian Forests in Southern California. *Ecosystems*, *13*(1), 99–107. https://doi.org/10.1007/s10021-009-9303-z

Bernhardt, E. S., Palmer, M. A., Allan, J. D., Alexander, G., Barnas, K., Brooks, S., Carr, J., Clayton, S., Dahm, C., Follstad-Shah, J., Galat, D., Gloss, S., Goodwin, P., Hart, D., Hassett, B., Jenkinson, R., Katz, S., Kondolf, G. M., Lake, P. S., … Sudduth, E. (2005). Synthesizing U.S. River Restoration Efforts. *Science*, *308*(5722), 636–637. https://doi.org/10.1126/science.1109769

Blake, W. H., Wallbrink, P. J., & Droppo, I. G. (2009). Sediment aggregation and water quality in wildfire-affected river basins. *Marine and Freshwater Research*, *60*(7), 653–659. https://doi.org/10.1071/MF08068

Boano, F., Harvey, J. W., Marion, A., Packman, A. I., Revelli, R., Ridolfi, L., & Wörman, A. (2014). Hyporheic flow and transport processes: Mechanisms, models, and biogeochemical implications. *Reviews of Geophysics*, *52*(4), 603–679. https://doi.org/10.1002/2012RG000417

Bosworth, L., Smith, R. M., Culbertson, A., Jamison, L. R., Burnett, P., & Brooks, P. D. (2025). Streamflow and Groundwater Response to Stream Restoration Using Beaver Dam Analogues in a Semi-Arid Perennial Stream. *JAWRA Journal of the American Water Resources Association*, *61*(1), e13254. https://doi.org/10.1111/1752-1688.13254

Brunner, P., & Simmons, C. T. (2012). HydroGeoSphere: A Fully Integrated, Physically Based Hydrological Model. *Ground Water*, *50*(2), 170–176. https://doi.org/10.1111/j.1745-6584.2011.00882.x

Castro, J. M., & Thorne, C. R. (2019). The stream evolution triangle: Integrating geology, hydrology, and biology. *River Research and Applications*, *35*(4), 315–326. https://doi.org/10.1002/rra.3421

Christensen, N. D., Prior, E. M., Czuba, J. A., & Hession, W. C. (2024). Stream Restoration that Allows for Self-Adjustment Can Increase Channel-Floodplain Connectivity. *Journal of Ecological Engineering Design*, *1*(1), Article 1. https://doi.org/10.21428/f69f093e.e8ffa1a3

Collins, B. D., Montgomery, D. R., Fetherston, K. L., & Abbe, T. B. (2012). The floodplain large-wood cycle hypothesis: A mechanism for the physical and biotic structuring of temperate forested alluvial valleys in the North Pacific coastal ecoregion. *Geomorphology*, *139–140*, 460–470. https://doi.org/10.1016/j.geomorph.2011.11.011

Di Virgilio, G., Evans, J. P., Blake, S. A. P., Armstrong, M., Dowdy, A. J., Sharples, J., & McRae, R. (2019). Climate Change Increases the Potential for Extreme Wildfires. *Geophysical Research Letters*, *46*(14), 8517–8526. https://doi.org/10.1029/2019GL083699

Doherty, J. (2015). *Calibration and Uncertainty Analysis for Complex Environmental Models*. Watermark Numerical Computing. https://pesthomepage.org/pest-book

Emlid, (2025). *Reach RS2+ Multi-band RTK GNSS Receiver with Centimeter Precision.* https://emlid.com/reachrs2plus/. Accessed on October 13th, 2025.

Eyster, T. (2018). *MODELING DAM REMOVAL IN A MOUNTAIN MEADOW WITH MODFLOW-NWT*. https://dx.doi.org/10.14288/1.0375844

Fairfax, E., & Whittle, A. (2020). Smokey the Beaver: Beaver-dammed riparian corridors stay green during wildfire throughout the western United States. *Ecological Applications*, *30*(8), e02225. https://doi.org/10.1002/eap.2225

Fencil, K. (2020). RTK GNSS Accuracy Test: Emlid Reach RS2 vs. Topcon Hiper VR. *E38 Survey Solutions*. https://e38surveysolutions.com/blogs/news/rtk-gnss-accuracy-test-emlid-reach-rs2-vs-topcon-hiper-vr.

Florsheim, J. L., Chin, A., Kinoshita, A. M., & Nourbakhshbeidokhti, S. (2017). Effect of storms during drought on post-wildfire recovery of channel sediment dynamics and habitat in the southern California chaparral, USA. *Earth Surface Processes and Landforms*, *42*(10), 1482–1492. https://doi.org/10.1002/esp.4117

Formann, E., Egger, G., Hauer, C., & Habersack, H. (2014). Dynamic disturbance regime approach in river restoration: Concept development and application. *Landscape and Ecological Engineering*, *10*(2), 323–337. https://doi.org/10.1007/s11355-013-0228-5

Furman, A. (2008). Modeling Coupled Surface–Subsurface Flow Processes: A Review. *Vadose Zone Journal*, *7*(2), 741–756. https://doi.org/10.2136/vzj2007.0065

Graham, D. N., & Butts, M. B. (2006). *Flexible, integrated watershed modeling with MIKE SHE*. In Watershed Models, Eds. C.P. Singh & D.K. Frevert Pages 245-272, CRC Press. ISBN: 0849336090.

Gray, D. D. (2016). *A First Course in Fluid Mechanics For Civil Engineers* (2nd ed.). Water Resources Publishing. ISBN 13: 978-1-887201-8-72.

Gregory, S. V., Swanson, F. J., McKee, W. A., & Cummins, K. W. (1991). An Ecosystem Perspective of Riparian Zones. *BioScience*, *41*(8), 540–551. https://doi.org/10.2307/1311607

UNSW Connected Waters Initiative. (2017). Groundwater Levels and Aquifer Storage. https://www.connectedwaters.unsw.edu.au/schools-resources/fact-sheets/groundwater-levels-and-aquifer-storage

Harbaugh, A. W. (2005). MODFLOW-2005: The U.S. Geological Survey modular ground-water model--the ground-water flow process. *Techniques and Methods*, Article 6-A16. https://doi.org/10.3133/tm6A16

Hill, M. C., Banta, E. R., Harbaugh, A. W., & Anderman, E. R. (2000). MODFLOW-2000, the U.S. Geological Survey modular ground-water model; user guide to the observation, sensitivity, and parameter-estimation processes and three post-processing programs. In *Open-File Report* (Nos. 2000–184; pp. 1–209). U.S. Geological Survey. https://doi.org/10.3133/ofr00184

Huayhuaca, C., Cheng, A., Beeton, T., Sanderson, J., Barton, A., Kimple, A., Colavito, M., Zebrowski, J., & Dunn, J. (2023). Preparing landscapes and communities to receive and recover from wildfire through collaborative readiness. *Southwest Ecological Restoration Institutes*.

Hunt, R. J., Walker, J. F., Selbig, W. R., Westenbroek, S. M., & Regan, R. S. (2013). Simulation of climate-change effects on streamflow, lake water budgets, and stream temperature using GSFLOW and SNTEMP, Trout Lake Watershed, Wisconsin. In *Scientific Investigations Report* (Nos. 2013–5159). U.S. Geological Survey. https://doi.org/10.3133/sir20135159

Jarrett, R. D. (1984). Hydraulics of High-Gradient Streams. *Journal of Hydraulic Engineering*, *110*(11), 1519–1539. https://doi.org/10.1061/(ASCE)0733-9429(1984)110:11(1519)

Kurth, A.-M., Weber, C., & Schirmer, M. (2015). How effective is river restoration in re-establishing groundwater–surface water interactions? – A case study. *Hydrology and Earth System Sciences*, *19*(6), 2663–2672. https://doi.org/10.5194/hess-19-2663-2015

Lai, Yong G. (2020). SRH-2D User's Manual: Sediment Transport and Mobile-Bed Modeling. United States Bureau of Reclamation.

Lewandowski, J., Meinikmann, K., & Krause, S. (2020). Groundwater-Surface Water Interactions: Recent Advances and Interdisciplinary Challenges. Water, 12(1), 296. https://doi.org/10.3390/w12010296

Markstrom, S. L., Niswonger, R. G., Regan, R. S., Prudic, D. E., & Barlow, P. M. (2008). *GSFLOW—Coupled Ground-Water and Surface-Water Flow Model Based on the Integration of the Precipitation-Runoff Modeling System (PRMS) and the Modular Ground-Water Flow Model (MODFLOW-2005)*. https://pubs.usgs.gov/tm/tm6d1/

Marshall, A., Zhang, X., Sawyer, A. H., Wohl, E., & Singha, K. (2023). Logjam characteristics as drivers of transient storage in headwater streams. *Water Resources Research*, 59, e2022WR033139. https://doi.org/10.1029/2022WR033139

McCluney, K. E., Poff, N. L., Palmer, M. A., Thorp, J. H., Poole, G. C., Williams, B. S., Williams, M. R., & Baron, J. S. (2014). Riverine macrosystems ecology: Sensitivity, resistance, and resilience of whole river basins with human alterations. *Frontiers in Ecology and the Environment*, *12*(1), 48–58. https://doi.org/10.1890/120367

Nathan, A. (2024). Emlid Reach RS2+ Review & RTK Set Up. *Point One Navigation. https://pointonenav.com/news/easy-rtk-setup-on-the-emlid-reach-rs2-with-polaris-rtk/.*

Niswonger, R. G., Panday, S., & Ibaraki, M. (2011). MODFLOW-NWT, a Newton formulation for MODFLOW-2005. In *Techniques and Methods* (Nos. 6-A37). U.S. Geological Survey. https://doi.org/10.3133/tm6A37

Niswonger, R. G., Prudic, D. E., & Regan, R. S. (2006). Documentation of the Unsaturated-Zone Flow (UZF1) Package for modeling Unsaturated Flow Between the Land Surface and the

Water Table with MODFLOW-2005. *Techniques and Methods*, Article 6-A19. https://doi.org/10.3133/tm6A19

Ntona, M. M., Busico, G., Mastrocicco, M., & Kazakis, N. (2022). Modeling groundwater and surface water interaction: An overview of current status and future challenges. *Science of The Total Environment*, *846*, 157355. https://doi.org/10.1016/j.scitotenv.2022.157355

Oliver, T. H., Heard, M. S., Isaac, N. J. B., Roy, D. B., Procter, D., Eigenbrod, F., Freckleton, R., Hector, A., Orme, C. D. L., Petchey, O. L., Proença, V., Raffaelli, D., Suttle, K. B., Mace, G. M., Martín-López, B., Woodcock, B. A., & Bullock, J. M. (2015). Biodiversity and Resilience of Ecosystem Functions. *Trends in Ecology & Evolution*, *30*(11), 673–684. https://doi.org/10.1016/j.tree.2015.08.009

Parise, M., & Cannon, S. H. (2012). Wildfire impacts on the processes that generate debris flows in burned watersheds. *Natural Hazards*, *61*(1), 217–227. https://doi.org/10.1007/s11069-011-9769-9

Petticrew, E. L., Owens, P. N., & Giles, T. R. (2006). Wildfire Effects on the Quantity and Composition of Suspended and Gravel-Stored Sediments. In B. Kronvang, J. Faganeli, & N. Ogrinc (Eds.), *The Interactions Between Sediments and Water* (pp. 283–292). Springer Netherlands. https://doi.org/10.1007/978-1-4020-5478-5_29

Pettit, N. E., & Naiman, R. J. (2007). Fire in the Riparian Zone: Characteristics and Ecological Consequences. *Ecosystems*, *10*(5), 673–687. https://doi.org/10.1007/s10021-007-9048-5

Pugh, B. E., Colley, M., Dugdale, S. J., Edwards, P., Flitcroft, R., Holz, A., Johnson, M., Mariani, M., Means-Brous, M., Meyer, K., Moffett, K. B., Renan, L., Schrodt, F., Thorne, C., Valman, S., Wijayratne, U., & Field, R. (2022). A possible role for river restoration

enhancing biodiversity through interaction with wildfire. *Global Ecology and Biogeography*, *31*(10), 1990–2004. https://doi.org/10.1111/geb.13555

Reneau, S. L., Katzman, D., Kuyumjian, G. A., Lavine, A., & Malmon, D. V. (2007). Sediment delivery after a wildfire. *Geology*, *35*(2), 151–154. https://doi.org/10.1130/G23288A.1

Rhoades, C. C., Nunes, J. P., Silins, U., & Doerr, S. H. (2019). The influence of wildfire on water quality and watershed processes: New insights and remaining challenges. *International Journal of Wildland Fire*, *28*(10), 721–725. https://doi.org/10.1071/WFv28n10_FO

Rosell, F., Bozsér, O., Collen, P., & Parker, H. (2005). Ecological impact of beavers Castor fiber and Castor canadensis and their ability to modify ecosystems. *Mammal Review*, *35*(3–4), 248–276. https://doi.org/10.1111/j.1365-2907.2005.00067.x

Sahoo, G. B., Ray, C., & De Carlo, E. H. (2006). Calibration and validation of a physically distributed hydrological model, MIKE SHE, to predict streamflow at high frequency in a flashy mountainous Hawaii stream. *Journal of Hydrology*, *327*(1), 94–109. https://doi.org/10.1016/j.jhydrol.2005.11.012

Scamardo, J., Munger, W., Loria, K., Nauman, B., Wang, J., Leopold, S., Heggli, A., Huntly, N., Baker, M., & Meadow, A. M. (2025). Trends in the Outcomes, Practice, and Law of Low-Tech Process-Based Restoration in Western Rangelands. *Rangeland Ecology & Management*, *98*, 344–356. https://doi.org/10.1016/j.rama.2024.08.032

Scamardo, J., & Wohl, E. (2020). Sediment storage and shallow groundwater response to beaver dam analogues in the Colorado Front Range, USA. *River Research and Applications*, *36*(3), 398–409. https://doi.org/10.1002/rra.3592

Sevier, E. C., Pope, K. L., Dralle, D. N., Wagenbrenner, J. W., Cummings, A. K., Richardson, P., & Lang, M. (2024). Rapid Hydrological Responses Following Process-Based Restoration

in a Degraded Sierra Nevada Meadow. *Hydrological Processes*, *38*(11), e70005. https://doi.org/10.1002/hyp.70005

Shakesby, R. A., & Doerr, S. H. (2006). Wildfire as a hydrological and geomorphological agent. *Earth-Science Reviews*, *74*(3), 269–307. https://doi.org/10.1016/j.earscirev.2005.10.006

Soil Survey Staff, Natural Resources Conservation Service, United States Department of Agriculture. Web Soil Survey. Available online at the following link: http://websoilsurvey.sc.egov.usda.gov/. Accessed 2024.

Stanford, J. A., Ward, J. V., Liss, W. J., Frissell, C. A., Williams, R. N., Lichatowich, J. A., & Coutant, C. C. (1996). A General Protocol for Restoration of Regulated Rivers. *Regulated Rivers: Research & Management*, *12*(4–5), 391–413. https://doi.org/10.1002/(SICI)1099-1646(199607)12:4/5<391::AID-RRR436>3.0.CO;2-4

Svejcar, T. (1997). Riparian Zones: 1) What Are They and How Do They Work? *Rangelands*.

Swain, A. N. (2021). *Modeling the Groundwater Basin in the Northern Cities Management Area* [M.Sc., California Polytechnic State University]. https://www.proquest.com/docview/2838439304/abstract/91AC4DBE541446BPQ/1

Swanson, F. J. (1981). Fire and geomorphic processes. *Mooney, HA; Bonnicksen, TM; Christensen, NL; Lotan, JE*, 401–420.

Swanson, F. J., Kratz, T. K., Caine, N., & Woodmansee, R. G. (1988). Landform Effects on Ecosystem Patterns and Processes. *BioScience*, *38*(2), 92–98. https://doi.org/10.2307/1310614

Talebmorad, H., & Ostad-Ali-Askari, K. (2022). Hydro geo-sphere integrated hydrologic model in modeling of wide basins. *Sustainable Water Resources Management*, *8*. https://doi.org/10.1007/s40899-022-00689-y

Warrick, J. A., Hatten, J. A., Pasternack, G. B., Gray, A. B., Goni, M. A., & Wheatcroft, R. A. (2012). The effects of wildfire on the sediment yield of a coastal California watershed. *GSA Bulletin*, *124*(7–8), 1130–1146. https://doi.org/10.1130/B30451.1

Waseem, M., Kachholz, F., Klehr, W., & Tränckner, J. (2020). Suitability of a Coupled Hydrologic and Hydraulic Model to Simulate Surface Water and Groundwater Hydrology in a Typical North-Eastern Germany Lowland Catchment. *Applied Sciences*, *10*(4), Article 4. https://doi.org/10.3390/app10041281

Wheaton, J., Bennett, S., Bouwes, N., Maestas, J., & Shahverdian, S. (2019). *Low-Tech Process-Based Restoration of Riverscapes: Design Manual. Version 1.0*. https://doi.org/10.13140/RG.2.2.19590.63049/2

Wohl, E., Fryirs, K., Grabowski, R. C., Morrison, R. R., & Sear, D. (2024). Enhancing the natural absorbing capacity of rivers to restore their resilience. *BioScience*, *74*(11), 782–796. https://doi.org/10.1093/biosci/biae090

Wohl, E., Kramer, N., Ruiz-Villanueva, V., Scott, D. N., Comiti, F., Gurnell, A. M., Piegay, H., Lininger, K. B., Jaeger, K. L., Walters, D. M., & Fausch, K. D. (2019). The Natural Wood Regime in Rivers. *BioScience*, *69*(4), 259–273. https://doi.org/10.1093/biosci/biz013

Wohl, E., Lininger, K. B., & Scott, D. N. (2018). River beads as a conceptual framework for building carbon storage and resilience to extreme climate events into river management. *Biogeochemistry*, *141*(3), 365–383.

Wohl, E., Marshall, A. E., Scamardo, J., White, D., & Morrison, R. R. (2022). Biogeomorphic influences on river corridor resilience to wildfire disturbances in a mountain stream of the Southern Rockies, USA. *Science of The Total Environment*, *820*, 153321. https://doi.org/10.1016/j.scitotenv.2022.153321

Wolman, M. G. (1954). A method of sampling coarse river-bed material. *Eos, Transactions American Geophysical Union*, *35*(6), 951–956. https://doi.org/10.1029/TR035i006p00951

Wunder, S., Lehmann, B., & Nestmann, F. (2011). Determination of the drag coefficients of emergent and just submerged willows. *International Journal of River Basin Management*, *9*(3–4), 231–236. https://doi.org/10.1080/15715124.2011.637499

APPENDIX A: DATA PROCESSING

A.1 Groundwater Well Data

When the data from the HOBO loggers were downloaded, the well was bailed to remove any sediment that may affect the data. The elevations of each logger within the well were known by surveying in the cap of the groundwater well using real time kinetic positioning (RTK) survey then measuring the distance from the top of the cap to the logger. Temperature of the water affects the water density therefore the following equations from (Gray, 2016) were used to determine the water density as temperature varied:

$$\rho = \frac{a}{(1 + 18.159725x10^{-3}T)}$$

$$a = (999.8396 + 18.224944T - 0.00792221T^2 - 55.44846x10^{-6}T^3 + 149.7562x10^{-9}T^4 - 393.2952x10^{-12}T^5)$$

The water stage (or depth) above the logger in the well was calculated using the following equation:

$$h = \frac{p}{\rho g}$$

where h is water depth, p is pressure, ρ is water density, and g is gravity.

APPENDIX B: SUPPLEMENTAL CALIBRATION METRICS

The following tables represent calibration metrics for each individual well. The naming nomenclature includes the groundwater well transect (T1 through T5), which side of the stream they are on (Tx.1 – Stream Left Floodplain, Tx.2 – Stream Left Near the Channel, Tx.3 – Stream Right near the Channel, and Tx.4 – Stream Right Floodplain).

Table B-1: Calibration Metrics for Each Well Including All Data

Observation	R2	RMSE (m)
T1.2	0.045659	1.012883
T1.3	0.0480668	1.144436
T1.4	0.0103329	2.429805
T2.4	0.0025563	5.678717
T2.3	0.003195	2.271913
T2.1	0.0322574	3.809762
T3.1	0.0038279	6.024937
T3.2	0.0595806	1.82569
T3.3	0.0419147	1.779091
T3.4	0.0030098	6.766323
T4.1	0.0073136	2.615344
T4.3	0.0395709	0.803093
T4.2	0.0809238	0.780767
T4.4	0.0040204	1.546676
T5.3	0.0171491	0.88934
T5.2	0.120587	0.369073
T5.1	0.0066895	1.767873

Table B-2: Calibration Metrics for Each Well Excluding 30.48 m. Spikes

Observation	R2	RMSE (m)
T1.2	0.045659	1.012883
T1.3	0.0480668	1.144436
T1.4	0.0103329	2.429805
T2.4	0.0183315	1.959737
T2.3	0.003195	2.271913
T2.1	0.0322574	3.809762
T3.1	0.0224125	1.641556
T3.2	0.0595806	1.82569
T3.3	0.0419147	1.779091
T3.4	2.051E-05	2.735651
T4.1	0.0073136	2.615344
T4.3	0.0395709	0.803093
T4.2	0.0809238	0.780767
T4.4	0.0040204	1.546676
T5.3	0.0171491	0.88934
T5.2	0.120587	0.369073
T5.1	0.0066895	1.767873

Table B-3: Calibration Metrics for Each Well Excluding 1.83 m. Spikes

Observation	R2	RMSE (m)
T1.2	0.2933982	0.235598
T1.3	0.4114925	0.344388
T1.4	0.2120042	0.253985
T2.4	0.0950216	0.526066
T2.3	0.2373162	0.286202
T2.1	0.099679	0.290677
T3.1	0.0517685	0.449164
T3.2	0.3745956	0.331969
T3.3	0.3885144	0.643043
T3.4	0.0800697	0.72341
T4.1	0.3073052	0.404394
T4.3	0.3278407	0.364138
T4.2	0.3706616	0.50598
T4.4	0.3011567	0.406486
T5.3	0.1965603	0.220263
T5.2	0.4392091	0.291412
T5.1	0.1593876	0.327242

APPENDIX C: SUPPLEMENTAL RESTORATION SCENARIO DATA

Figure C-1 identifies the locations of the relic beaver dams at the Elkhorn Creek study site.

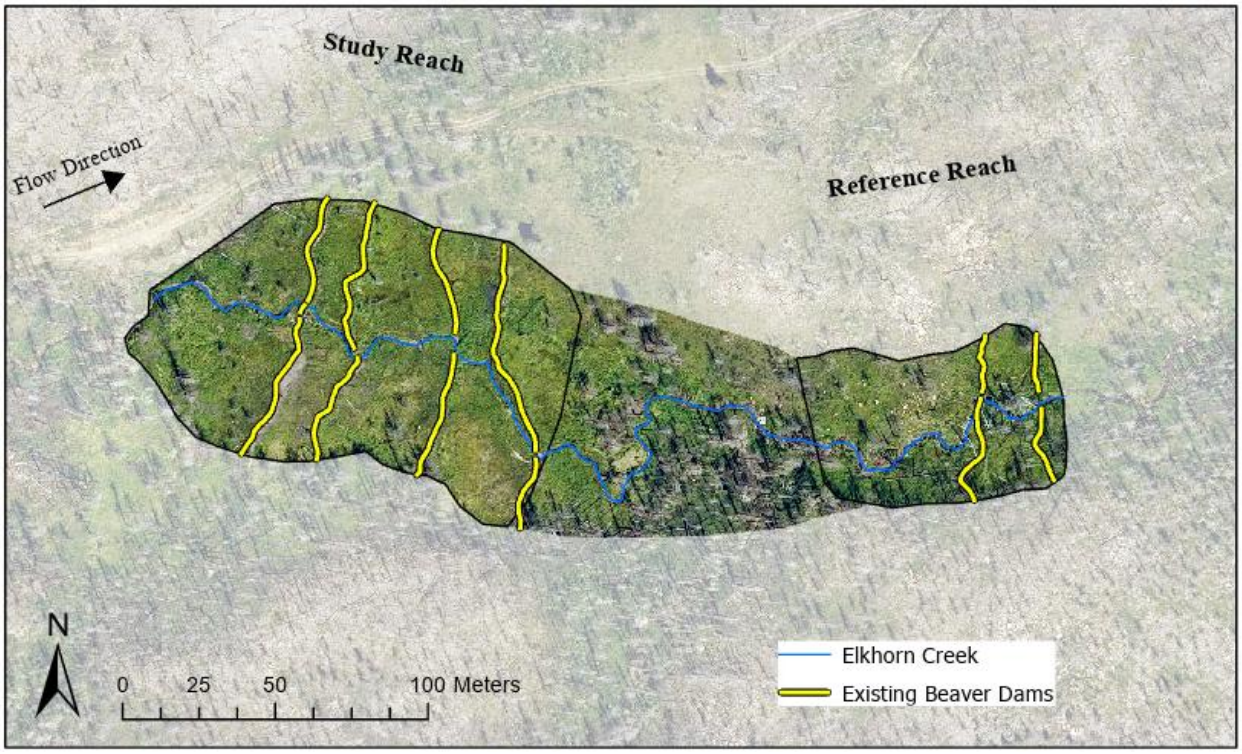

Figure C-1: Existing Beaver Dams at Elkhorn Creek Study Site

PALS were inserted into the hydrodynamic model at different locations based on restoration scenario. Restoration Scenario 1 was not included due to no PALS being inserted. The following figures show the location of PALS based on specified scenario.

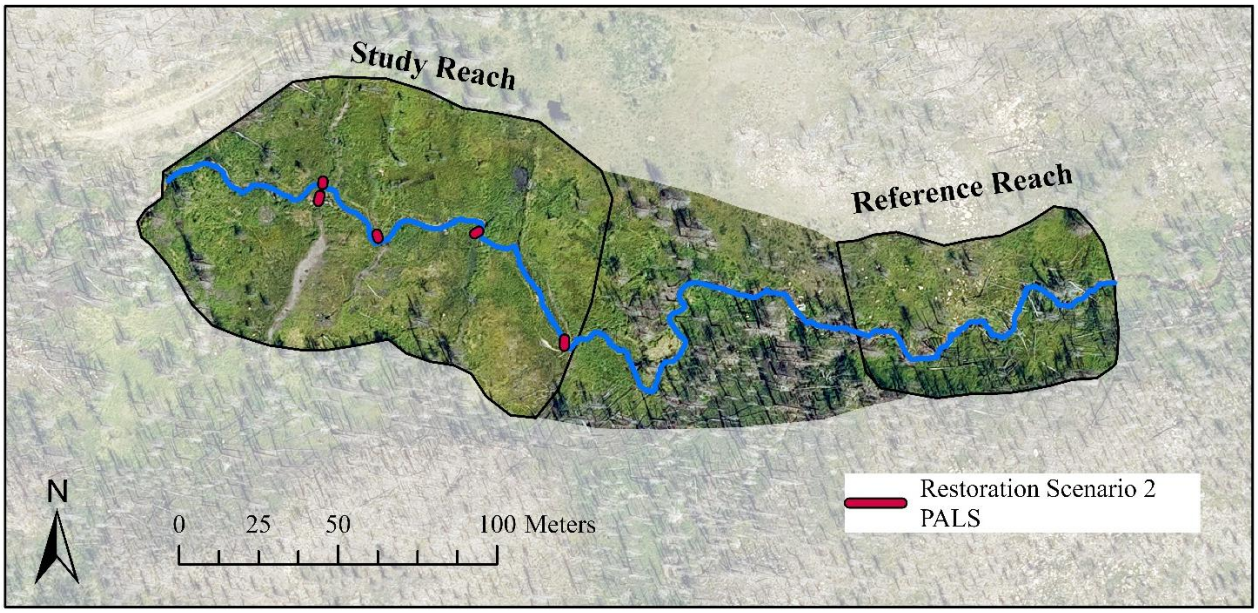

Figure C-2: Restoration Scenario 2 PALS Location

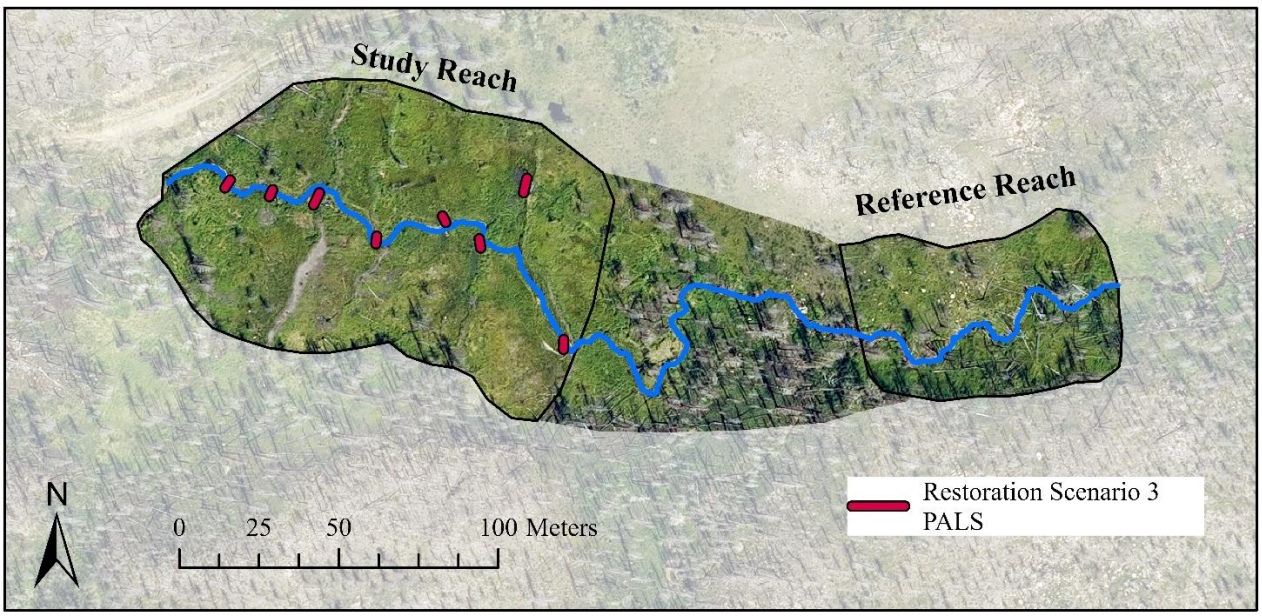

Figure C-3: Restoration Scenario 3 PALS Location

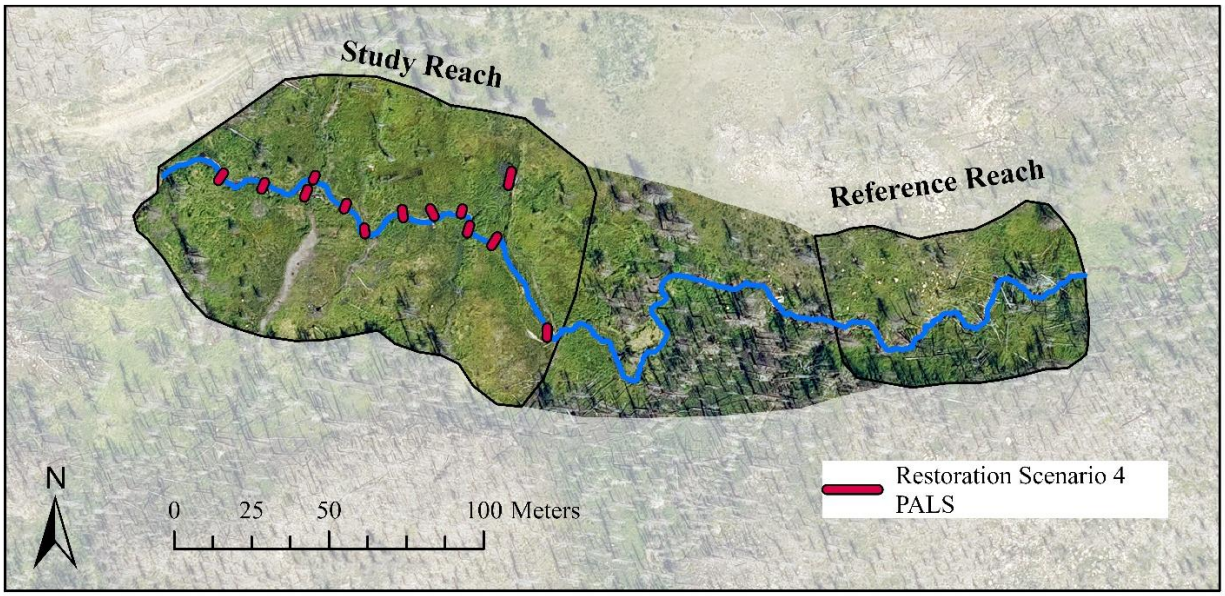

Figure C-4: Restoration Scenario 4 PALS Location

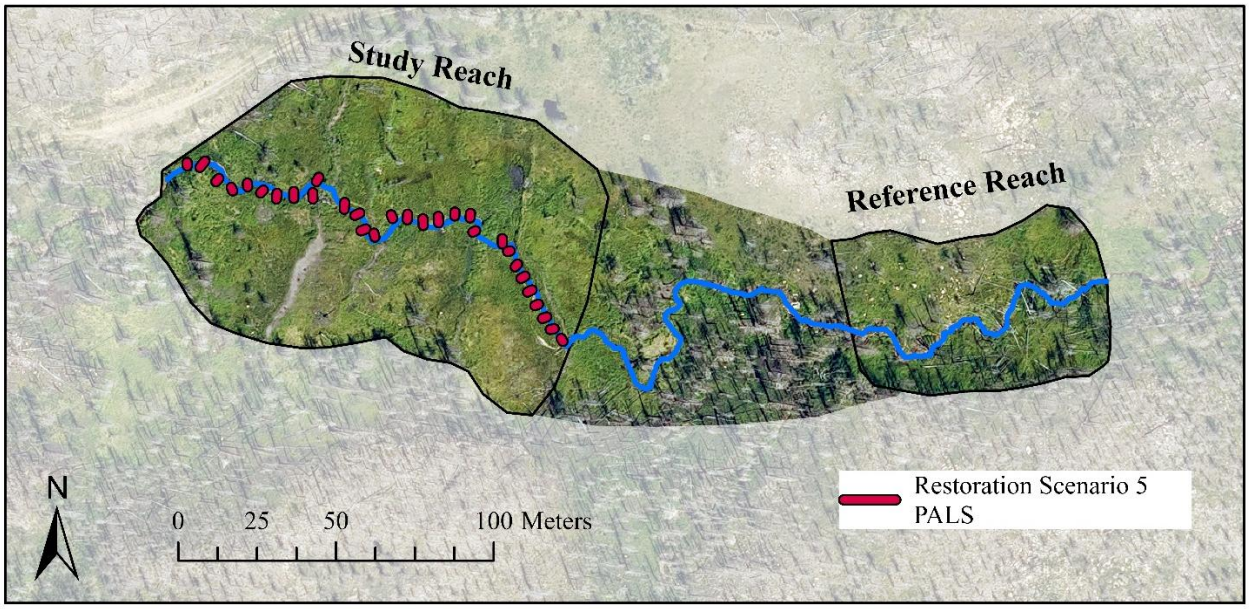

Figure C-5: Restoration Scenario 5 PALS Location

Due to the varying PALS locations between restoration scenarios, the surface water extent also varied in the hydrodynamic model. The following figures represent the surface water extend for each flowrate for each restoration scenario in the MODFLOW-NWT model.

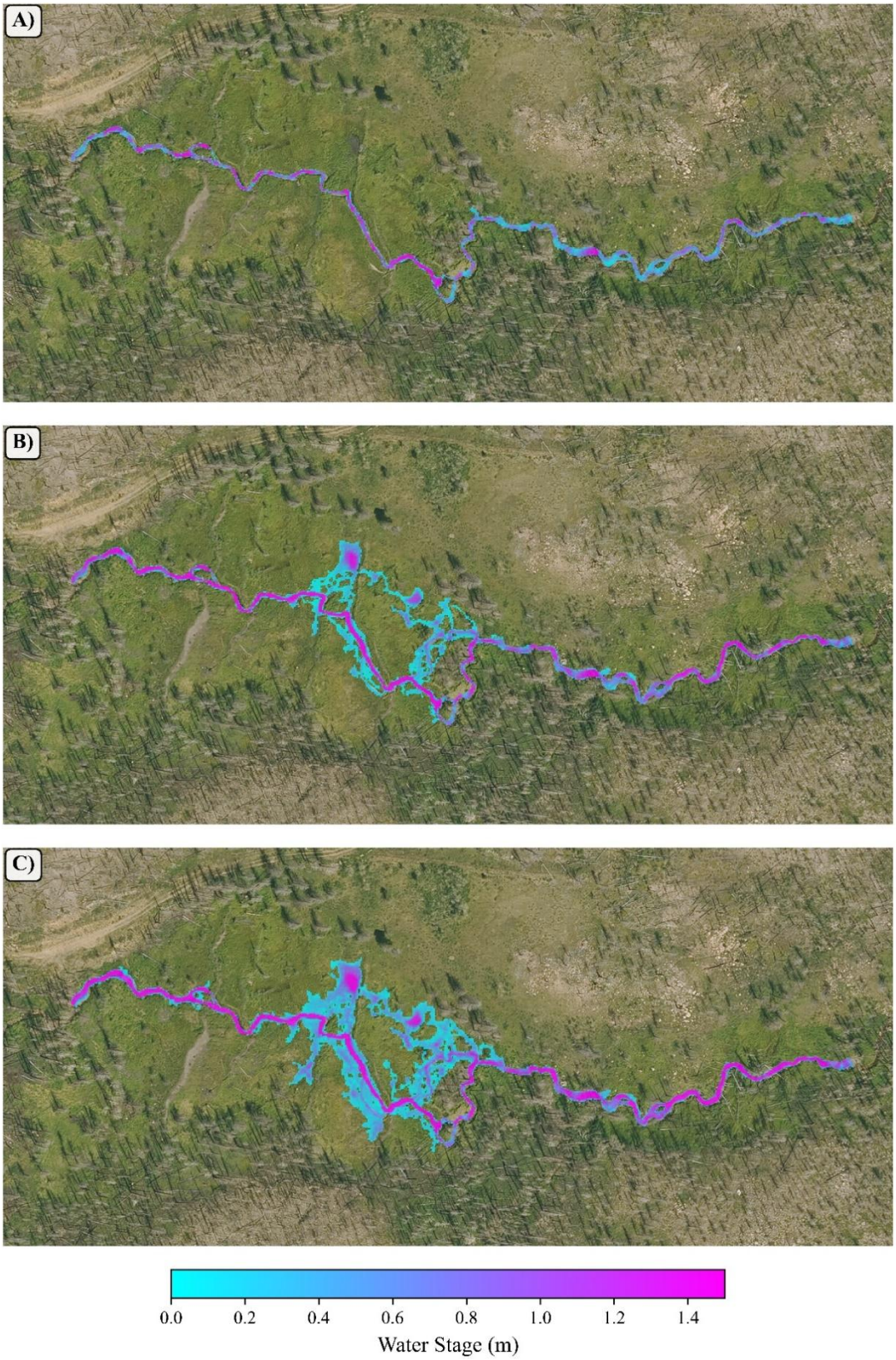

Figure C-6. Restoration Scenario 2 SRH-2D Results. A) Flowrate: 0.11 m^3/s B) Flowrate: 0.34 m^3/s C) Flowrate: 0.57 m^3/s

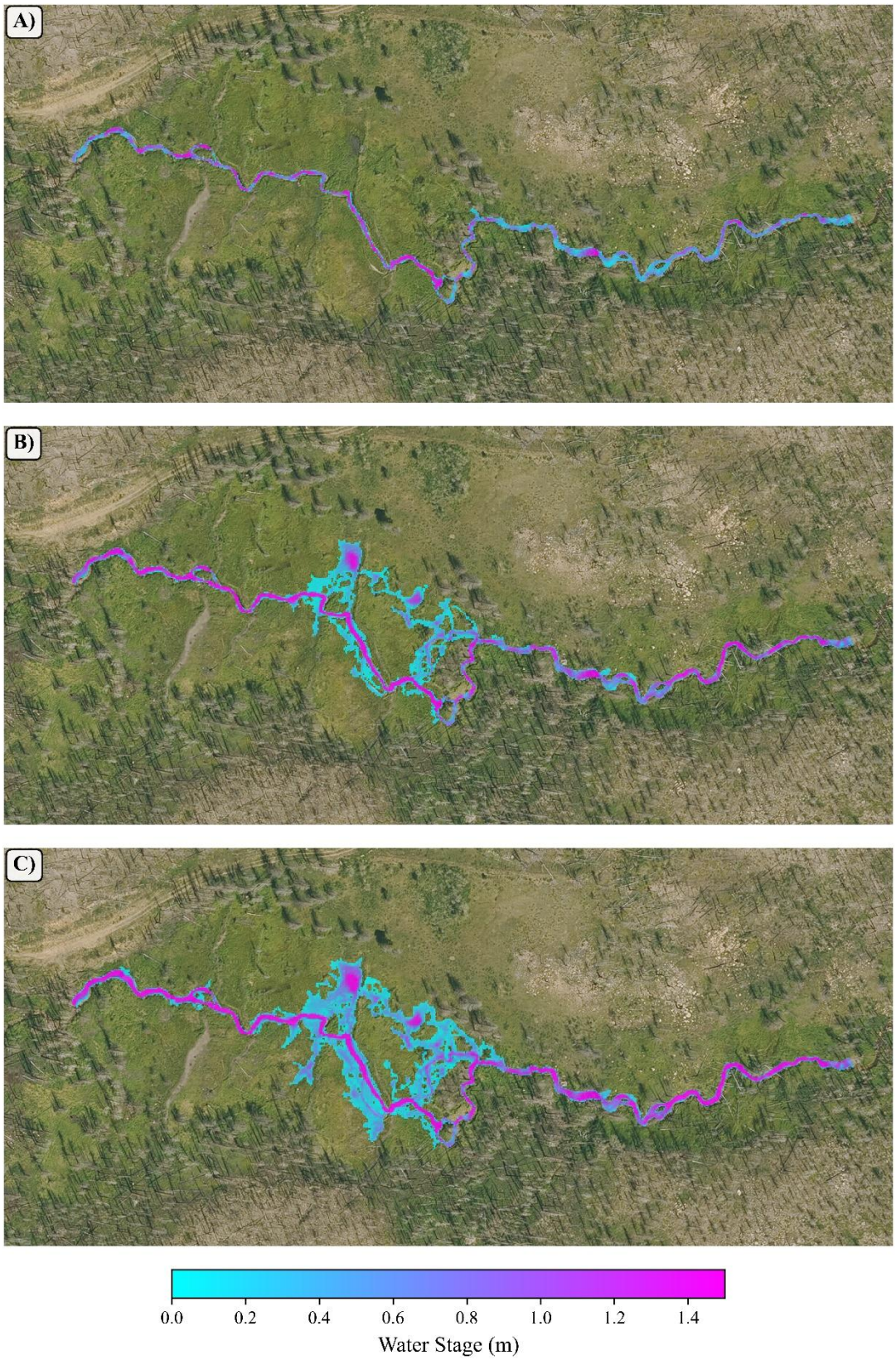

Figure C-7. Restoration Scenario 4 SRH-2D Results A) Flowrate: 0.11 m^3/s B) Flowrate: 0.34 m^3/s C) Flowrate: 0.57 m^3/s

APPENDIX D: SUPPLEMENTAL GROUNDWATER DATA OBSERVATIONS

Additional time series of groundwater elevation data for PALS 3 Groundwater Well Transect, PALS 5 Groundwater Well Transect, and DS 2 Groundwater Well Transect are shown.

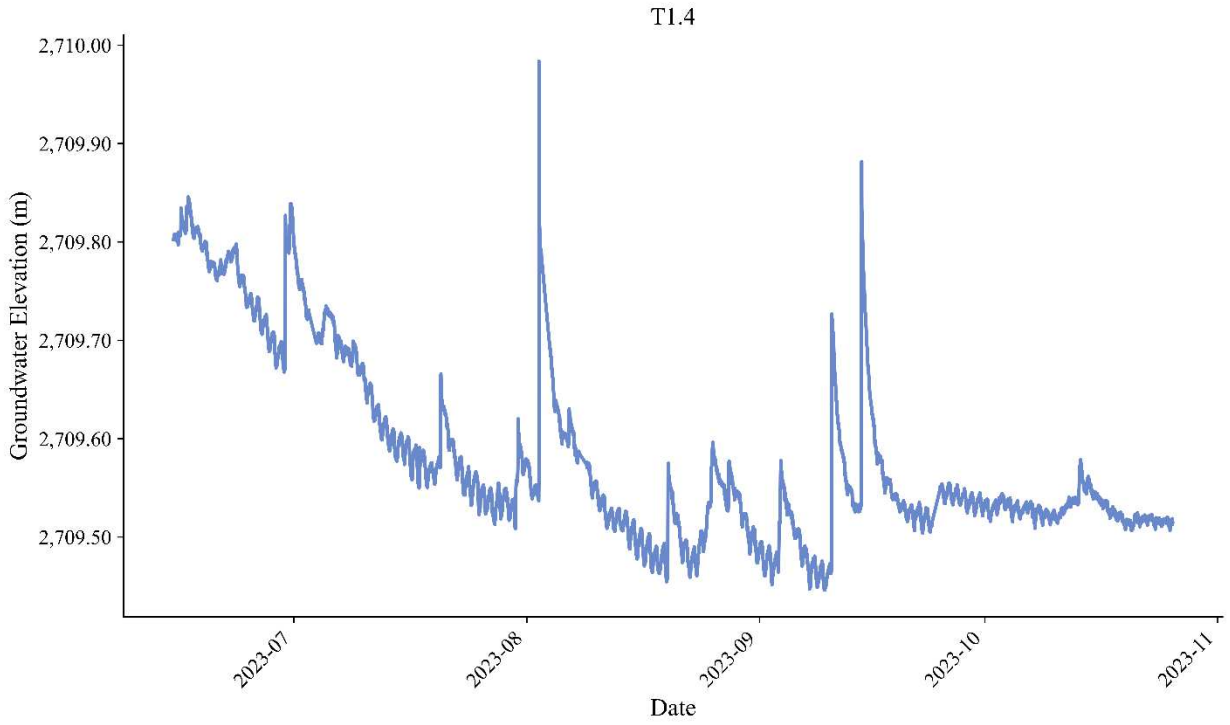

Figure D-1. T1.4 Groundwater Observation Elevations at Transect 1

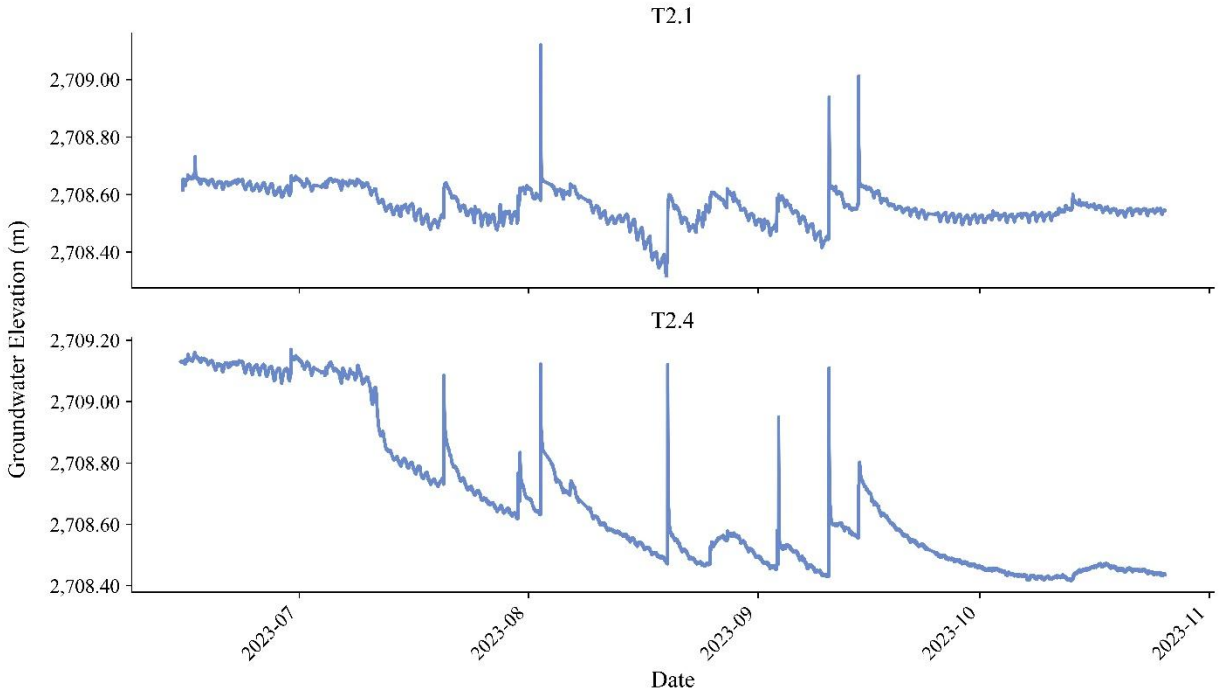

Figure D-2. Groundwater Observation Elevations at Transect 2

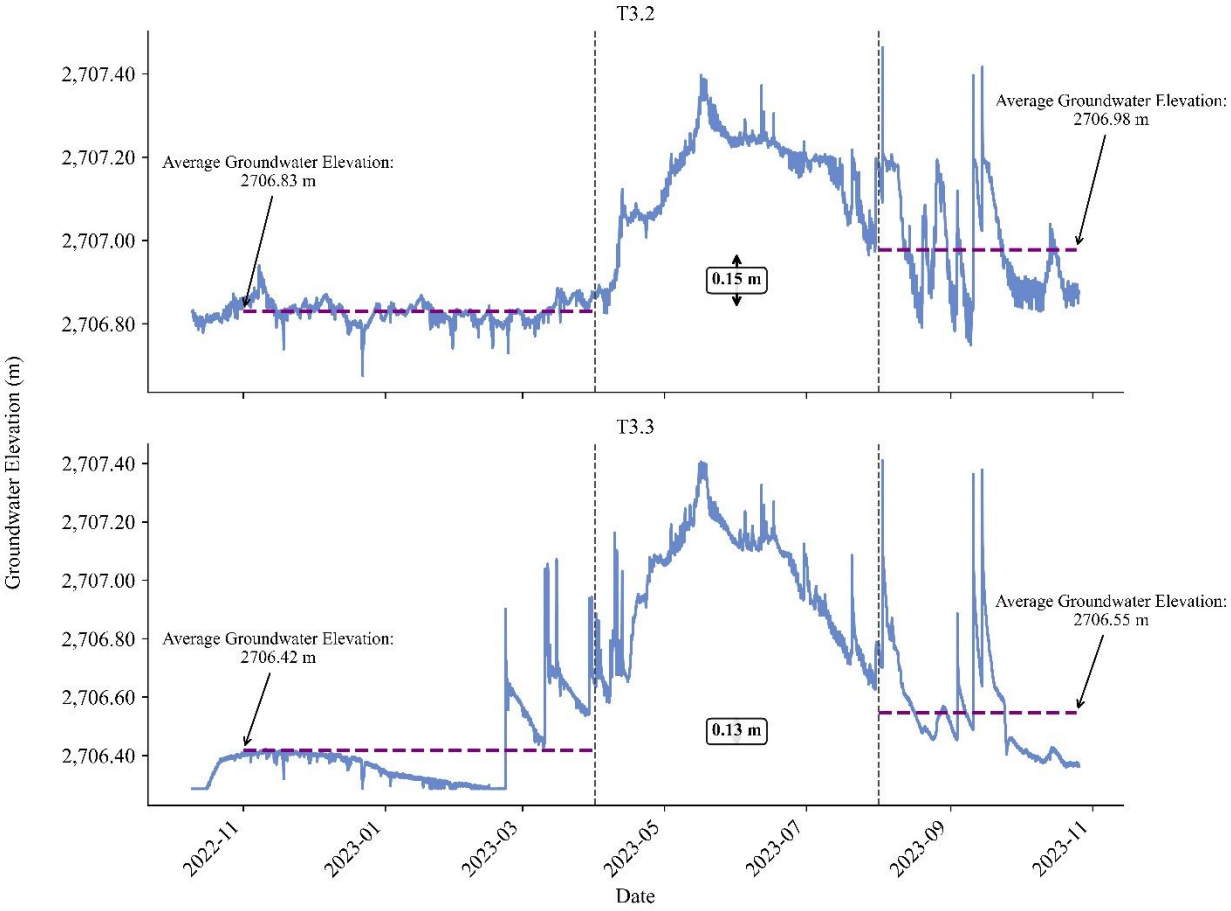

Figure D-3: Groundwater Observation Elevations at Transect 3. Average groundwater elevation showed an increase of 0.15 m (T3.2) and 0.13 m (T3.3) between the pre-runoff baseflow period and the post-runoff baseflow period as indicated by the vertical dotted lines.

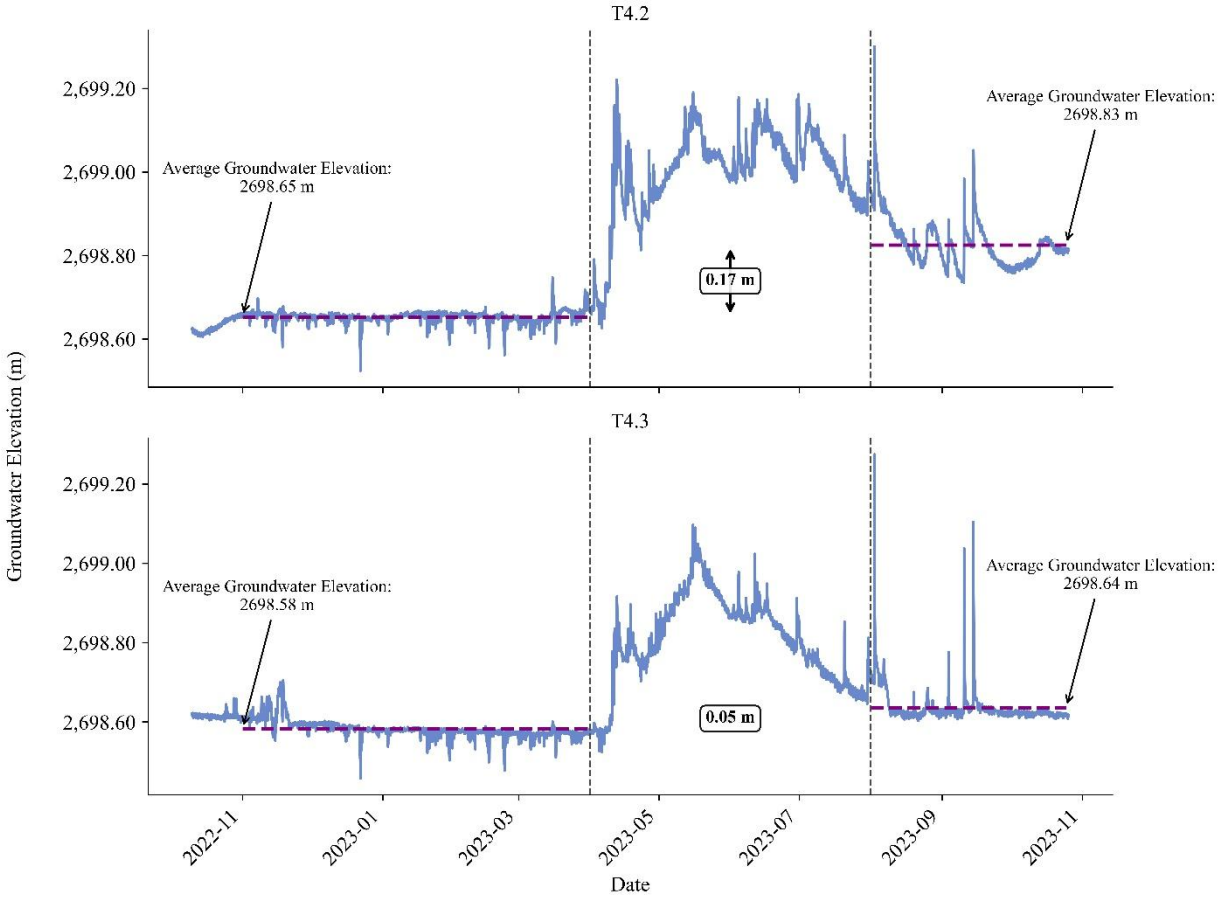

Figure D-4. Groundwater Observation Elevations at Transect 4. Average groundwater elevation showed an increase of 0.17 m (T4.2) and 0.05 m (T4.3) between the pre-runoff baseflow period and the post-runoff baseflow period as indicated by the vertical dotted lines.

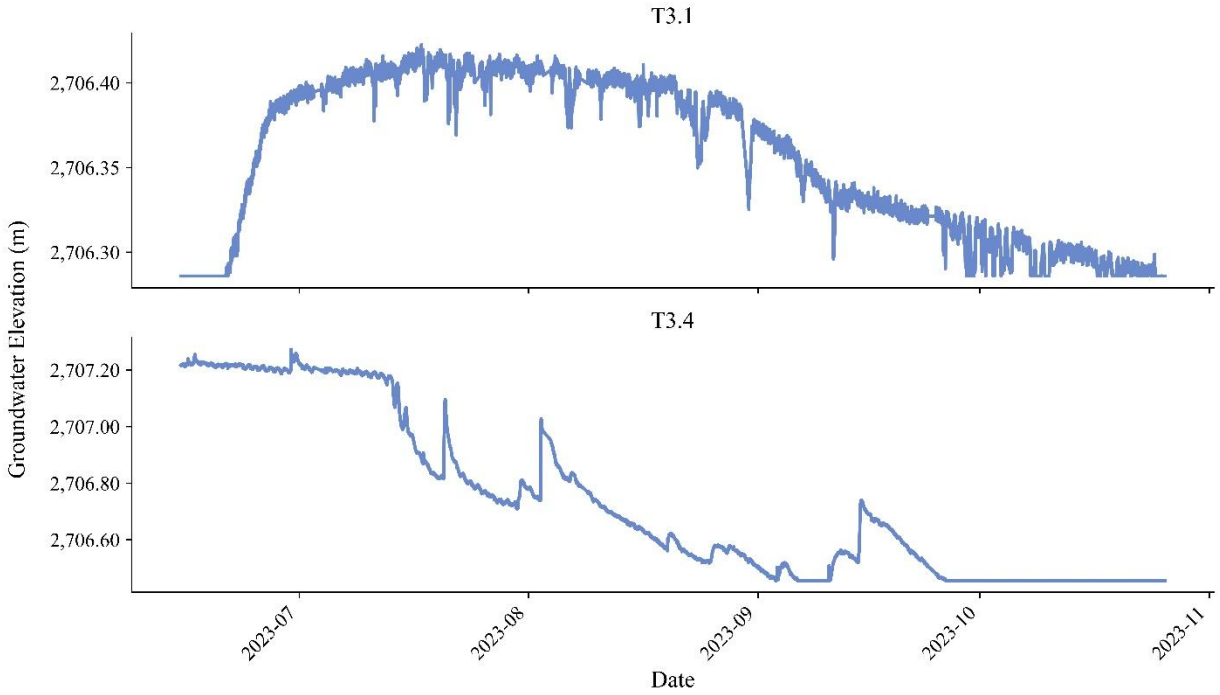

Figure D-5. Groundwater Observation Elevations at Transect 3

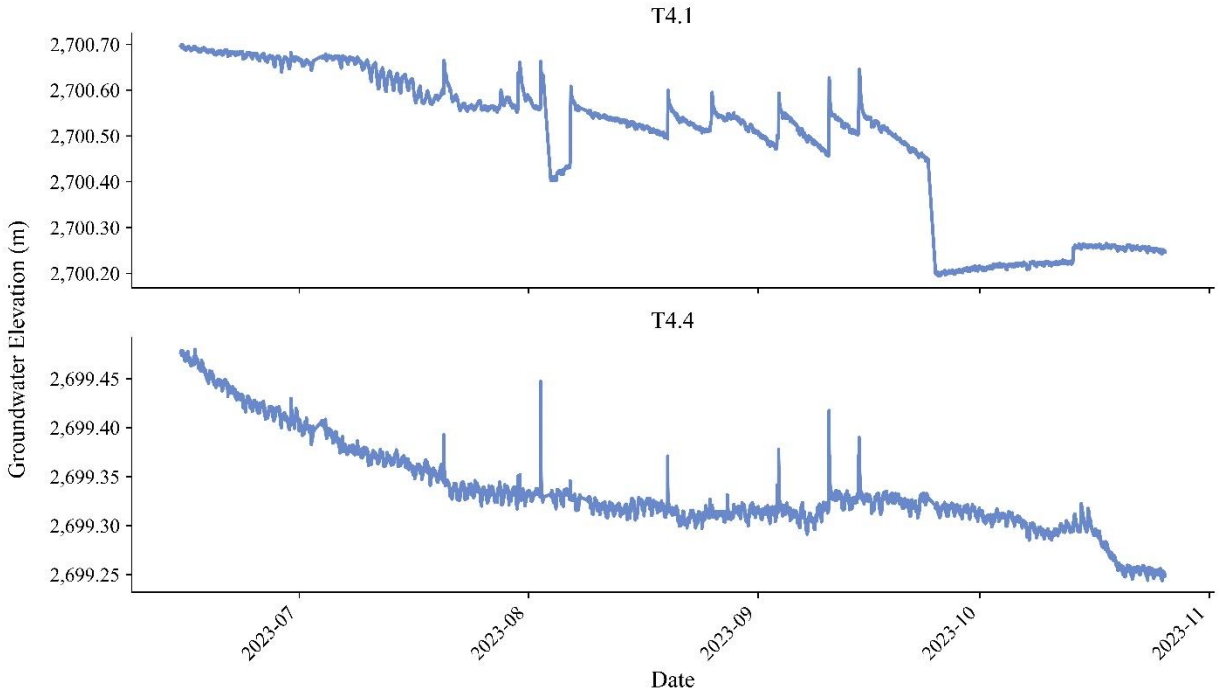

Figure D-6. Groundwater Observation Elevations at Transect 4

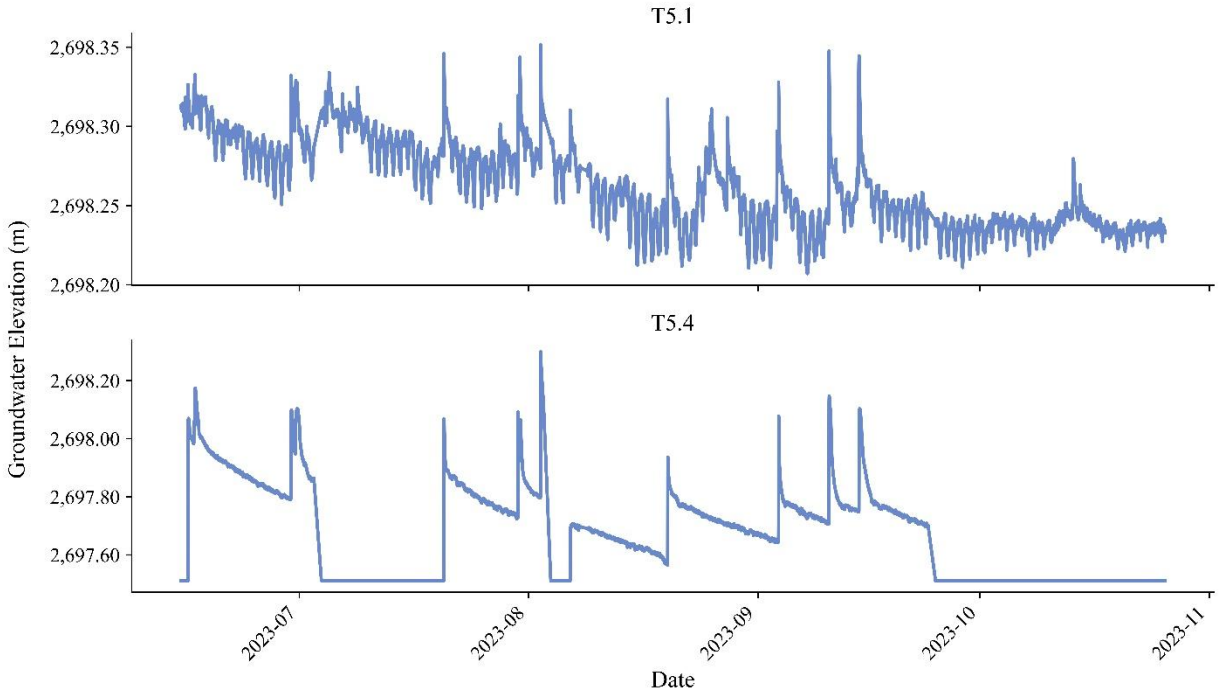

Figure D-7. Groundwater Observation Elevations at Transect 5

APPENDIX E: SEDIMENT SIZE DATA

Wolman pebble counts were conducted to monitor sediment size difference prior to and after restoration. The results are shown below. The first seven figures are surveys done upstream (US) of the PALS while the last seven figures are surveys done downstream (DS) of the PALS.

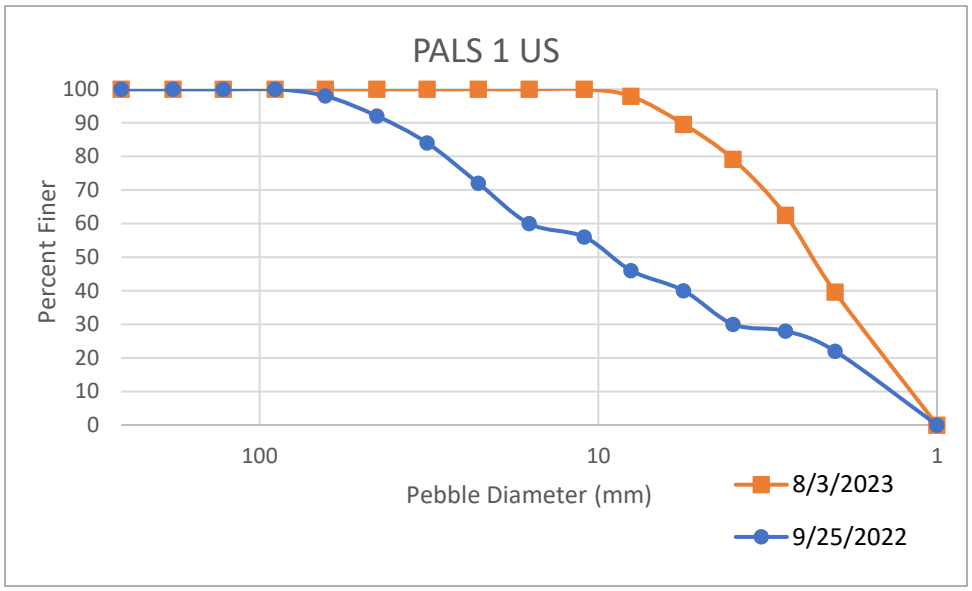

Figure E-1: Grain Size Distribution Upstream of PALS 1

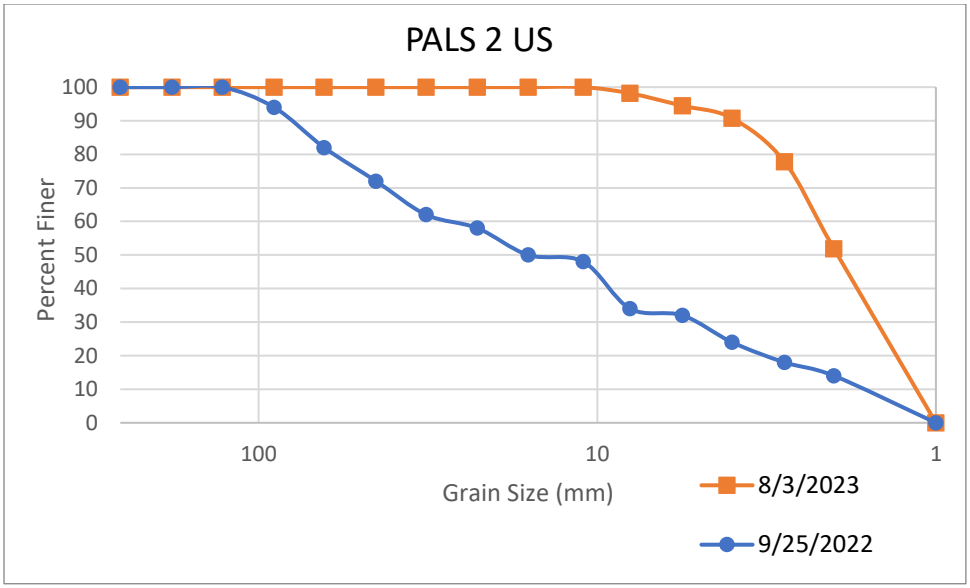

Figure E-2: Grain Size Distribution Upstream of PALS 2

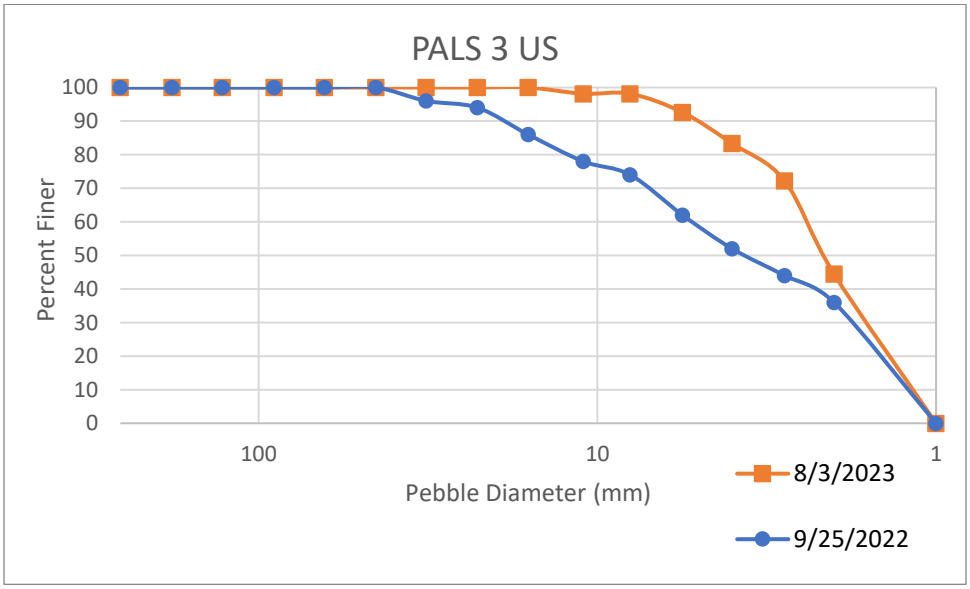

Figure E-3: Grain Size Distribution Upstream of PALS 3

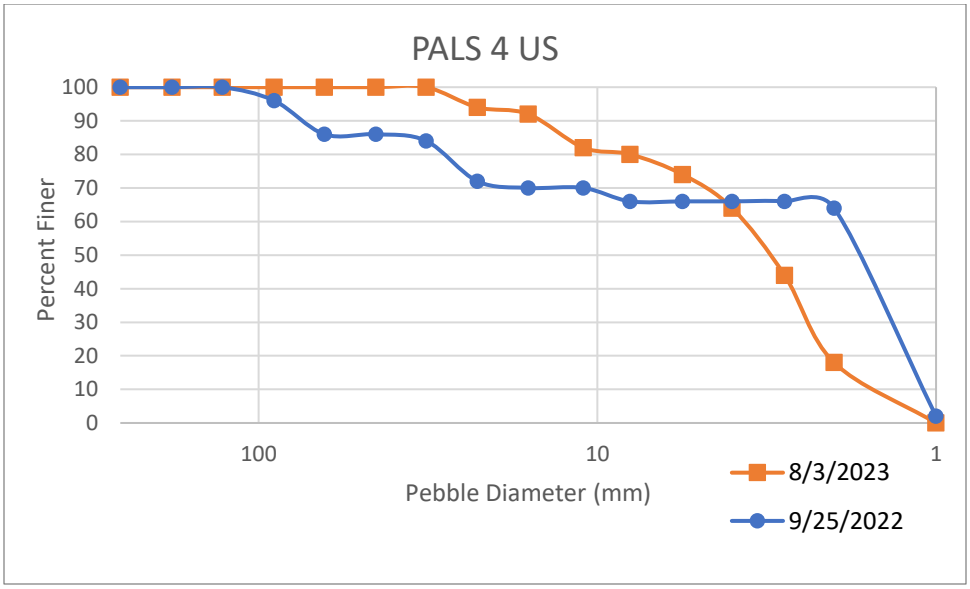

Figure E-4: Grain Size Distribution Upstream of PALS 4

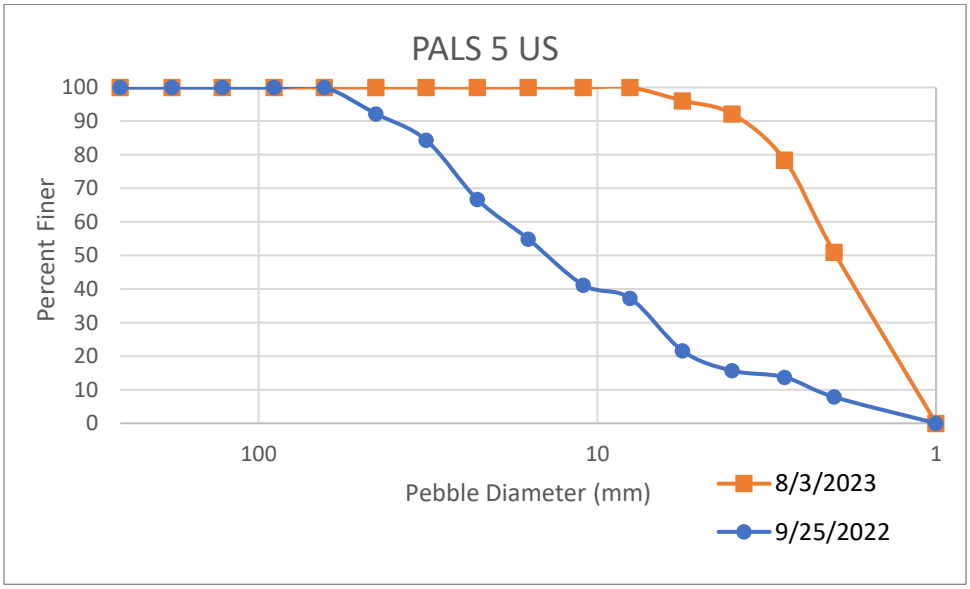

Figure E-5: Grain Size Distribution Upstream of PALS 5

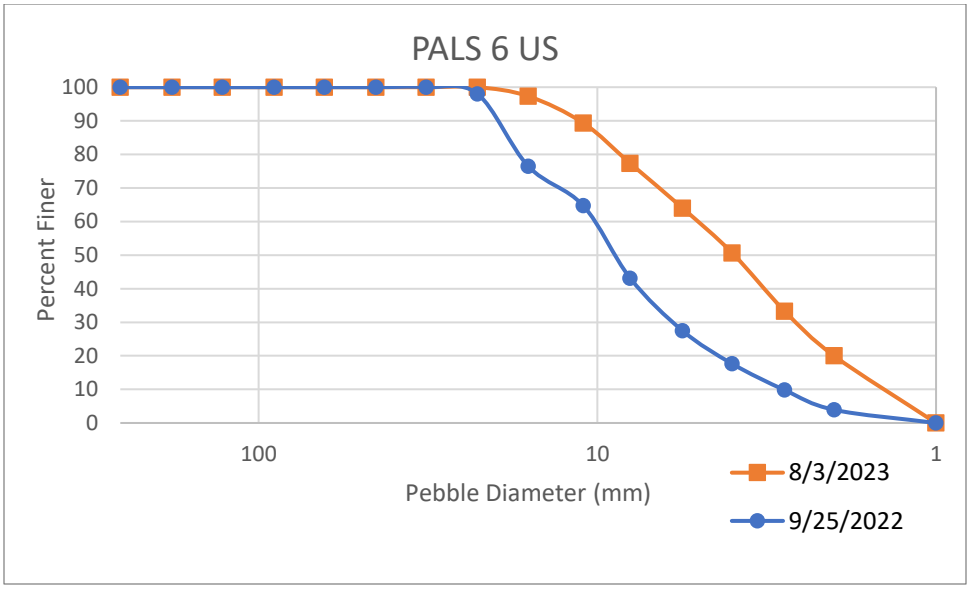

Figure E-6: Grain Size Distribution Upstream of PALS 6

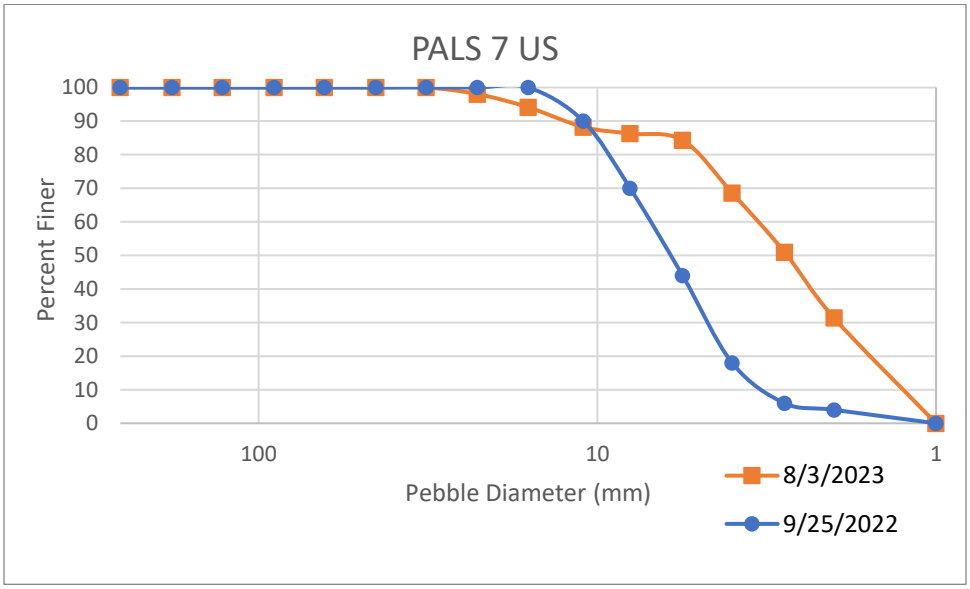

Figure E-7: Grain Size Distribution Upstream of PALS 7

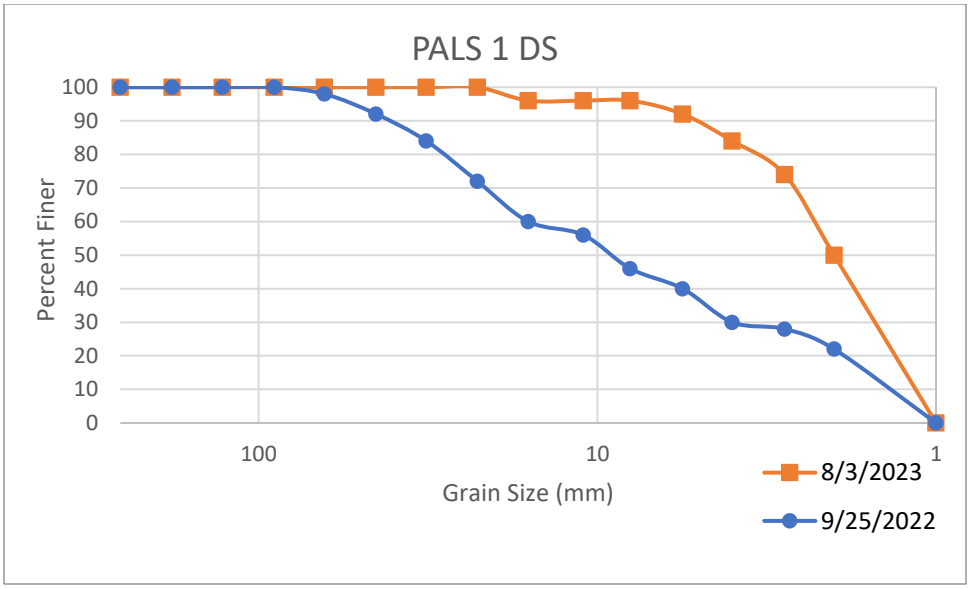

Figure E-8: Grain Size Distribution Downstream of PALS 1

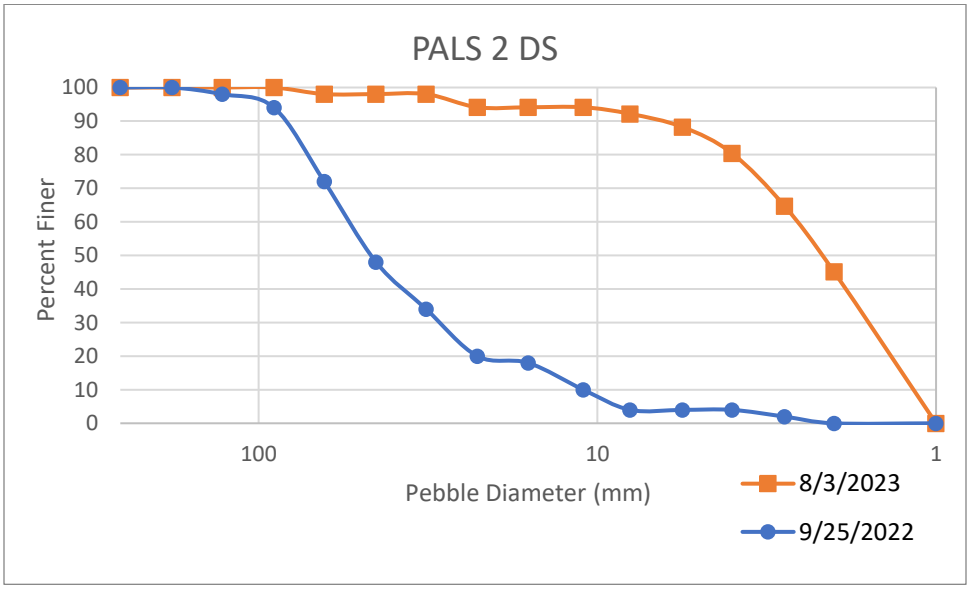

Figure E-9: Grain Size Distribution Downstream of PALS 2

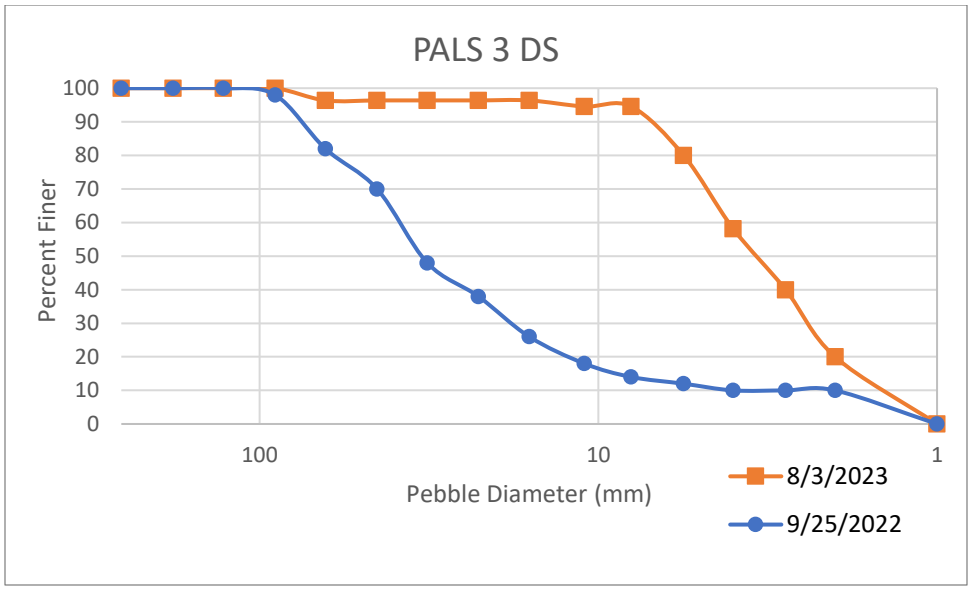

Figure E-10: Grain Size Distribution Downstream of PALS 3

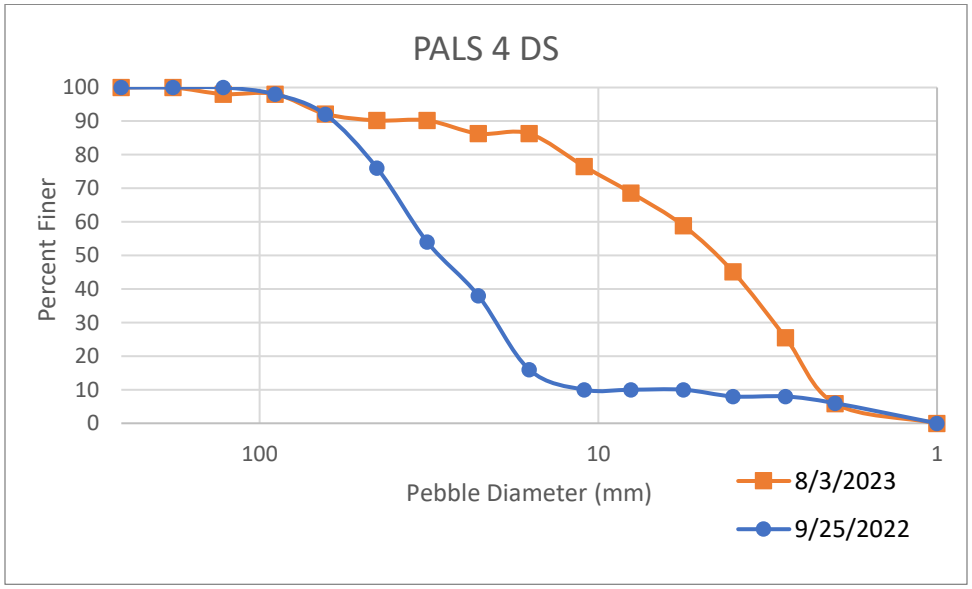

Figure E-11: Grain Size Distribution Downstream of PALS 4

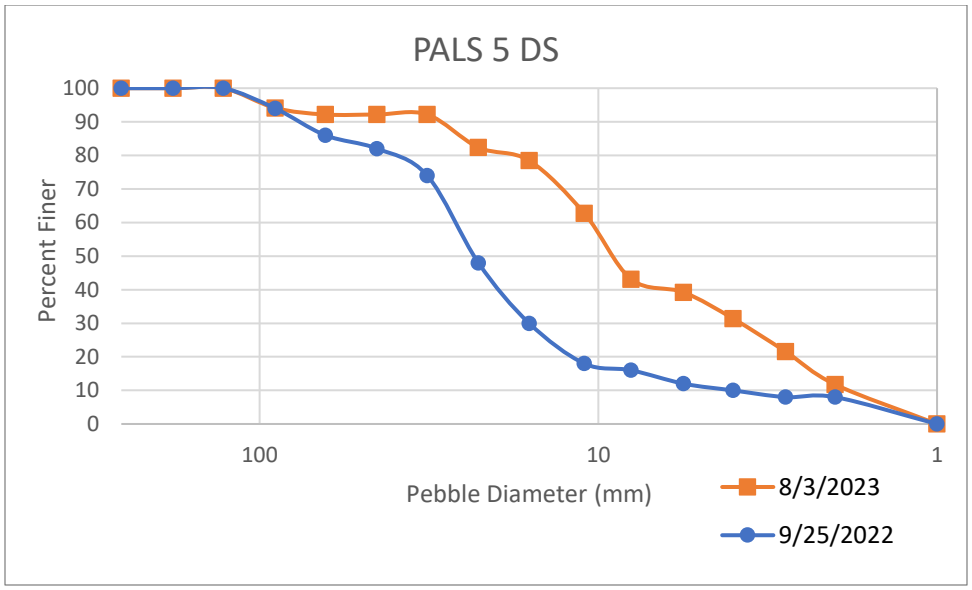

Figure E-12: Grain Size Distribution Downstream of PALS 5

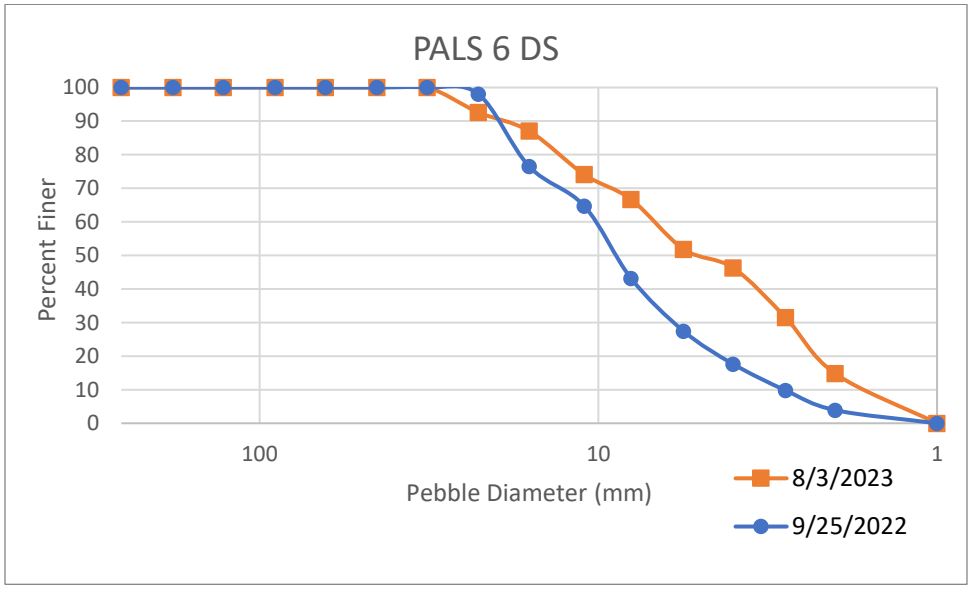

Figure E-13: Grain Size Distribution Downstream of PALS 6

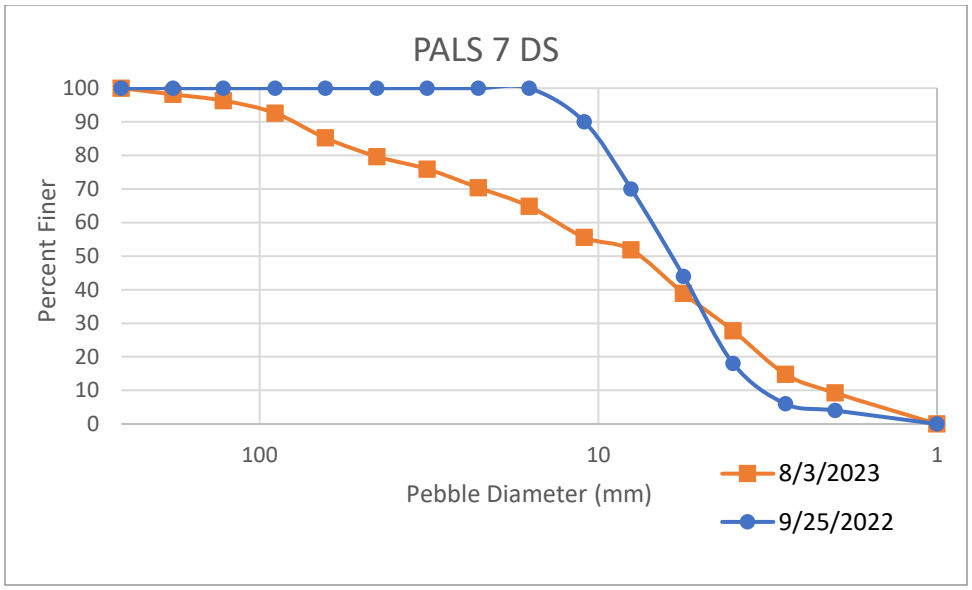

Figure E-14: Grain Size Distribution Downstream of PALS 7

APPENDIX F: SUPPLEMENTAL MODFLOW RESULTS

The following figures show additional modeling results.

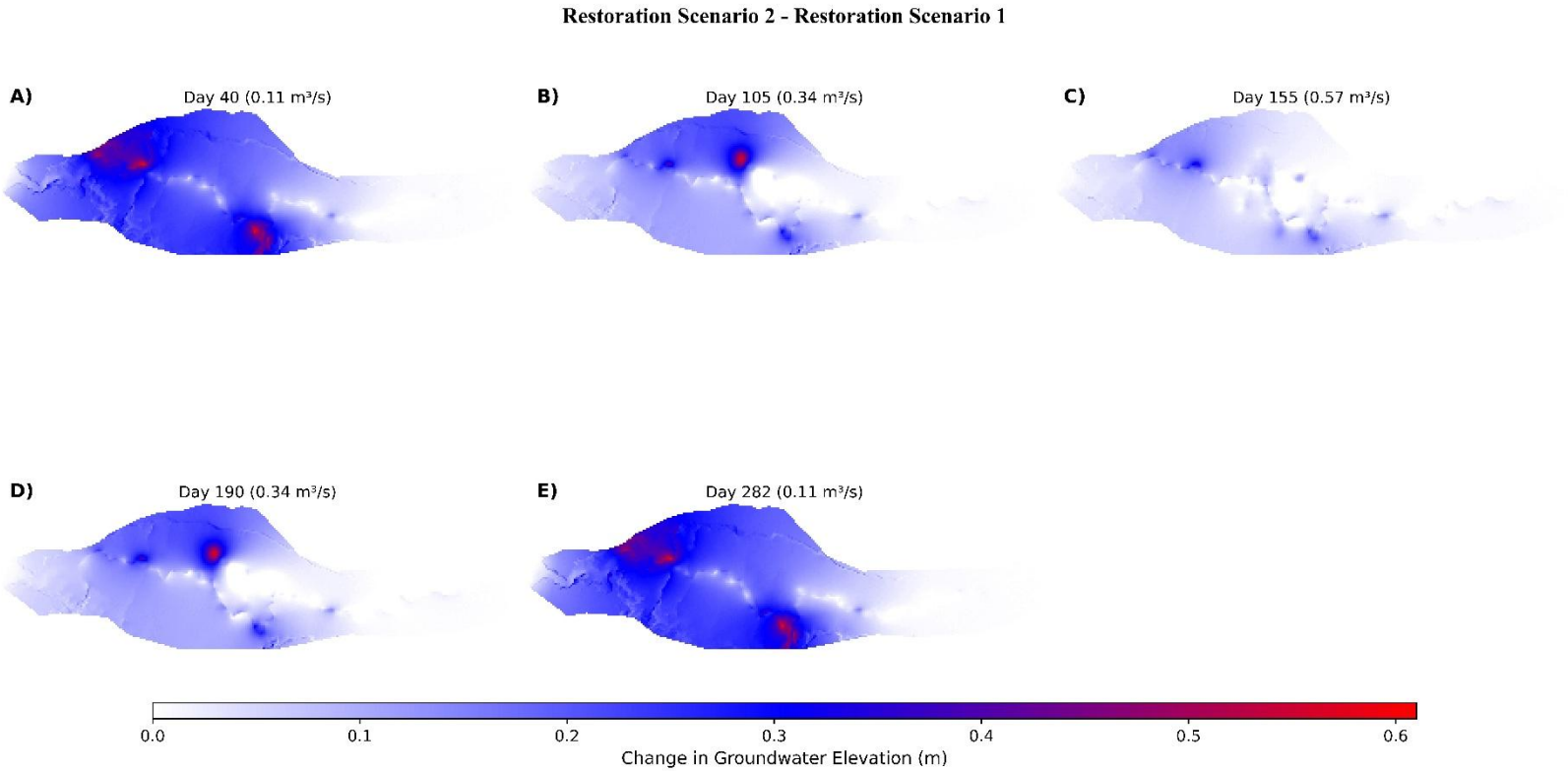

Figure F-1: Scenario 2 – Scenario 1 Groundwater Difference Maps through Time.

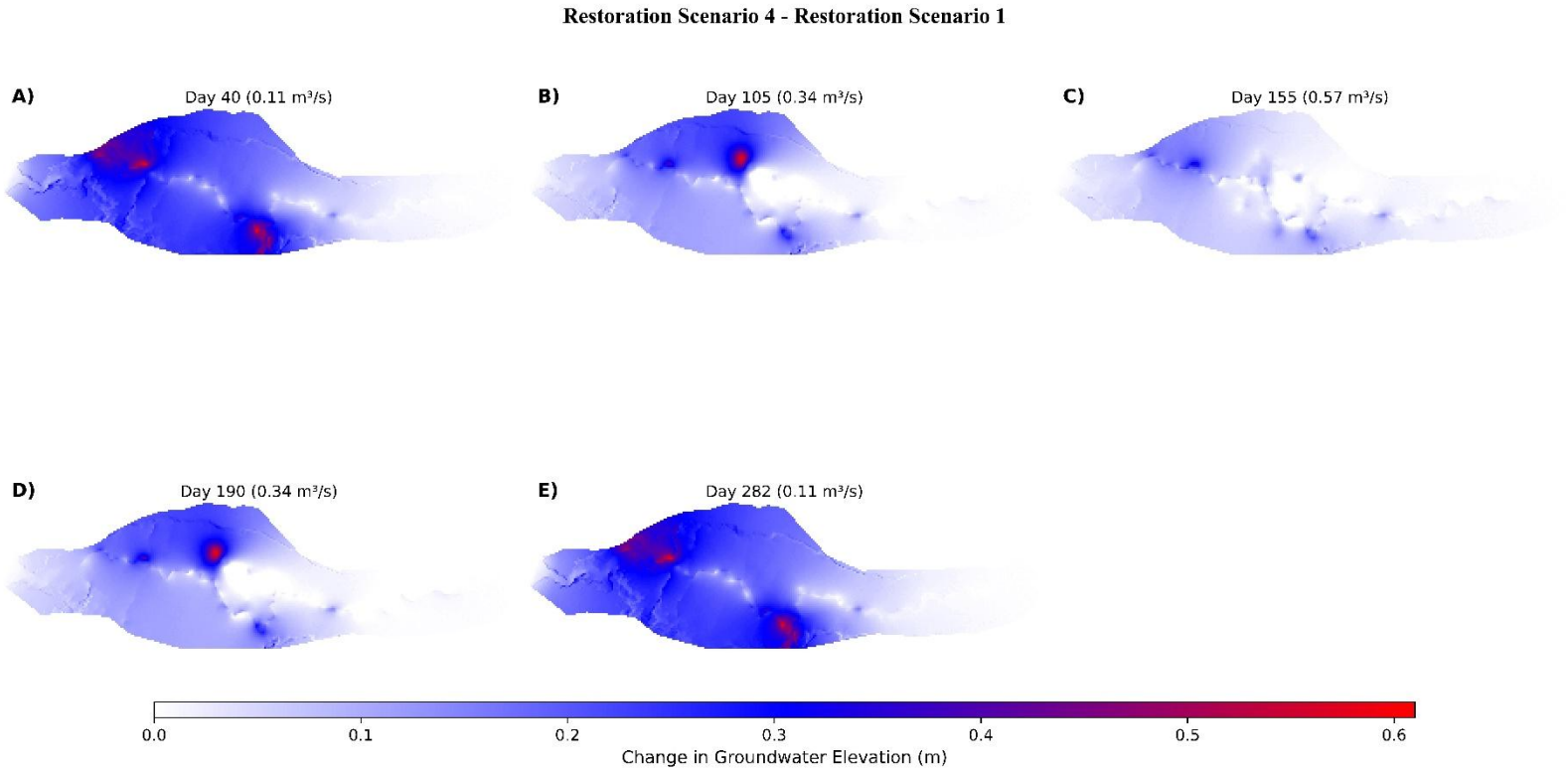

Figure F-2: Scenario 4 – Scenario 1 Groundwater Difference Maps through Time.

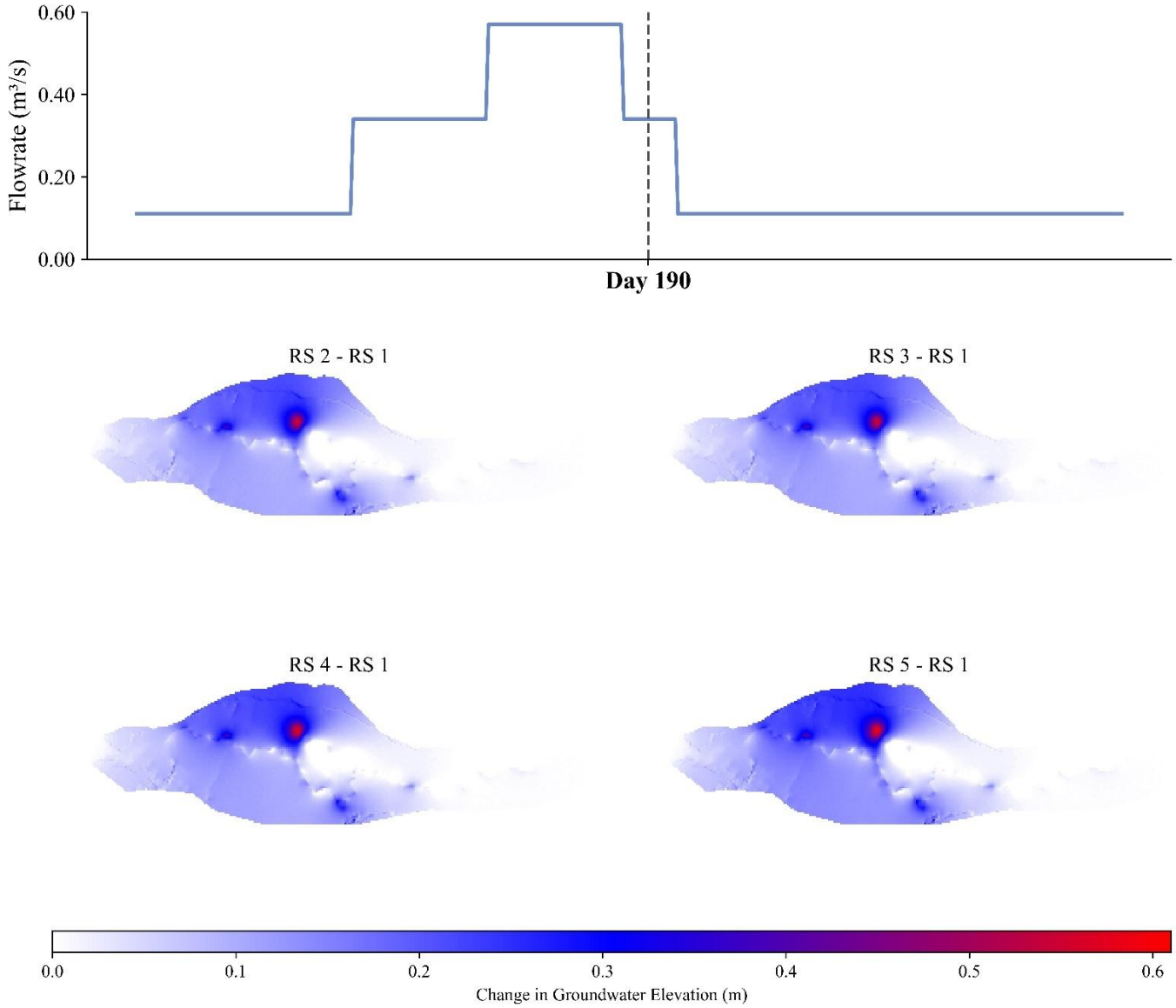

Figure F-3: Groundwater Elevation Difference Maps at Day 190, 0.34 cms.

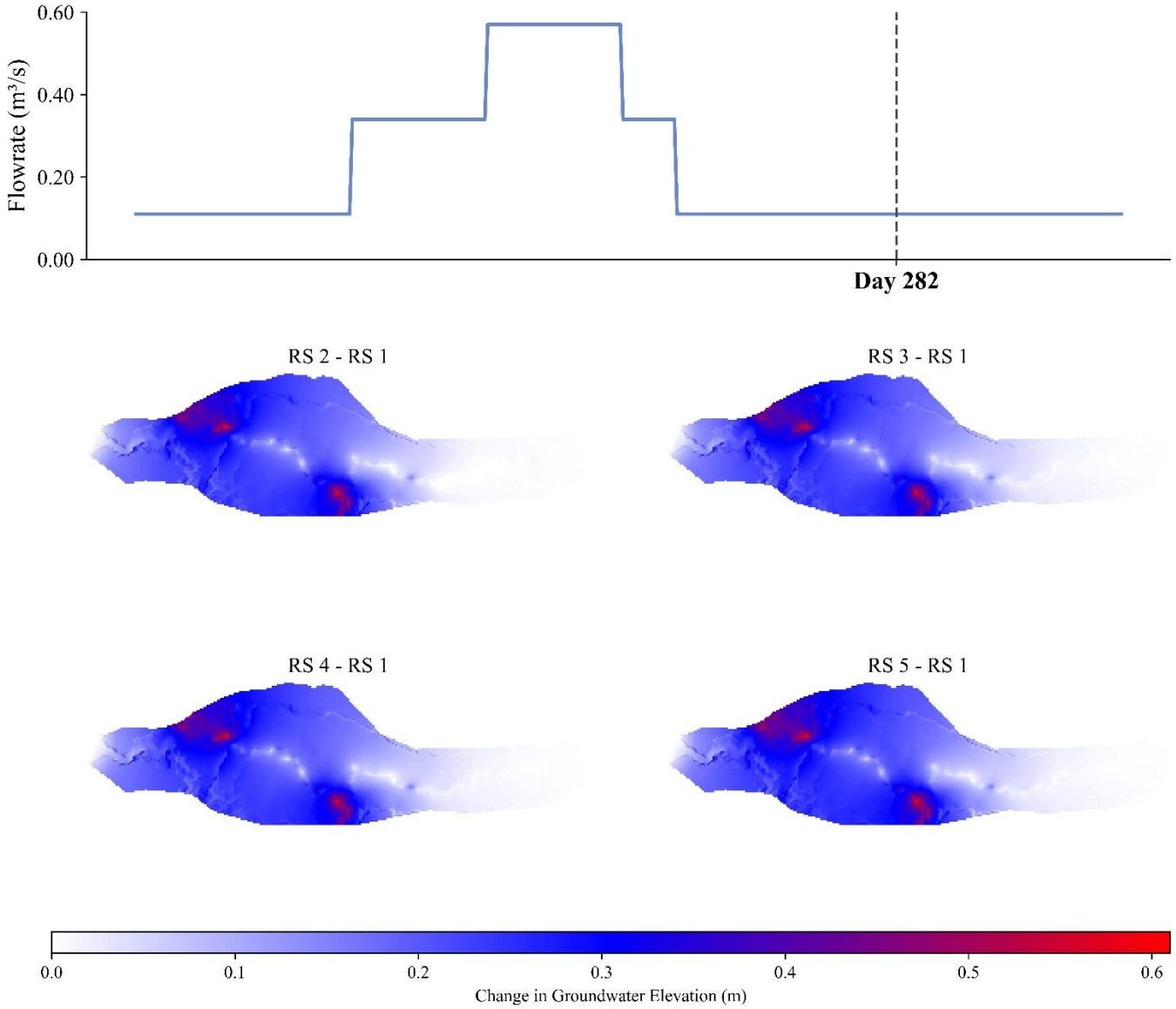

Figure F-4: Groundwater Elevation Difference Maps at Day 282, 0.11 cms.

APPENDIX G: ANNUAL PRECIPITATION DATA

U.S. Department of Commerce
National Oceanic & Atmospheric Administration
National Environmental Satellite, Data, and Information Service

Current Location: Elev: 5004 ft. Lat: 40.5763° N Lon: 105.0858° W
Station: **FORT COLLINS, CO US USC00053005**

Global Summary of the Year
2022 - 2024
Generated on 09/18/2024

National Centers for Environmental Information
151 Patton Avenue
Asheville, North Carolina 28801

Date	Liquid Precipitation (Inches)			Frozen Precipitation (Inches)					Number of Days				
Elem->	PRCP	EMXP		SNOW	EMSN		EMSD		DP01	DP10	DP1X	DYHF	DYTS
Year	Total Liquid Content	Extreme Max Precip	Date of Occurrence	Snowfall	Extreme Max Snowfall	Date of Occurrence	Extreme Max Snow Depth	Date of Occurrence	Precip >= 0.01"	Precip >= 0.10"	Precip >= 1.00"	FG+	TS
2022	13.26	1.97	Jul-28	50.4	7.8	Feb-02	11	Feb-02	83	36	1		2
2023	24.20	2.45	Aug-01	49.5	8.8	Mar-27	6	Nov-25	94	54	4		21
2024													16

Notes

(Blank) Data element not reported or missing.

X Monthly means or totals based on incomplete time series.

\+ Occurred on one or more previous dates during the month. The date in the Date field is the last day of occurrence.

A Accumulated amount.

T Trace Amount.

FG+ Heavy Fog

TS Thunderstorms